12-1-2013

Gene-environment interactions affect long-term depression (LTD) through changes in dopamine D2 receptor affinity in Snap25 haplodeficient mice

Michael Baca

Michael J. Baca
Candidate

Biomedical Sciences
Department

This dissertation is approved, and it is acceptable in quality and form for publication:

Approved by the Dissertation Committee:

Dr. L. Donald Partridge , Chairperson

Dr. Michael C. Wilson

Dr. Andrea Allan

Dr. Conrad James

Gene-environment interactions affect long-term depression (LTD) through changes in dopamine D2 receptor affinity in *Snap25* haplodeficient mice

by

MICHAEL J. BACA

DISSERTATION

Submitted in Partial Fulfillment of the
Requirements for the Degree of

Doctor of Philosophy
Biomedical Sciences

The University of New Mexico
Albuquerque, New Mexico

December, 2013

Dedication

I would like to dedicate this dissertation to my parents, John and Emily Baca, for instilling in me the lifelong desire for learning and the value of education. I would also like to also dedicate this to my uncle, Dr. Mario L. M. Baca, who is an inspiration through his continued dedication to education up to and including his retirement despite his lifelong battle with multiple sclerosis.

Acknowledgments

I would like to acknowledge my advisor Dr. Don Partridge, for giving me the opportunity to work within his lab, for teaching me the basic techniques and fundamentals involved in electrophysiology, and for all of his tireless support in developing, performing and presenting the hypothesis and results of this research. I would also like to acknowledge two of my advisors on my committee, Dr. Michael Wilson and Dr. Andrea Allan, both for allowing me to work within their labs and for their steadfast guidance in performance of this research. Dr. Michael Wilson was instrumental both in permitting the use of Snap25 haplodeficient mutant colonies necessary for this research, and for his invaluable critiques throughout the research and encouragement to go beyond my engineering mindset to write and think more like a scientist. Dr. Andrea Allan was invaluable in developing and understanding how to perform the binding assays as well as how to perform and interpret statistical analysis of the results.

I would also like to acknowledge another of my advisors, Dr. Conrad James for opening up opportunities within Sandia National Laboratories which permitted me tie this research to ongoing Sandia related bioscience projects, and for his constant support throughout this process. I would also like to thank Sandia National Laboratories itself for providing the opportunity to pursue this research. I would also like to thank Dr. Dan Savage and Dr. Martina Rosenberg for helpful guidance in developing and the use of their lab for the [^{35}S]-GTP-γ-S binding assay. I would also thank Amy Lucero for managing the mouse colonies including the administration of nicotine and genotyping.

Additional thanks go to a couple of my lab mates, Chessa Scullin and Adrian Schiess. They both provided invaluable help in learning electrophysiological techniques and critiques of this research. Acknowledgement for participation in the ongoing research presented in Appendix 2 includes Adrian Schiess, Dr. Conrad James, Devin Jelinek, and Dr. Don Partridge.

Finally, last but not least I would like to thank my family for their continual support and patience through out this process, including my wife Linda, and my children Samuel, Abigail and Jacob.

Gene-environment interactions affect long-term depression (LTD) through changes in dopamine D2 receptor affinity in *Snap25* haplodeficient mice

by

Michael J. Baca

B.S. Electrical Engineering, University of New Mexico, 1987

M.S. Electrical Engineering, New Mexico State University, 1989

PhD, Biomedical Sciences, University of New Mexico, 2013

Abstract

Genes and environmental conditions interact in the development of cognitive capacities and each plays an important role in neuropsychiatric disorders such as attention deficit/hyperactivity disorder (ADHD) and schizophrenia. Multiple studies have indicated that the gene for the SNARE protein, SNAP-25 is a candidate susceptibility gene for ADHD, as well as schizophrenia, while maternal smoking is a candidate environmental risk factor for ADHD. In this study, mice heterozygous for a *Snap25* allele and deficient in SNAP-25 expression were utilized to model genetic effects in combination with prenatal exposure to nicotine to explore genetic and environmental (G × E) factors and interactions.

Striatal long-term depression (LTD) is a form of synaptic plasticity in which there is a reduction in the glutamate released by cortical afferents onto striatal medium spiny neurons (MSNs). The glutamatergic inputs activate ionotropic and group I metabotropic glutamate receptors while dopaminergic inputs from the substantia nigra pars compacta activate type-2 dopamine receptors (D2Rs), which collectively lead to post-synaptic production of endocannabinoids that diffuse in a retrograde manner to activate pre-synaptic type-1 cannabinoid (CB1) receptors on to pre-synaptic terminals. The CB1 receptors initiate signaling cascades that lead to the long-term decrease in glutamate release in pre-synaptic glutamate terminals. Using a high frequency stimulus (HFS) electrophysiological paradigm for LTD induction in striatal MSNs, I first characterized synaptic depression in four G × E groups representing mice prenatal nicotine exposed or not or having Snap25 deficiency or not, that showed responses which could be divided by cluster analysis into populations expressing LTD and short-term depression (STD). STD is characterized by an initial decrease in amplitude in the response to the HFS followed by near full recovery of the response within 30 minutes, while LTD occurs when the initial decrease remains attenuated for at least 30 minutes. I found that prenatal exposure to nicotine in *Snap25* heterozygote mice produced a less robust LTD population and less return to baseline in the STD population. Using receptor antagonists in the same HFS electrophysiological paradigm I next examined the roles of dopaminergic D2Rs and cannabinoid CB1Rs, both critical for LTD induction in the striatum. I found that prenatal exposure to nicotine in *Snap25* heterozygote mice produced a deficit in the D2R-dependent induction of LTD, although the CB1R involvement in plasticity was not impaired.

From these results I developed the hypothesis that the impaired induction of LTD due to prenatal exposure to nicotine in *Snap25* heterozygote mice, could be related to changes in D2R affinity and/or changes in the number of D2R receptors. This was initially tested using a [^{35}S]-GTPγS binding assay to measure the agonist-stimulated response of G-protein-coupled D2R receptors. Indeed, the agonist-stimulated response was found to be reduced in *Snap25* heterozygote mice prenatally exposed to nicotine, which was consistent with a reduction in affinity of the agonist for the D2R receptor, and/or reduced GPCR coupling to downstream signaling, but not with changes in the

number of receptors. Next, a D2R agonist saturation binding assay, using [^{3}H]-quinpirole (a D2R selective agonist) followed by Scatchard analysis, showed that *Snap25* heterozygote mice prenatally exposed to nicotine exhibited significantly lower affinity (higher K_d) for D2R binding without a significant change in B_{max}, which would reflect a change in the number of receptors.

Collectively, these results support individually (G and E factors) and in combination (G × E interactions), the HET genotype and prenatal nicotine exposure lead to an impaired D2R GPCR signaling resulting from decreased agonist affinity and possibly receptor-effector coupling of the D2R receptors These receptor binding observations are consistent with the electrophysiological results showing that, in the presence of a D2R antagonist, cortico-striatal circuits in *Snap25* heterozygote mice prenatally exposed to nicotine exhibit a significant deficit in LTD induction.

This study demonstrates that genetic conditions present in a *Snap25* haplodeficient mouse model together with prenatal nicotine exposure can together alter specific receptor affinity and signaling in dopaminergic D2 receptors (D2Rs) with functional consequences in synaptic long-term depression (LTD). Since *SNAP25* is a candidate susceptibility gene for cognitive disorders such as ADHD and schizophrenia and additionally prenatal exposure to nicotine is a candidate environmental risk factor for ADHD, these studies have important translational relevance. The study also presents a general set of experimental procedures by which potential G × E interactions can be explored to determine if they alter receptor function and/or synaptic plasticity in specific brain regions.

Table of Contents

List of Figures

List of Tables

Chapter 1 – Introduction

Basal ganglia circuitry

The basal ganglia are a set of nuclei found in the forebrain and midbrain. Before discussing the neuronal circuitry of the basal ganglia, it is important to first describe its basic anatomy. As shown in Fig. 1.1, the four principle nuclei of the rodent basal ganglia are the striatum (Str), globus pallidus (GP), substantia nigra (SN) and subthalamic nuclei (STN). The striatum in turn is subdivided into a dorsal region consisting of the caudate and putamen, and a ventral region also referred to as the nucleus accumbens. The dorsal and ventral striatum are not as well differentiated in rodents as they are in primates, so the dorsal region is simply referred to as the dorsal striatum and ventral region as the nucleus accumbens (NAc). The globus palladus (also referred to as the pallidum) consists of an external segment, globus pallidus external (GPe), and internal segment, globus palladus internal (GPi). The substantia nigra in turn consists of two regions, the substantia nigra pars compacta (SNc) and substantia nigra pars reticulata (SNr).

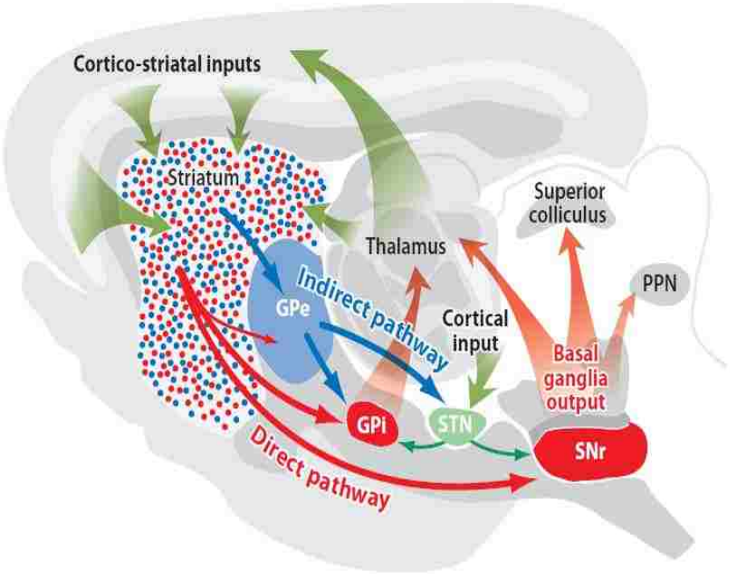

Fig. 1.1: Rodent basal ganglia nuclei and connections. Figure shows key nuclei in the basal ganglia and key connections between nuclei involved in inputs and output to the basal ganglia. Figure does not show dopaminergic connections into the striatum from the SNc (Gerfen and Surmeier, 2011)

Fig. 1.1 shows that the striatum is the primary input nuclei for the basal ganglia since it receives major excitatory glutamatergic input from all areas of cortex (referred to as cortico-striatal inputs) and the thalamus (referred to as thalamo-striatal inputs). The striatum also receives modulatory dopaminergic input from the SNc and serotonergic input from the dorsal raphé (not shown). The striatum consists primarily of medium spiny neurons (MSNs), which make up to 90% of the neurons in the striatum (Bolam et al., 2000), which receive these glutamatergic inputs as well as modulatory inputs and project inhibitory GABAergic outputs primarily to the GP and SNr. There are two D1-like dopamine receptor types, D1 and D5 receptors and three D2-like dopamine receptor types: D2, D3 and D4 receptors (Seeman and Van Tol, 1994; Vallone et al., 2000). All D2-class receptors are expressed in MSNs in the dorsal striatum with D2 receptors normally expressed ~2 fold higher that D3 and D4 receptors combined (Surmeier et al., 1996). In this document D2 receptors (D2Rs) will specifically refer to the D2 receptor subtype within the D2-like receptor class which in turn will be referred to as the D2-like receptors. The MSNs make up to 90% of striatal neurons and divide into roughly two equally expressed types of projecting neurons; those that express D1Rs known as striatonigral or direct pathway neurons and those that express D2Rs known as striatopallidal or indirect pathway neurons. A portion of D1R-striatopallidal and D2R-striatonigral neurons express other dopamine receptors, for example, D1R-striatonigral neurons express D3Rs, and D4Rs as well (Surmeier et al., 1996). As shown in Fig. 1.1, direct pathway MSNs project primarily to the GP (GPi and GPe) and SNr, while indirect pathway MSNs project primarily to the GPe. GPe neurons further project inhibitory GABAergic outputs to the GPi and STN to complete the indirect pathway. The STN also receives cortical glutamatergic input and projects glutamatergic outputs to the GPi and SNr. The major basal ganglia output circuits are inhibitory GABAergic projections from the GPi and SNr to the thalamus. There are also projections from the SNr to the superior colliculus and pendunculopontine nucleus (PPN). MSNs in the NAc also receive glutamatergic inputs from the amygdala and hippocampus and modulatory dopaminergic inputs from the ventral tegmental area (VTA).

Basal ganglia and behavior

The basal ganglia have long been associated with the coordination of movement. This can be understood in part by the complementary roles played by the direct and indirect MSN projections associated with movement (Gerfen and Surmeier, 2011). Fig. 1.2 is a diagram of basal ganglia inputs and outputs similar to Fig. 1.1, but simplified to show the differences between activation of direct and indirect pathway MSNs and their effect on motor control. As shown in Fig. 1.2, upon sufficient convergent glutamatergic excitation either direct (left) or indirect (right) MSNs will be activated to make a transition from the DOWN to the UP state and fire action potentials. Direct pathway neurons (left) project directly to inhibit basal ganglia output targets (GPi or SNr). For motor circuits from direct pathway MSNs, this results in a net inhibition of these output GABAergic neurons, which project to the motor thalamus resulting in a net disinhibition of these circuits. Through thalamocortical feedback from the motor thalamus to the pre-motor and motor cortex, this leads to promotion of movement. In contrast, indirect pathway neurons (right) project indirectly to the GPe, which ultimately results in activation of glutamatergic STN neurons onto the target outputs of the basal ganglia (GPi or SNr). For motor circuits from indirect pathway MSNs, this results in a net excitation of these output GABAergic neurons, which project to the motor thalamus resulting in a net inhibition of these circuits. Through thalamocortical feedback from the motor thalamus to the pre-motor and motor cortex, this leads to an inhibition of movement.

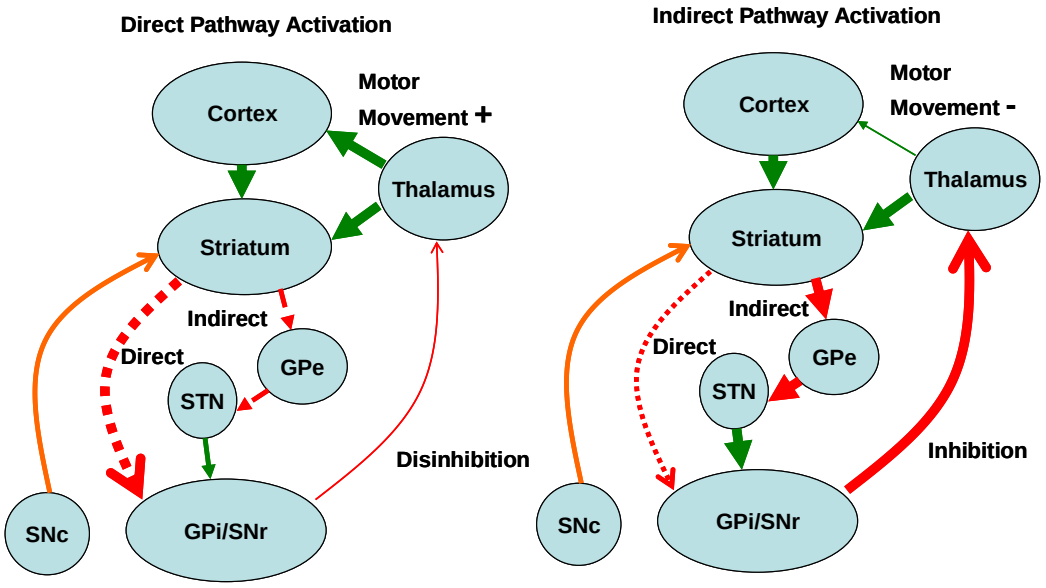

Fig. 1.2: Activation of direct and indirect pathway neurons on motor movement. Figure shows how activation of direct pathway MSNs (right) promotes movement and indirect pathway (left) inhibits movement (green arrows- glutamate; red arrows – GABA; orange arrows – dopamine; thickness of arrow represents relative amount of activation of each part of the pathway)

Evidence that the basal ganglia are involved in control of movement has also been found with its role in progressive neurodegenerative disorders such as Parkinson's disease and Huntington's disease. Parkinson's disease patients experience slowness of movement, rigidity, tremors, and problems in maintaining balance. These symptoms are related to degeneration of dopaminergic projection neurons from the SNc to the striatum leading to a greater disruption of direct pathway MSNs versus indirect pathway MSNs. This ultimately causes an increased GABAergic output to the thalamus and depression of motor activity in the cortex and spinal cord. Animals supplied with dopamine neurotoxins such as reserpine, 6-OHDA, or MPTP replicate both behavioral and circuit changes associated with Parkinson's disease supporting the role of the indirect pathway in motor suppression (Shen et al., 2008).

Huntington's disease is a progressive neurodegenerative disorder resulting from a recessive dominant gene for the huntingtin protein involving excessive CAG repeats within the gene, with usual onset in midlife with fatality within 15-20 years of onset. The disease causes inclusion bodies to form in neurons starting in the striatum and then spreading to other brain regions leading to excitotoxic cell death of neurons. These result

in involuntary movements called chorea's as well as emotional and cognitive difficulties. In contrast to the case in Parkinson's disease, indirect pathway neurons are more heavily disrupted causing them to be less active.

Additional evidence that the basal ganglia is involved with movement is provided by studies in which dopamine and glutamate receptor agonists and antagonists are injected *in vivo* into striata of animals, since these are both important neurotransmitters in the striatum. Numerous studies have shown that D1R agonists perfused into the striatum enhance movement while D1R antagonists inhibit movement; conversely, D2R agonists perfused into the striatum inhibit movement while D2R antagonists enhance movement. Both of these results support the roles of D1-direct pathway neurons in promoting movement and D2-indirect pathway in inhibiting movement (David et al., 2005). Because glutamate agonists activate both pathways in MSNs, their effects on movement have been found to be more complex and more difficult to summarize (David et al., 2005) .
In addition to the evidence, described above, that the basal ganglia are important for initiation of movement, recent work is bringing to light their role in the coordination of movement. Currently there are at least two competing hypothesis as to what these roles might be in terms of coordination of movement as further discussed below including adjustment of motor sequences (Marsden, 1987), and selection of competing motor programs (Mink, 1996).

As discussed, the basal ganglia receive cortical and thalamic inputs, which then project to output structures including the GPi and SNr via the indirect and direct pathway MSNs, which in turn make inhibitory GABAergic projections to the thalamus as well as other output targets. There is evidence that these cortical and thalamic inputs and outputs are connected topographically such that input and output connections to and from the basal ganglia form quasi-independent control loops, which control different aspects of movement (and other functions) (Bolam et al., 2000; Tisch et al., 2004). For example, the skeletomotor loop links the premotor, supplementary motor, and motor cortex with basal ganglia and motor thalamus to be involved with coordination of skeletal muscles. Additional basal ganglia loops including the occulomotor loop associated with eye movements and loops, which connect to cortical areas associated with somatosensory and limbic functions. The limbic areas also receive inputs primarily from the ventral striatum

(NAc), the hippocampus, and the amygdala, and have been shown to be involved in reinforcement learning, a role for the basal ganglia distinct from direct motor coordination.

We can compare the similarities and differences of competing hypotheses for the overall role of the basal ganglia in the skeletomotor loop in coordination of movement of limbs. One hypothesis is that the basal ganglia are involved in adjusting motor sequences through opposing actions of the direct and indirect pathways (Marsden, 1987). This is essentially a reiteration of the roles played by the direct and indirect pathway in their disinhibition or inhibition of movement. In this model, cortical inputs and thalamic motor outputs are filtered through the striatum to dynamically fine tune movements as they are occurring by coordinating basal ganglia outputs in the GPi/SNr. A slightly more sophisticated hypothesis is that the basal ganglia have a role in selecting competing motor programs (Mink, 1996). One of the fundamental problems in motor control is determining which motor program to execute at any given time for a given task or situation, given that there may be many competing inputs from different brain regions. The chorea involved in Huntington's disease or response to dopaminergic medications for Parkinson's disease indirectly shows how conflicting signals may affect the coordination of movement. As shown in Fig. 1.1, cortical inputs are delivered to the striatum as well as the STN. In this model, a general motor program is sent to the STN and the focused selection program is carried out through inputs in the striatum, which either activate or inhibit this motor program through coordinated regulation of the direct and indirect pathways. For example, if the desired program is to extend the arm, the basal ganglia outputs will disinhibit motor outputs that are associated with extending the arm and inhibit motor outputs that are associated with flexing the arm. Further research has extended this paradigm to argue that the basal ganglia circuitry is involved in movement selection in an adaptive manner such that beneficial movement sequences are enhanced and those which are harmful, are suppressed. Mechanisms in neuronal plasticity, such as long-term depression (LTD) and long-term potentiation (LTP), may be involved in adjustments of basal ganglia circuitry involved in selection of motor programs. Some preliminary research, which links LTD to behavior in the striatum is discussed below, following a discussion of the process of LTD induction in the striatum.

Striatal long-term depression (LTD) induction and signaling in MSNs

The mechanisms that underlie the induction of long-term depression (LTD) in the striatum are the basis of many recent reviews (Di Filippo et al., 2009; Kreitzer and Malenka, 2008; Lovinger, 2010; Surmeier et al., 2007). The following is a summary of the process of induction of LTD as it is currently understood (Fig. 1.3). Long-term decreases in synaptic efficacy, known as LTD, occur in MSNs in the striatum as a result of high frequency stimulation (HFS) of the glutamatergic inputs or as the result of paired activation of pre- and post-synaptic neurons known as spike timing dependent plasticity (STDP). LTD is expressed as a decrease in the probability of glutamate release by cortical or thalamic pre-synaptic inputs to MSNs. This is typically demonstrated by measuring the frequency and amplitude of miniature excitatory post-synaptic currents (mEPSCs) with frequency indicating the number of release events and amplitude indicating the response to these events. Striatal LTD is characterized by a decrease in mEPSC frequency, which is indicative of a pre-synaptic events and not amplitude, which would be characteristic of a post-synaptic event (Choi and Lovinger, 1997a; Choi and Lovinger, 1997b)

In the absence of glutamatergic input, the membrane potential of MSNs is near the potassium equilibrium potential of~-85 mV referred to as the DOWN state. In response to sufficient glutamatergic input, the MSN depolarizes to a potential of ~-55mV referred to as the UP state, which is above the threshold for action potential generation. The MSN must be in the UP state for the induction of LTD to occur (Choi and Lovinger, 1997a; Choi and Lovinger, 1997b). Sufficient glutamatergic input activates post-synaptic group I metabotropic glutamate receptors (mGluRs), which are necessary for LTD induction since their blockage by antagonists prevents LTD induction. Cav1.3 L-type Ca^{2+} channel activation appears to be necessary for LTD induction, since blockage by antagonists also prevents LTD induction (Wang et al., 2006). Sufficient dopaminergic input to D2 receptors (D2Rs) is also necessary for LTD induction, since their blockage by antagonists prevents LTD induction. Finally activation of pre-synaptically expressed cannabinoid type-1 receptors (CB1Rs) is necessary for LTD induction, since their blockage by antagonists also prevents LTD induction.

Fig. 1.3 shows the basic model which has been developed for LTD induction, which includes the so-called tri-synaptic circuit in which glutamatergic inputs converge with dopaminergic inputs onto MSN spines. The glutamatergic and dopaminergic inputs activate mGluRs and D2Rs. In addition, cholinergic interneurons may be also involved in LTD induction. The MSN depolarized from the DOWN state to the UP state leads to activation of Cav1.3 Ca^{2+} channels and Ca^{2+} signaling, which participates with the mGluR and D2R activation in the production of post-synaptic endocannabinoids, which transfer retrogradely to pre-synaptic cannabinoid CB1 receptors on glutamatergic input terminals to cause prolonged inhibition of glutamate release. The role of D2Rs in LTD induction in the striatum is well established, but their locus of action in this process has not been fully elucidated (Lovinger, 2010). Since D2Rs are expressed in MSN spines, activation of these D2Rs seem to be an obvious locus by which they are involved in LTD induction (shown in Fig 1.3 as D2R path1). Evidence includes the observation that D2R antagonists block LTD induction (Kreitzer and Malenka, 2005) as well as the additional observation that nAChR receptors are implicated in LTD induction (Partridge et al., 2002) possibly because of their inhibitory effects on dopamine release from dopaminergic inputs. Another locus of action (shown in Fig 1.3 as D2R path2) involves D2Rs expressed on cholinergic interneurons. According to this mechanism, a temporary pause in cholinergic interneuron firing due to D2R suppression of cholinergic interneuron firing in conjunction with glutamate excitation can lead to a temporary suppression of acetylcholine release onto muscarinic M1Rs on MSNs, suppression of which may be linked to the Cav1.3 Ca^{2+} channel activation involved in endocannabinoid production (Wang et al., 2006). This research also identified the Cav1.3 Ca^{2+} channel as the critical Ca^{2+} channel linked to LTD induction. Further research will be needed to elucidate whether D2R involvement is through path1 or path2 or both. Clearly the interactions of multiple transmitters, receptors, and channels are involved in LTD induction.

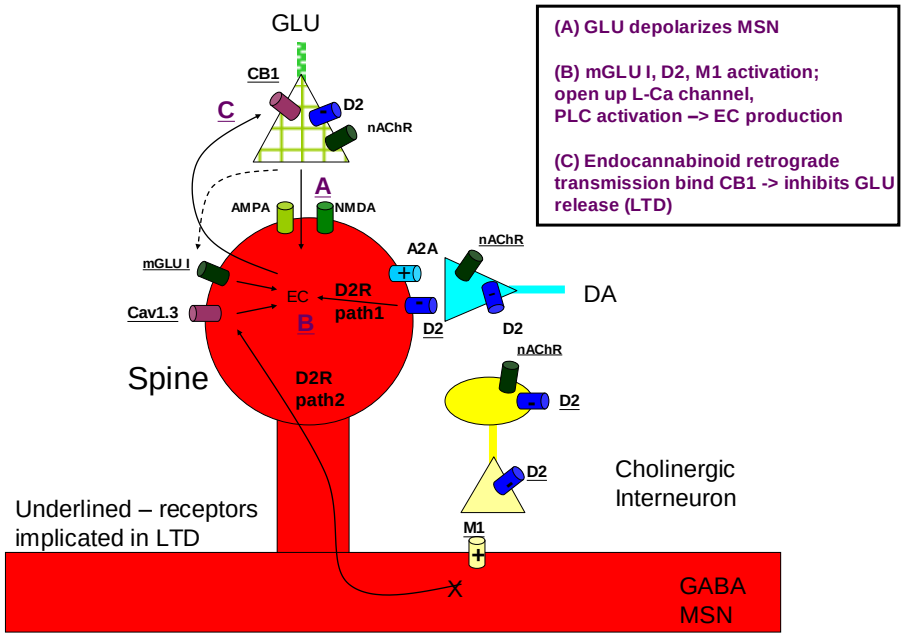

Fig. 1.3: Process of LTD induction in striatal MSNs. Schematic that illustrates how MSN spines interface with glutamatergic and dopaminergic inputs as well as inputs from cholinergic interneurons. The inset shows that following depolarization of an MSN by sufficient afferent glutamatergic stimulation, L-type Cav1.3 Ca^{2+} channels along with mGluR and D2R activation participate in the production of endocannabinoids which retrogradely transport to pre-synaptic CB1 receptors on glutamate terminals to lead to a long term decrease in the probability of glutamate release characteristic of MSN LTD. The figure also shows alternative paths by which D2Rs may be involved in LTD induction. D2R path1 in which binding of D2Rs expressed in MSNs directly contributes to endocannabinoid production and LTD or D2R path2 in which binding of D2Rs on cholinergic interneurons indirectly leads to suppression of acetylcholine release onto cholinergic interneurons, which in turn contributes to activation of L-type Cav1.3 Ca^{2+} channels, contributing to endocannabinoid production.

Dopamine D2Rs are seven-transmembrane (7TM) G protein coupled receptors (GPCRs) coupled to the $G_{i/o}$ family of trimeric G proteins which is also the case for D3Rs and D4Rs (Beaulieu and Gainetdinov, 2011). Group I mGluRs are GPCRs coupled to the G_q family of trimeric G proteins (Luscher and Huber, 2010). Activation of both of these receptors along with calcium influx from L-type Cav1.3 Ca^{2+} channels is necessary for LTD induction (Castillo et al., 2012). The two major endocannabinoids synthesized in MSN spines (Fig 1.3) are anandamide (Arachidonoylethanolomide; AEA) and 2-AG (2-arachidonoylgylcerol) (Kano et al., 2009). It is unclear which of these two endocannabinoids plays the principle role in LTD induction, but the current consensus is

that 2-AG may play a larger role (Castillo et al., 2012). Fig 1.4 illustrates one of the major anandamide synthesis pathways (top) and 2-AG synthesis pathway (bottom) indicating how activation of both pathways are Ca^{2+} dependent (Kano et al., 2009). It has also been established that one of the pathways of the synthesis of 2-AG is through G_q protein activation of phospholipase Cβ (PLCβ). It is less well established how mGluR signaling contributes to anandamide synthesis (Castillo et al., 2012). While D2Rs activation is critical to the LTD induction process, since antagonism of D2Rs leads to inhibition of LTD (Calabresi et al., 1992), its role (path1, path2 or both in Fig 1.3), in endocannabinoid production has not been clearly established. *In vivo* microdialysis measurements of anandamide in the striatum have shown that D2R activation by D2R agonists produces a multifold increase in anandamide indicating that D2R activation may be involved in endocannabinoid production during LTD induction (Giuffrida et al., 1999). As with mGluR, it is unclear how D2R signaling may influence anandamide synthesis. Given that one of the downstream effectors of D2Rs, as with mGluRs is PLCβ, this may be one mechanism by which D2R activation could be involved in 2-AG synthesis (Lee et al., 2004; Mathur and Lovinger, 2012).

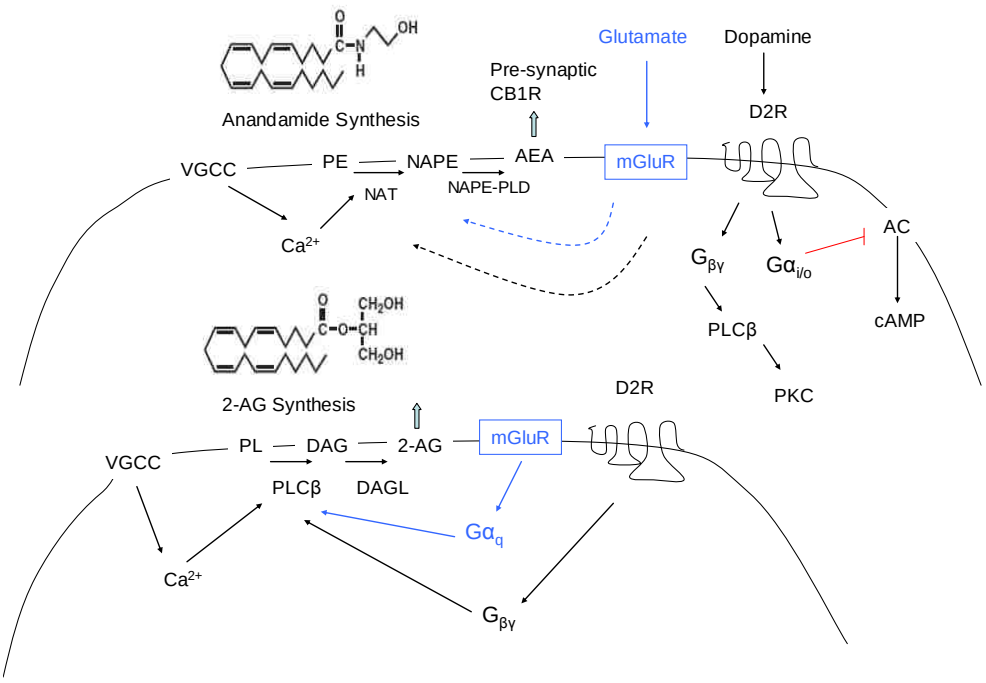

Fig. 1.4: Interaction of D2R and mGluR signaling with endocannabinoid production in MSNs. Top shows one synthesis pathway for endocannabinoid Anandamide (Arachidonoylethanolomide; AEA) as well as possible mGluR, D2R and VGCC (L-type Cav1.3 Ca^{2+} channel) interactions with Anandamide synthesis. Bottom shows one synthesis pathway for endocannabinoid 2-arachidonoylgylcerol (2-AG) as well as possible mGluR, D2R and VGCC (L-type Cav1.3 Ca^{2+} channel) interactions with Anandamide synthesis. Black arrows show activation of D2R downstream effectors as well as endocannabinoid synthesis pathways. Red lines show inhibition of D2R downstream effectors. Blue arrows show activation of mGluR downstream effectors. Dotted lines – black and blue, unclear how activation of D2Rs and mGluRs influences anandamide synthesis. Abbreviations: AC, adenylyl cyclase; cAMP, cyclic AMP; DAG, diacylglycerol; DAGL, diacylglycerol lipase; NAT, *N*-acyltransferase; NAPE, *N*-acyl-phosphatydlethanolamine; NAPE-PLD, *N*-acyl-phosphatydlethanolamine-hydrolyzing phospholipase D; PLCβ, phospholipase Cβ; PE, phosphatidylethanolamine; PKC, protein kinase C; PL, phospholipid. Chemical drawings of Anandamide and 2-AG, obtained from (Ueda et al., 2013)

The synthesis of endocannabinoids on the post-synaptic MSNs is followed by their transfer retrogradely to pre-synaptic CB1Rs expressed on glutamate terminals. The process of transfer to the pre-synaptic glutamate terminals has not been fully resolved as to whether it may involve carrier proteins or simple diffusion (Kano et al., 2009). Signal transduction through CB1Rs, which are $G_{i/o}$-coupled GPCRs, leads to reduction in the release of glutamate from pre-synaptic terminals leading to LTD. Why this transduction

process leads to sustained changes in glutamate release is currently not fully understood (Castillo et al., 2012; Mathur and Lovinger, 2012).

The D2R has two variants expressed by alternate splicing of the same gene, D2S (S=short; 414 amino acids) and D2L (L=long; 443 amino acids). The D2S is predominantly expressed pre-synaptically on input terminals including glutamatergic, dopaminergic, and cholinergic terminals on MSNs (Fig. 1.3) and D2L is expressed post-synaptically on MSNs spines (Usiello et al., 2000). The D2 receptor can exist in either a state of low or high affinity for dopamine ($D2^{Low}$ or $D2^{High}$, respectively) and the relative levels of each affinity state have been investigated (Seeman et al., 2006). The $D2^{Low}$ state represents the condition where the D2R GPCR is uncoupled from the heterotrimeric protein ($G\alpha_{i/o}$,G_{β},$G\gamma$) and the $D2^{High}$ state represents the condition where the D2R GPCR is coupled and the latter state is more readably able to bind dopamine and D2R agonists (van Wieringen et al., 2013). Studies using homogenized rat striata suggest that ~0.77 of D2Rs are normally in the $D2^{High}$ state (Seeman et al., 2006).

D2R receptors have important downstream signaling pathways in addition to those associated with endocannabinoid production. A brief summary of the major pathways associated with D2R signaling based upon information provided in recent reviews (Beaulieu and Gainetdinov, 2011; Cho et al., 2010; Yao et al., 2008) is presented below and illustrated in Fig. 1.5. Prior to D2R agonist binding, the trimeric G protein α subunit will be bound to GDP, and tightly associated with the β and γ subunits. There is some controversy as to whether the trimeric G protein complex can be pre-coupled to the D2R receptor prior to agonist binding, or whether it requires agonist binding in order to be coupled to the D2R. In either case, upon D2R agonist binding, the trimeric G protein complex associates with the D2R through the third intracellular loop and C terminus, and undergoes conformational changes, which allow an exchange of GTP for GDP on the Gα subunit causing the Gα subunit to become activated and to dissociate from the Gβγ subunit complex. Both the activated Gα subunit as well as Gβγ subunit complex can then trigger secondary downstream signaling pathways. The Gα subunit has intrinsic GTPase activity, which allows it to hydrolyze GTP permitting a return to the inactive state bound to the Gβγ subunit complex. Important regulators of G protein signaling (RGSs) can accelerate the rate of GTP hydrolysis. As long as agonist binding of the D2R remains,

multiple sets of heterotrimeric G proteins can be activated, amplifying the downstream signaling. Agonist binding further triggers recruitment of G protein receptor kinases (GRKs), which phosphorylate specific sites on the D2R intracellular loops allowing β-arrestins to bind the D2Rs and to the D2R in an activity-dependent manner. The β-arrestins also trigger clathrin-dependent internalization and recycling of the D2R receptors. Protein kinase A (PKA) and protein kinase C (PKC) also phosphorylate sites on the D2Rs and also may be involved in regulation of D2R signaling.

Since D2Rs are coupled to the $G_{i/o}$ family of trimeric G proteins, activation the Gα subunit inhibits adenylyl cyclase (AC) activity. This results in a net inhibition of PKA and its targets including those involved with dopamine and the 32kDa cAMP-regulated phosphatase DARPP-32. Inhibition of DARPP-32 depends upon de-phosphorylation by protein phosphatase 2B (PP2B, or calcineurin), which is a calcium-dependent process.

The D2R Gβγ subunit complex as discussed previously activates PLCβ and so may be involved in 2-AG endocannabinoid synthesis. The Gβγ subunit complex is also involved in other PLCβ-dependent signaling processes such as the activation of PKC and inositol 1,4,5-trisphosphate (IP_3)-dependent opening of IP_3 Ca^{2+} channels expressed in the endoplasmic reticulum (ER) lumen. The resultant release of Ca^{2+} is involved in PP2B activation as well as the activation of Ca^{2+}-calmodulin dependent protein kinase II (CAMKII). The PLCβ signaling is also negatively coupled to L/N Ca^{2+} channel opening and it promotes the opening of G-protein-coupled inward rectifying potassium (GIRK) channels, both of which act to inhibit the excitability of MSNs.

Finally, β-arrestin signaling, associated with D2R desensitization and receptor internalization, is involved, through protein phosphatase 2A (PP2A) activation, in the suppression of signaling associated with Akt (Protein kinase B; PKB).

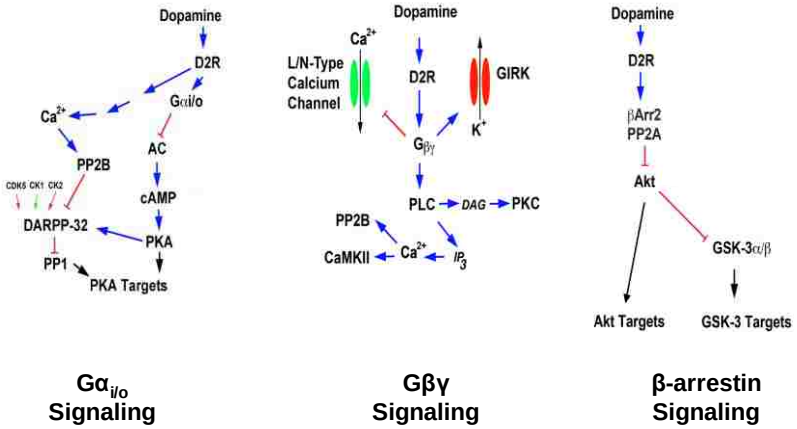

Fig. 1.5: Dopamine D2R signaling pathways. Adapted from (Beaulieu and Gainetdinov, 2011). Left shows D2R $G\alpha_{i/o}$ and Ca^{2+} signaling pathways. Center shows D2R $G\beta\gamma$ signaling pathways. Right shows β-arrestin2 signaling pathways. Blue arrows show activation of D2R downstream effectors. Red T lines show inhibition of D2R downstream effectors. Abbreviations: AC, adenylyl cyclase; Akt, also referred to as protein kinase B; cAMP, cyclic AMP; DAG, diacylglycerol; DARPP-32, dopamine and cAMP regulated phosphoprotein of 32 kDA; βArr2, β-arrestin2; CamKII, Ca^{2+} -calmodulin dependent protein kinase II, GSK-3α/β, glycogen synthase kinase 3α/3β; IP3, inositol 1,4,5-trisphosphate; PLCβ, phospholipase Cβ; PKA, protein kinase A; PKC, protein kinase C; PP1, protein phosphatase 1; PP2A, protein phosphatase 2A; PP2B, protein phosphatase 2B.

Striatal LTD and behavior

Given the ubiquity of LTD in the striatum, an increasingly important research question has been to try to identify how LTD might be linked to behavior (Lovinger, 2010). These studies require linking animal behavioral experiments with *in vivo* or *ex vivo* electrophysiology recordings in order to show that the behavioral changes are connected to changes in plasticity. For example, one study found differences in ability to undergo LTD in cortico-striatal circuits in association with the acquisition and consolidation phases of skilled learning task (Yin et al., 2009). In this study, mice were implanted with multi-electrode arrays in which *in vivo* recordings of the dorsal medial striatum (DMS) and dorsal lateral striatum (DLS) MSNs were recorded simultaneously while the mice learned a task of remaining on rotorod (rotating bar) for repeated trials

each day for several days. It was found that during the early training phase (day 1) DMS, but not DLS, neurons increased their firing rates simultaneous with improvement of the skill as measured in latency (seconds) remaining on the rotorod compared to the rates recorded from the same mice prior to training (non-trained naïve controls). During the late training phase (day 8), DLS neurons, but not DMS neurons, increased their firing rates compared to naïve controls but this did not correspond with improvements in latency. This indicated that DMS and DLS firing rates correlated with different time periods of the task. To examine possible changes in striatal plasticity associated with these changes in firing rates, *ex vivo* slice recordings were performed on representative naïve controls as well as early and late trained mice, which had undergone the same learning tasks. In both the DMS and DLS neurons an experimental paradigm known as the LTD saturation task was performed. This paradigm consisted of a 10 minute baseline set of population spike recordings delivered at half maximum stimulus followed by two 1 second trains of 100 Hz at maximum stimulus followed by 20 minute recordings at half maximum stimulus during which the population spike would typically decrease in amplitude compared to the baseline and partially recover to ~0.8 of the previous baseline. The same HFS train and 20 minute recording was repeated three times for a total of 4 HFS trains interspersed with 20 minute recovery periods for a 120 minute total recording time. The object of this paradigm was to determine when the responses to HFS reached saturation in which the response following a given stimulus train in the series failed to produce a significant depression of the population spike over that from the previous stimulus train. This was considered to be a saturation of the LTD response. It was found that for naïve mice, DMS slices required more HFS trains to reach saturation than DLS slices and thus were more malleable to modification in the naïve and early learning stages and this corresponded with the increased firing rates in early stages found with the *in vivo* recordings. Conversely for late stage mice, DLS slices required more HFS trains than DMS slices and were more malleable to modification in the late learning stages. These changes were interpreted to imply that the differences in firing rates recorded *in vivo* in the DLS versus the DMS neurons involving behavioral learning correlated to changes in responses to LTD saturation in *ex vivo* slices of the same animals, so that behavior could be potentially linked to LTD.

Another recent study compared knockout mice deficient in adenlylyl cyclase 5 (AC5), which is highly expressed in MSNs, where it serves as a downstream effector of D2Rs, to WT controls for different behavioral tasks as well as for changes in electrophysiology including LTD (Kheirbek et al., 2009). In a response learning task known to be dorsal striatum-dependent, in which mice were required to swim to locate a hidden platform arm by making the same body turn (left or right) each time, AC5 knockouts were found to take longer to acquire the success criteria (9/10 correct choices) than controls, during both the initial acquisition as well as during reverse learning where the opposite body turn was required, with a 2-3 fold increase in the number of trials for the AC5 knockouts to achieve success versus the controls. Similar to the previous research on DLS versus DMS (Yin et al., 2009), the latency to fall off of a rotorod was significantly less for AC5 knockouts versus controls, for latencies during daily trials, extended over three days. In subsequent whole-cell voltage-clamp recordings, differences were not found in basal firing or paired pulse facilitation between AC5 knockouts and controls. However when subject to four 1 second trains of 100 Hz at maximum stimulus intensity separated by 10 seconds, with 10 minutes of baseline recordings at half maximum stimulus prior to the 100 Hz trains, and 30 minutes of recordings following the 100 Hz trains, it was found that both AC5 knockouts and controls underwent a brief drop in amplitude following the 100 Hz trains, relative to the baseline recordings, but the AC5 knockouts returned to the baseline levels after 30 minutes, while the controls underwent a mild LTD of ~0.80 of the baseline levels. This experiment like the previous one, demonstrates how behavioral changes may be correlated with changes in LTD. Both of these studies also show how changes in response to LTD due to genetic differences or striatal location, may be related to and partially underlie associated behavioral changes.

Gene-environmental factors and interactions in neuropsychiatric diseases

It has been known for some time that a given trait expression is a product of both the genes underlying a particular trait as well as environmental conditions. For most traits, which are products of multiple genes and environmental factors, this is seen in the mathematically described heritability of a trait (h^2) where h^2 = genotypic variance/phenotypic variance (Falconer, 1989). A highly heritable trait is one in which

the underlying genes make a larger contribution to the trait's expression than do environmental factors. The heritability of a trait varies greatly because a given trait may be under the influence of many genes and diverse environmental factors. Furthermore, trait expression can be understood to be influenced both by the genetic coding as well as environmental factors. For example, changes in transcription factors can influence the amount of protein that a gene will express. Equivalently, changes in environmental conditions can modulate the levels of transcription factors available and thus influence protein expression. Environmental factors can be distinguished to some extent by whether they have their effects *in utero*, during early postnatal development, or throughout the lifetime of an organism.

It is not surprising that both genes and environmental conditions are involved in the development of cognitive capacities and that both can contribute to neuropsychiatric disorders. There is a growing body of research dedicated to determining the crucial role played by gene-environmental interactions in neuropsychiatric illnesses including depressive disorders, ADHD, schizophrenia, obesity, and substance abuse (Wermter et al., 2010). It has been known for some time that there are specific genes associated with susceptibility to certain neuropsychiatric disorders. At the same time, it is postulated that given a set of susceptibility genes for a given disorder, the likelihood of getting a specific disease will increase in the presence of specific environmental factors. A common example of the interaction of genes and environmental conditions in a non-neuropsychiatric disease is phenylketonuria (PKU). PKU results from a recessive mutation in which the gene for phenylalanine hydroxylase (PAH) that is necessary to convert the amino acid phenylalanine to tyrosine is non-functional. If PKU is undetected, phenylalanine accumulates and is converted to phenlyketone, which accumulates and if untreated can lead to seizures and mental retardation. Fortunately, detection at birth, and the use of phenylalanine-deficient diets can prevent the development of PKU. Thus, PKU illustrates how a gene mutation (PAH) combined with an environmental effect (consumption of phenylalanine) can lead to a disease PKU. Gene-environmental ($G \times E$) interactions in neuropsychiatric disorders are harder to identify than the simple case of PKU. This is due to the polygenic nature of neuropsychiatric disorders such as attention deficit hyperactivity disorder (ADHD), schizophrenia, and autism, in which the disorder

appears to be the product of the combined effects of many genes and not the effect of a small number of dominant genes as was the case in PKU.

A number of recent studies have examined the relationship of G × E factors in other disorders. An early set of studies (Caspi et al., 2002; Caspi et al., 2003) showed that a polymorphism of the gene encoding for monoamine oxidase A (MAO_A) combined with childhood maltreatment was associated with conduct disorder and antisocial personality. Follow-up studies failed to replicate the findings, but a meta-analysis of multiple studies still showed a significant interaction (Kim-Cohen et al., 2006). Several studies have linked obesity to G × E interactions, including one which linked a polymorphism in the fat mass and obesity associated gene (*FTO*), and low amounts of physical activity (Rampersaud et al., 2008). Another study found that a gene variant for the serotonin transporter and environmental adversity were involved in depression (Uher and McGuffin, 2008). Additionally, as described below, there is evidence for G × E interactions in attention deficit/hyperactivity disorder (ADHD) and schizophrenia. These studies provide impetus for studies with animal models to further probe the role of the interaction of G × E factors on behavior and neural circuits, which may underlie neuropsychiatric as well as other disorders.

G × E interactions can be evaluated by performing analysis of variance (ANOVA) between groups of animals with differences in genes and environmental conditions. For example, as described further in the Methods, I have used a 2 × 2 design to evaluate the interactions of genotype and environment using *Snap25* heterozygote knockout male mice (HET) bred with wild type C57BL/6J female mice (WT) (genotype control) under either saccharine (environmental control) or prenatal nicotine exposure (PNE) conditions during pregnancy to produce four experimental groups of mice representing genotype (HET) × environmental (PNE) interactions. A two-way ANOVA was used evaluate if there are main genotype (HET v WT) factors, main environmental factors (PNE v Sac), and/or factors due to gene-environmental interactions. Analysis of a given experiment will reveal whether combinations of distinct genotypic and/or environmental factors as well as gene-environmental interactions contribute to the comparative differences of the experimental groups.

Role of SNAP-25, and prenatal nicotine exposure in ADHD

Attention deficit/hyperactivity disorder (ADHD) is a common, albeit heterogeneous, neuropsychiatric disorder with a prevalence of greater than 5% worldwide (Faraone et al., 2003; Polanczyk et al., 2007). ADHD is first detected in childhood and often extends into adulthood (Biederman et al., 2011) and is characterized by the debilitating social and behavioral symptoms of excessive inattention, hyperactivity, and impulsivity (American Psychiatric Association, DSM IV-TR, 2000).

The role of the basal ganglia and the dorsal striatum in particular in ADHD is well established (Swanson et al., 2007). For example, in human ADHD patients, the caudate is smaller than these structures in control groups, and prefrontal cortex to striatal networks have been found to be functionally less active compared to controls (Swanson et al., 2007). Genetic association studies have demonstrated that ADHD has strong heritability, although it appears to have a complex multigenic etiology (Faraone et al., 2005; Faraone and Mick, 2010) consistent with small effects due to multiple genes. Multiple studies have consistently found certain gene variants implicated in ADHD including the *SNAP25* gene, several dopamine related genes (*DRD4*, *DRD5*, *DAT*, dopamine β-hydroxylase) as well as serotonin related genes (Faraone et al., 2005). Some of these candidate ADHD genes, such as *DRD4* and *DAT*, are directly involved in cortico-striatal circuitry. While the striatum has traditionally been directly associated with motor control, it has increasingly been seen to be critical in other forms of behavior as well (Schultz et al., 2003). The therapeutic response to psychostimulant treatment has implicated the involvement of dopamine and norepinephrine systems with implications for cortico-striatal circuitry and executive function (Swanson et al., 2007). Recent imaging studies further suggest the contribution of a wide range of neural networks to the diversity of ADHD symptoms (Castellanos and Proal, 2012). Based on the evidence for alterations in dopaminergic neurotransmitter systems, a number of genes that encode proteins involved in dopamine transmission have been examined in genetic studies and have been shown to be associated with ADHD (Faraone and Mick, 2010).

The *SNAP25* gene is one candidate susceptibility gene for ADHD. *SNAP25* encodes the pre-synaptic protein SNAP-25, which is one of the t-SNAREs that have been shown to play a role in Ca^{2+}-dependent vesicular fusion and is thus a protein critical to

evoked neurotransmitter release (Jahn and Scheller, 2006; Rizo and Sudhof, 2012). In order for neurotransmitter to be released from a pre-synaptic terminal, a neurotransmitter-filled vesicle must fuse with the pre-synaptic membrane. This fusion process requires the interaction of target-membrane-associated-soluble N-ethylmaleimide fusion protein attachment protein receptor proteins (t-SNAREs) and vesicle-membrane-associated-soluble N-ethylmaleimide fusion protein attachment protein receptor proteins (v-SNAREs). These SNARE components interact to form a 4 barrel coiled-coil structure, which makes a zipper-like interaction to reduce the distance between the plasma membrane and vesicular membrane thereby allowing the two membranes to fuse and form a fusion pore through which neurotransmitter is released into the synaptic cleft.

Furthermore, a number of studies have implicated a role for environmental toxins, including prenatal exposure to tobacco smoke and alcohol as well as and postnatal lead exposure, as significant risk factors for ADHD (Braun et al., 2006; Linnet et al., 2003). Given the evidence for both a genetic contribution from the *SNAP25* gene and an environmental contribution from prenatal nicotine in ADHD, both of these factors have been studied in this research to examine the potential effects of G × E factors and interactions in synaptic depression in a *Snap25* null mouse mutant.

Experiments with rats have shown that prenatal nicotine exposure affects nACh receptor expression and activity as well as dopamine release in the striatum relative to controls (Gold et al., 2009). Thus, one potential target of prenatal nicotine exposure could be nACh receptors in the striatum with subsequent effects on dopamine release. Several subtypes of the nAChR are expressed on striatal glutamate and dopamine terminals, as well as on MSNs and on cholinergic interneurons themselves (Quik et al., 2007). Importantly, nAChR antagonists also have been shown to block LTD induction, so nAChRs, along with D2Rs, mGluRs, and CB1Rs are necessary for LTD induction (Partridge et al., 2002). Using an adenovirus carrying a cre-inducible channelrhodopsin gene targeted to cholinergic interneurons, Cragg and colleagues (Threlfell et al., 2012) were able to demonstrate that cholinergic interneurons can directly activate dopamine release through nAChRs expressed on dopaminergic terminals. Dani and colleagues have demonstrated similar effects with nicotine (Zhang et al., 2009). Another study found that prenatally nicotine-exposed mice exhibit an upregulation of nAChR binding and

decreased dopamine efflux in the striatum compared to controls for adolescent (PN42) versus younger animals (PN10) (Gold et al., 2009). This study also found changes in cortical and thalamic responses of nAChR receptors, both of which are expressed on cortical and thalamic glutamatergic terminal inputs to the striatum, and thus could have additional affects on the LTD induction pathway in the striatum. Thus multiple studies support a role for nAChRs in modulating dopamine release, involvement in LTD both of which could be affected by prenatal nicotine exposure.

Snap25 animal models for ADHD

Animal models have been invaluable in the characterization of mechanisms that may underlie human neuropsychiatric disorders. The *coloboma* mouse mutant, heterozygous for a ~2 cM deletion of chromosome 2 (*Cm*) that encompasses the gene encoding SNAP-25, is one of several experimental constructs that meet the criteria of a valid animal model of ADHD (Fan et al., 2012; Wilson, 2000). This SNAP-25 haplodeficient mouse, which exhibits a 50% reduction of SNAP-25 expression (Hess et al., 1992), displays certain hallmarks of ADHD (Fan et al., 2012) including hyperactivity, which is ameliorated by the psychostimulant amphetamine (Hess et al., 1996), as well as inattention and impulsivity (Bruno et al., 2007). Moreover, the hyperkinesis and amphetamine responsiveness of these mutants have been shown to be mediated through D2 dopamine receptors (Fan and Hess, 2007; Fan et al., 2010). Interestingly, the robust hyperactive behavior of this mutant appears not to be recapitulated in heterozygote *Snap25* null mutants (Washbourne et al., 2002), although it was recently reported that these mice do display more subtle behavioral deficits and a susceptibility to seizures (Corradini et al., 2012). Additionally, using microdialysis to assay dopamine efflux in freely moving *coloboma* mice, Hess and colleagues have demonstrated markedly increased basal levels of extracellular dopamine in the striatum that is further increased by amphetamine administration (Fan and Hess, 2007).

Both genetic and environmental factors have been shown to contribute to the inattentive, hyperactive/impulsive, and combined subtypes of ADHD (Swanson et al., 2007; Thapar et al., 2007). Given that G × E interactions are very complex in heterogeneous human populations, an animal model based on well-defined genetics and

pharmacological exposure is proposed in this research that should provide better understanding of this interaction and the mechanisms by which it contributes to ADHD.

Snap25 and Schizophrenia

Social impairment, along with other cognitive and emotional dysfunctions, is characteristic of schizophrenia (American Psychiatric Association, DSM IV-TR, 2000). There are a range of symptoms associated with schizophrenia, as well as distinct subtypes to the disorder. Among these symptoms are multimodal hallucinations (auditory, visual, olfactory, etc.) as well as delusions including an extreme sense of being persecuted, in different degrees depending on the subtype of the disorder.

In addition to ADHD, *SNAP25* has been identified as a candidate gene for schizophrenia based upon genome wide analysis (Lewis et al., 2003). A transgenic mouse bearing a variant of the human disrupted in-schizophrenia (*DISC1)* gene encoding a truncated DISC1 protein associated with schizophrenia, also exhibit a 30% decrease in expression of SNAP-25, which may contribute to deficits in social interactions, as well as to the spontaneous hyperactivity found in these mutants (Pletnikov et al., 2008). In a *Snap25* gain of function mutant mouse, *Bdr*, proposed to model elements of schizophrenia (Jeans et al., 2007), prenatal exposure to stress not only enhances sensorimotor gating defects, but also produces deficits in social interaction and reveals depression-like behavior (Oliver and Davies, 2009). Thus, there is evidence that suggests a role for *Snap25* in mice with schizophrenia-like behaviors.

Additional background data on *Snap25* null mutant mice

Unpublished i*n vivo* microdialysis measurements of glutamate and dopamine in the striatum of heterozygous *Snap25* null mutants (*Snap25* $^{+/-}$ mice; equivalent to the HET/Sac group used in this research) performed by Dr. Ellen Hess and colleagues found that these mice had significantly increased evoked extrasynaptic dopamine release, but lower glutamate release in response to potassium-induced depolarization when compared to wild type controls (Fig. 1.6). Amphetamine also increased dopamine release in the *Snap25* null mutants relative to controls (Fan, Wilson, Hess, unpublished observations).

These findings indicate that the *Snap25* null mutants utilized in this study, exhibit *hyperdopaminergic* together with *hypoglutamatergic* transmission. The potential implications of these phenotypic differences on the results of this research are presented in the Discussion.

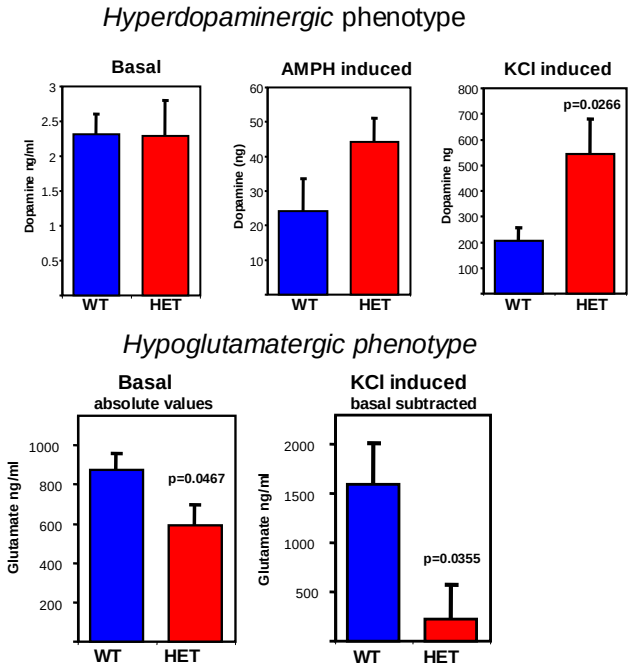

Fig. 1.6: *In vivo* microdialysis measurements show *hyperdopaminergic* and *hypoglutamatergic* phenotype of HET mice vs. controls.

Independent behavioral research was performed in parallel to this work to test for G × E interactions in behavior by using the same adolescent (PN35 – PN50) *Snap25* null mutant heterozygotes (*Snap25*$^{+/-}$) and control littermates (*Snap25*$^{+/+}$) (Washbourne et al., 2002) and the same prenatal nicotine exposure paradigm (Paz et al., 2007) as is used in this research and recently published (Baca et al., 2013). The four G × E experimental groups were assessed for spontaneous locomotor activity in a novel environment and their social interaction phenotypes were determined (Fig. 1.7A, B). For these behaviors, the mice were tested during their nocturnal active phase. Cumulative data collected for the locomotor activity over 180 minutes is shown in Fig. 1.7A. The activity of the HET/PNE group was found to be significantly greater (~1.5 – 3.5 fold) than the other groups (Fig. 1.7A) indicating increased locomotor activity among the HET mice exposed

to prenatal nicotine. Importantly, significantly increased activity of the HET control group compared to WT mice was not observed, consistent with an initial report on the behavior of these mice (Washbourne et al., 2002). However, in agreement with earlier findings (Paz et al., 2007), the PNE treatment did result in greater activity of the wild type offspring (WT/PNE group) compared to saccharine-treated wild type controls (WT/Sac group; ~2.2 fold, p <0.01). Nevertheless, the significant ~3.5 fold increase of spontaneous activity observed in HET/PNE groups compared to WT/Sac groups was more comparable to the hyperactivity of coloboma mutants discussed above, which was 3-4 fold greater compared to their control wild type littermates when tested over a similar time course (Hess et al., 1996).

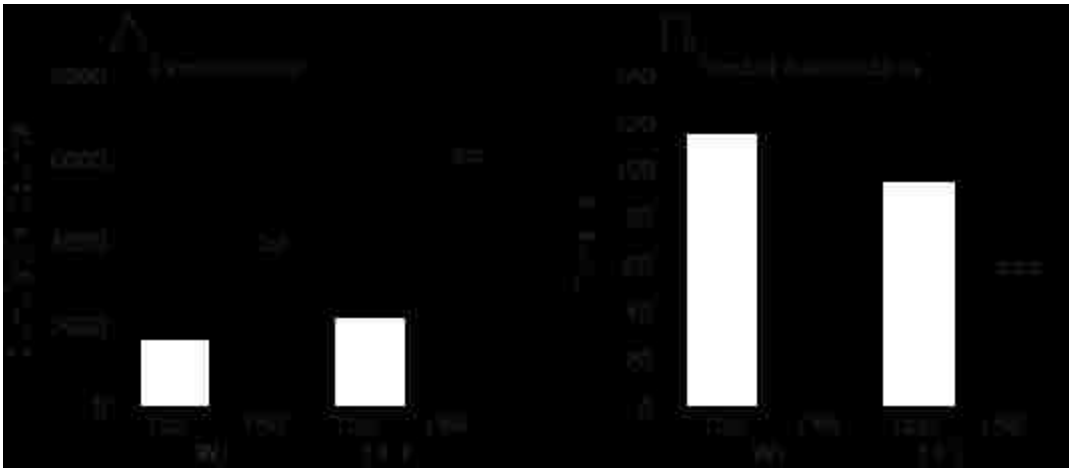

Fig. 1.7: Locomotor activity and social interaction in the four G × E groups.
A Locomotor activity of animals from the four G × E experimental groups were monitored in individual photocell activity cages. Values shown (mean ± SEM, n = 4 – 5 animals) represent beam breaks recorded over a 180 minute period. A two-way ANOVA of the data obtained from the two genotype (HET v WT) × two prenatal treatment (PNE v Sac) group comparisons revealed a significant effect of genotype ($F_{(1,14)}$ = 14.11, p < 0.01), treatment ($F_{(1,14)}$=51.76, p <0.001), as well as a significant interaction of genotype × treatment ($F_{(1,14)}$=4.70, p <0.05). Post-hoc revealed HET/PNE group had significantly greater activity than other groups (p < 0.01) and WT/PNE significantly greater than the WT/Sac control group (p < 0.01). **B** Social interaction of animals from the four G × E groups was monitored individually. Values shown (mean ± SEM, n = 7 – 8 animals) represent time spent interacting with novel mouse. A two-way ANOVA revealed a significant effect of genotype ($F_{(1,26)}$=20.80, p < 0.001), treatment ($F_{(1,26)}$=10.82, p <0.01), and a significant interaction of genotype × treatment ($F_{(1,26)}$=6.02, p <0.05). Post-hoc tests for social interaction revealed HET/PNE group interacted significantly less frequently than other groups (p < 0.001).

To examine a more complex behavior, the four groups of mice were subjected to a social interaction test in which the mice were assessed for the amount of time spent with an unfamiliar mouse of the same sex and age (Fig. 1.7B). The social interaction of the HET/PNE group was found to be significantly less (~0.3 - 0.4 fold) than the other groups (Fig. 1.7B) indicating reduced social interaction among the HET mice exposed to prenatal nicotine.

When taken together, these results provided evidence that prenatal exposure to nicotine has a pronounced effect on the behavior of *Snap25* heterozygote mutant mice that is greater than its effect on wild type littermates, consistent with the idea that a SNAP-25 deficiency during brain development confers a vulnerability to the behavioral consequences of *in utero* nicotine exposure. In this study, I followed up on these behavioral findings by investigating the cellular and molecular mechanisms that underlie long-term synaptic plasticity.

This chapter has provided an overview of basal ganglia function; striatal LTD induction; a potential relationship between striatal LTD and behavior; some examples of the interaction of gene-environmental interactions and neuropsychiatric disorders; evidence that *Snap25* deficiency and prenatal nicotine exposure are factors in ADHD and schizophrenia; and finally the use of animal models to shown how these genetic and environmental factors may be involved in the etiology of these disorders. The hypothesis of this research is that gene-environmental factors and interactions deriving from *Snap25* deficiency and prenatal nicotine exposure lead to long term impairments in D2 receptor functionality in striatal MSNs. I show that this occurs by impairments of D2 receptor affinity and possibly receptor-effector coupling leading to functional impairments of the process of striatal LTD induction. The methods used and results of electrophysiology and binding studies which support this hypothesis as well as a discussion of the implications of these results are presented in the chapters that follow.

Chapter 2 – Hypothesis and Specific Aims

Genes and environmental conditions interact in the development of cognitive capacities so both would be expected to play a role in neuropsychiatric disorders. As outlined in the Introduction, the gene for the SNARE protein, SNAP-25, has been identified as one of the candidate susceptibility genes for ADHD as well as for schizophrenia (Faraone and Mick, 2010). Similarly, the environmental risk factor of maternal smoking has been associated with ADHD (Linnet et al., 2003). Deficits in the striatum have been implicated in ADHD, and models have been proposed to account for changes in attention, motor functions, and behavior due to alterations in the striatum and specific genes are implicated in some of these (Swanson et al., 2007). This study aims to determine how genetic contributions from a *Snap25* haplodeficient mouse model together with prenatal nicotine exposure may together alter specific receptor affinity and signaling in dopaminergic D2 receptors (D2Rs) as well as synaptic long-term depression (LTD), which is in part dependent on these receptors. The linkage of *Snap25* haplodeficiency has to ADHD has been studied extensively in the well established *coloboma* mouse model of ADHD, which includes *Snap25* haplodeficiency, by Michael Wilson, Ellen Hess and other researchers, which provide a foundation for further studies (Fan et al., 2012). Thus, this interaction of genetic and environment factors should provide insight into mechanisms contributing to cognitive disorders such as ADHD and schizophrenia. The study also presents a general set of experimental procedures by which potential gene-environmental interactions can be explored to determine if they alter receptor function and/or synaptic plasticity in specific brain regions.

The induction of LTD was characterized in the striatum as early as 1992 using high frequency stimulus (HFS) paradigms, based on both extracellular (field potential) and intracellular (voltage-clamp) techniques (Calabresi et al., 1992). These initial experiments found that a 100 Hz HFS paradigm as described below was capable of inducing LTD using both recording techniques. Furthermore, the use of D2R antagonists implicated a role for dopaminergic D2Rs during the induction paradigm. Subsequent work has identified several other receptors including the pre-synaptic CB1 receptors as also necessary for LTD induction (Surmeier et al., 2007). Since both the D2 and CB1

receptors have been established as important elements in LTD induction, these two receptor types were chosen as important candidates to probe the G × E factors and interactions involved in LTD induction. An additional basis for examining D2Rs was that a preliminary microdialysis study identified *Snap25* haplodeficient mice as *hypoglutaminergic* and *hyperdopaminergic* as discussed in the Introduction, suggesting that the normal glutamatergic and dopaminergic interactions found in LTD may have been affected by the *Snap25* gene.

Experiments in all specific aims utilized a 2 × 2 design, which was developed to evaluate the factors and interactions of genotype and environment on cortico-striatal signaling. *Snap25* heterozygote knockout male mice (HET) (Washbourne et al., 2002) were bred with wild type C57BL/6J female mice (WT) under either saccharine or prenatal nicotine (PNE) bottle-fed conditions during pregnancy according to standard protocols to produce four G × E experimental groups of mice representing genotype (HET) × environmental (PNE) interactions designated as: WT/Sac, WT/PNE, HET/Sac and HET/PNE. Wild type (WT) and heterozygous (HET) offspring were evaluated between 35-50 days of age (average ~PN 40 for each group) to model an adolescent stage of brain maturation.

The following hypothesis and specific aims are proposed:

Hypothesis: **Gene-environment factors and interactions in *Snap25* deficiency and prenatal nicotine exposure lead to long-term impairments in D2 receptor affinity in striatal medium spiny neurons resulting in impairments of the process of striatal LTD induction.**

Aim 1-To characterize gene-environment factors and interactions in long-term synaptic depression using a high frequency stimulus (HFS) LTD induction paradigm.

The effect of G × E factors and interactions in a *Snap25* haplodeficient mouse model was measured in the four G × E experimental groups. A high frequency stimulus (HFS) paradigm in the dorsal striatum is used to induce long-term (LTD) or short-term (STD) depression as has been previously reported (Lovinger et al., 1993). The D2

receptor (D2R) antagonist, sulpiride, and the CB1 receptor (CB1R) antagonist, AM251, was used to pharmacologically isolate the neurotransmitter systems involved in the G × E factors and interactions, since each of these neurotransmitter systems has been shown to be essential for the induction of LTD in the cortico-striatal pathway (Surmeier et al., 2007). Each set of experiments also used paired pulses separated by a 50 ms interpulse interval (IPI) to assess changes in the paired pulse ratio (PPR) during induction of LTD or STD as well as in the presence of a D2R or CB1R antagonist.

1a- Characterize G × E factors and interactions in synaptic depression (LTD and STD) in the four G × E groups. The effect of G × E factors and interactions on synaptic plasticity was determined using cluster analysis followed by two-way ANOVA to determine STD or LTD induction. Each set of experiments also used paired pulses at a 50 ms IPI to assess changes in paired pulse ratio (PPR) during induction of LTD or STD.

1b- Characterize the effect of D2R antagonists in long-term synaptic depression in the four G × E groups. These experiments used the same protocol as 1a above, except that slices were pre-incubated for ~20 minutes in the D2R antagonist, 10 μM sulpiride, prior to the start of the experiment and sulpiride will be continually perfused in the bath during the experiment. It was important to assess antagonism of D2Rs because D2R activation has been demonstrated to be crucial for induction of LTD in the striatum (Calabresi et al., 1992; Surmeier et al., 2007), and because preliminary *in vivo* microdialysis data of HET/Sac mice showed that they were *hyperdopaminergic*, which suggests that the dopamine system is affected by the *Snap25* heterozygote condition. Each set of experiments used paired pulses at a 50 ms IPI to assess changes in paired pulse ratio (PPR) during induction of LTD or STD in the presence of the D2R antagonist.

1c- Characterize the effect of CB1R antagonists in long-term synaptic expression in the four G × E groups. These experiments used the same protocol as 1a above, except that slices were preincubated for ~20 minutes in the CB1R antagonist, 2 μM AM251, prior to the start of the experiment and AM251 will be continually perfused

in the bath during the experiment. It was important to assess antagonism of CB1Rs because CB1Rs have been implicated as crucial for induction of LTD in the striatum (Surmeier et al., 2007). Each set of experiments also used paired pulses at a 50 ms IPI to assess changes in paired pulse ratio (PPR) during induction of LTD or STD in the presence of the CB1R antagonist.

Aim 2-To characterize gene-environmental factors and interactions in striatal D2Rs using a dopamine agonist-stimulated [^{35}S]-GTP-γ-S binding assay to quantify changes in D2R affinity, receptor coupling and number of receptors.

An agonist-stimulated [^{35}S]-GTPγS binding assay was used to characterize changes of the binding kinetics of D2Rs in the dorsal striatum in the four G × E experimental groups. The method targets D2R G-protein coupled receptors (GPCRs) and detects effects due to changes in affinity and/or receptor-effector coupling (Sovago et al., 2001).

2a- Determine approximate EC_{50} and EC_{100} values using a dopamine agonist stimulated [^{35}S]-GTP-γ-S binding assay. Initial experiments were performed in WT/Sac controls to determine approximate EC_{50} and EC_{100} values in order to calibrate experiments performed on all four G × E groups.

2b- Characterize D2R changes produced by G × E factors and interactions using a dopamine agonist stimulated [^{35}S]-GTP-γ-S binding assay. These experiments utilized previously determined EC_{50} and EC_{100} values (Aim 2a) in experiments to compare agonist binding under each of the conditions. The [^{35}S]-GTP-γ-S binding assay is an indirect method in that it measures dopamine agonist stimulated GTP binding, so it does not distinguish between agonist binding of GPCRs and effects due to coupling of Gα proteins and downstream effectors.

Aim 3- To characterize* G × E *factors and interactions in striatal D2Rs using a [^{3}H]-quinpiriole dopamine agonist radioligand saturation binding assay to further quantify changes in D2R affinity and number of receptors .

As a follow up to Aim 2, a [^{3}H]-quinpirole dopamine agonist radioligand saturation binding assay and Scatchard analysis was used to determine if D2R affinity (K_d) and maximum binding (B_{max}) in the dorsal striatum are affected by G × E interactions. These experiments were carried out with striatal brain homogenates (Levant et al., 1992) using comparable sets of mice as described in Aims 1 and 2.

3a- Use saturation binding assays to determine the range of [^{3}H]-quinpirole dopamine agonist levels and verify the efficacy of the antagonist. These preliminary experiments were carried out in WT/Sac controls to determine the proper ranges of D2R agonists and appropriate concentrations of the D2R antagonist for the saturation experiments.

3b- Determine changes in affinity and maximum binding produced by G × E factors and interactions using a [^{3}H]-quinpirole dopamine agonist radioligand saturation binding assay. Based on preliminary values determined in aim 3a, these experiments were used to determine if changes in D2R affinity (K_d) and maximum binding (B_{max}) in the dorsal striatum are affected by G × E factors. These experiments were carried out in striatal brain homogenates and used Scatchard analysis of the resulting saturation binding assays of the four G × E groups to determine K_d and the B_{max} values.

Chapter 3- Methods

The majority of the methods corresponding to the mouse breeding, electrophysiology and binding studies are found in our recent publication (Baca et al., 2013).

Mouse breeding and experimental design

All experiments were approved by the University of New Mexico Health Sciences Center Laboratory Animal Care and Use Committees and the National Institutes of Health. Mice used for all experiments were maintained in a 12 hour reverse light/dark cycle; lights on at 8PM and lights off at 8AM.

A 2 × 2 design was developed to evaluate the interactions of genotype and environment on cortico-striatal signaling and this design was used in all specific aims. *Snap25* heterozygote knockout male mice (HET) (Washbourne et al., 2002) were bred with wild type C57BL/6J female mice (WT) under either saccharine bottle fed conditions or prenatal nicotine exposure (PNE) bottle fed conditions during pregnancy according to standard protocols (Paz et al., 2007) This design produced four experimental groups of mice representing genotype (HET) × environmental (PNE) factors and interactions designated as: WT/Sac, WT/PNE, HET/Sac and HET/PNE as illustrated in Fig. 3.1.

Wild type (WT) and heterozygous (HET) offspring were evaluated between 35-50 days of age (average ~PN 40 for each group, shown in Table 3.1) to model an adolescent stage of brain maturation. No significant differences were found among the different groups in weights of the mice at PN40.

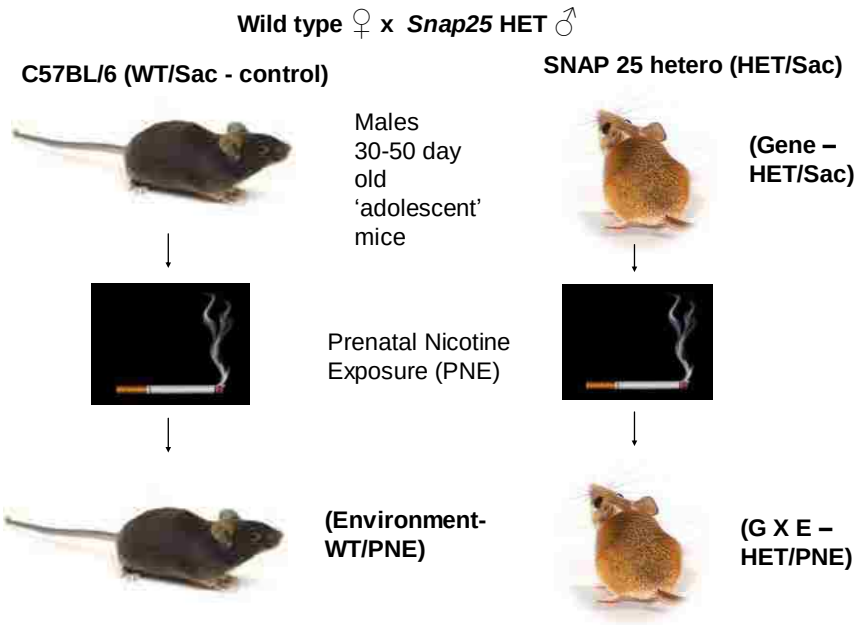

Fig. 3.1: Experimental paradigm used to generate G × E groups in all experiments.

Group	Age (PN day)		Weight (g)	
	Male	Female	Male	Female
WT/Sac	40.2 ± 0.7	37.8 ± 0.4	20.5 ± 0.3	17.0 ± 0.3
WT/PNE	38.8 ± 0.6	39.1 ± 0.4	20.8 ± 0.3	18.2 ± 0.5
HET/Sac	39.6 ± 1.0	38.0 ± 0.4	19.9 ± 0.4	16.5 ± 0.3
HET/PNE	39.8 ± 0.5	39.5 ± 0.6	20.6 ± 0.3	17.1 ± 0.3

Table 3.1: Average age and weight of mice used in all experiments.
Males were used in electrophysiology and binding studies (n=24- 31 animals). Females were used in addition to males (n=10 animals) only for [^{3}H]-Quinpirole D2R agonist saturation binding experiments. Values shown are mean ± SEM. No significant differences were found between ages used or weights of mice in any of the experiments.

***Snap25* heterozygote mice**

Heterozygous *Snap25* deficient mice (referred to as HET/Sac or HET/PNE groups depending on whether they were provided with drinking water containing saccharine or nicotine as described below) (Washbourne et al., 2002) were maintained by brother/sister heterozygote matings for 7 backcrossed generations to C57Bl/6 mice at the UNM HSC Animal Resource Facility. The heterozygous *Snap25* deficient mice, also referred to as *Snap25* haplodeficient mice are equipped with one wild type Snap25 gene and one null Snap25 gene. SNAP-25 coding sequence was disrupted in the target construct by replacing exon 5a and 5b with a PGK-neo gene cassette (Washbourne et al., 2002) to generate the disrupted *Snap25* gene as shown in Fig. 3.2. Genotyping was performed by PCR as described previously (Washbourne et al., 2002) by tail clips taken after brains were removed for electrophysiology and binding experiments as described below.

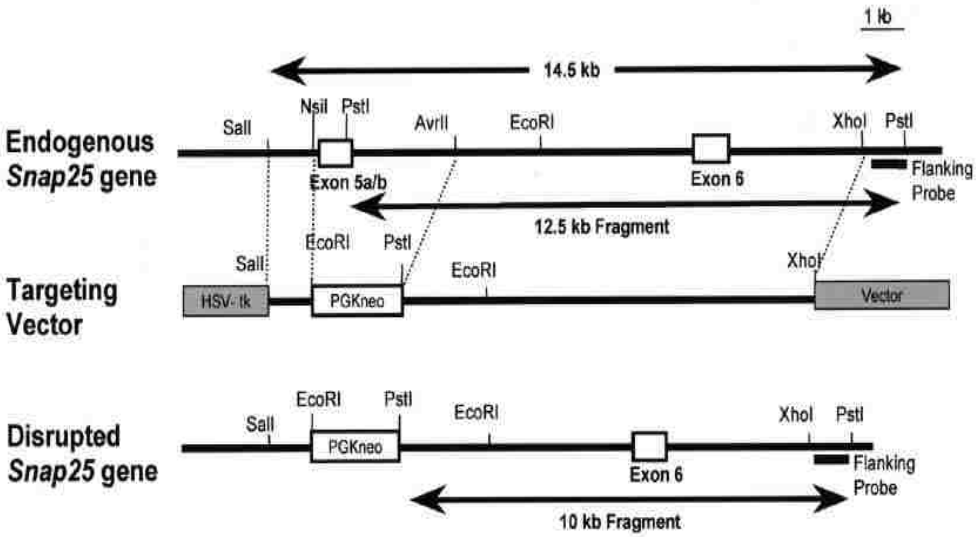

Fig. 3.2: *Snap25* heterozygotes generated by knockout of Exon 5a/5b (Washbourne et al., 2002).

Prenatal nicotine exposure

Mice were exposed prenatally to nicotine via drinking water as previously described (Paz et al., 2007). In this paradigm, breeding pairs were provided either with drinking water containing nicotine and saccharine (0.05 mg/ml and 0.6 mg/ml, respectively; PNE) or saccharine alone (Sac) *ad libitum* prior to and throughout gestation. To avoid potential effects due to an interaction between nicotine and a SNAP-25

deficient intrauterine environment, wild type females and heterozygote *Snap25* null males were used as breeding pairs. The prenatal nicotine exposed (PNE) dams were provided with 0.05 mg/ml nicotine and saccharine two weeks prior to pregnancy, during pregnancy, while the saccharine control dams were provided with saccharine during the same period (Paz et al., 2007). This nicotine dose corresponds to ~20 ng/ml in blood plasma or approximately levels equivalent in humans to ~1 pack/day. Following birth, the nicotine/saccharine content of the drinking water was gradually tapered down over one week to standard drinking water to limit any possible effects on perinatal brain development.

Slice preparation for electrophysiology

Electrophysiology experiments were performed in coronal striatal slices prepared from 35-50 day old male mice using standard techniques (Schiess et al., 2006). Briefly, animals were deeply anaesthetized by I.P. injection of 250 mg kg^{-1} ketamine, brains were rapidly removed, and slices cut at 300 μm with a vibroslicer (Pelco 101, St Louis, MO, USA) in an ice bath with a cutting solution containing (mM): 220 sucrose, 3 KCl, 1.2 NaH_2PO_4, 26 $NaHCO_3$, 12 $MgSO_4$, 0.2 $CaCl_2$, 10 glucose and 0.01 mg ml^{-1} ketamine equilibrated with 95%O_2–5%CO_2. Slices were then transferred to artificial cerebrospinal fluid (ACSF) containing (mM): 126 NaCl, 3 KCl, 1.25 NaH_2PO_4, 1 $MgSO_4$, 26 $NaHCO_3$, 2 $CaCl_2$ and 10 glucose equilibrated with 95%O_2–5%CO_2 at 30 °C for 1 h and then maintained at room temperature until recording in a constant flow chamber (Warner Instruments, Hamden, CT, USA or Scientific Systems Design, Mercerville, NJ, USA) maintained at 32 °C and continuously perfused at 2 ml min^{-1} with ACSF saturated with 95%O_2–5%CO_2.

Population spike recordings

Standard electrophysiological techniques were used for field potential (fEPSP) population spike (PS) recordings (Schiess et al., 2006) in the dorsal striatum (approximately 0.5-1.0 mm from the corpus callosum (CC) border) following stimulation of cortical layer V afferents (Fig. 3.3). The resulting PSs represent predominately activity of medium spiny neurons (MSNs) (Surmeier et al., 1996). fEPSPs were recorded

with an Axoclamp 2B (Molecular Devices, Sunnyvale, CA), amplifier and a Digidata 1322A interface using pCLAMP 9.2 software (Molecular Devices) for experimental control and data analysis. Recordings were digitized at 500 kHz and filtered at 2 kHz.

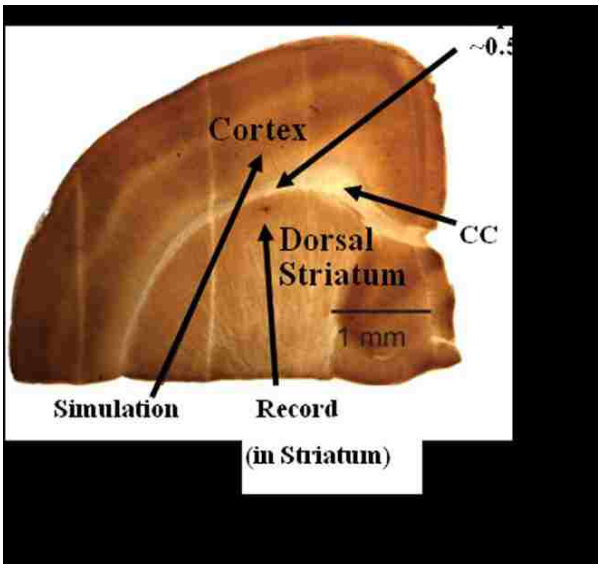

Fig. 3.3: Illustration of stimulation and recording of population spikes of MSNs in the dorsal striatum.

PS amplitudes were calculated by subtracting the average of the peak of the two positive phases (RP1 and RP2) of the fEPSP from the maximum intervening negative spike as shown in the example population spike on the left side of Fig. 3.5. Paired pre-synaptic constant current pulses (150 μs duration) with a 50 ms interpulse interval were applied at 20 second intervals with an Iso-Flex constant current stimulator (API Instruments, Jerusalem, Israel) through a concentric bipolar electrode (FHC, Bowdoinham, ME, USA). Test (~1/2 maximum) or HFS (~maximum) stimulus intensities were determined from an input-output curve. An example input-output curve showing the amplitude of the PS plotted as a function of the stimulus current amplitude is shown in Fig. 3.4.

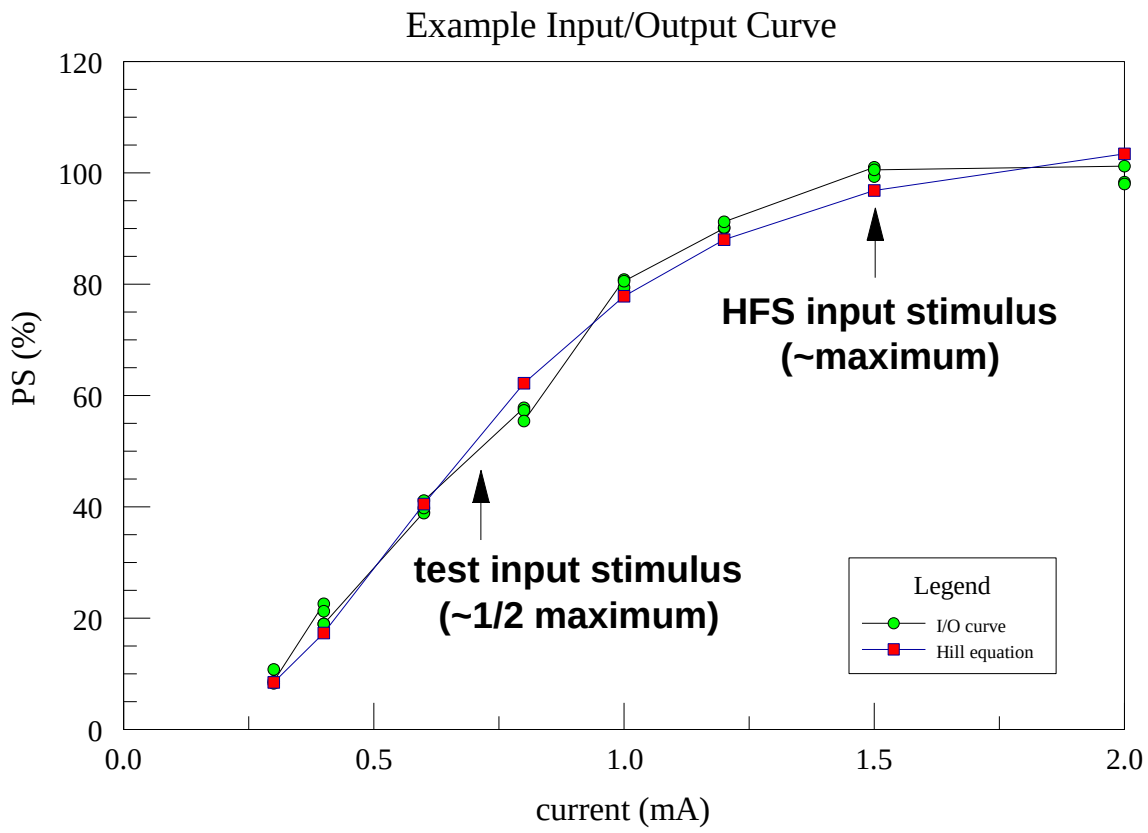

Fig. 3.4: Example input-output curve used to determine current inputs associated with half maximum and maximum population spike amplitudes.

To assess long-term synaptic plasticity in the cortico-striatal field, a 10 minute baseline was established at ½ maximum (test) stimulus intensity, then a high frequency (HFS) paradigm consisting of 4 sets of 1 s 100 Hz pulses at the maximum intensity was applied, and finally 30 minutes of recordings were obtained again at ½ maximum stimulus intensity to determine the time course of the effect of the HFS. The efficacy of alternative paradigms on their ability to induce long-term plasticity is discussed in Appendix 2. The average amplitude of the final 10 PSs of the 30 minute recovery period following the HFS (results- R) was compared to the average amplitude of 32 PSs during the 10 minute pre-HFS baseline (B) in order to determine the percentage of change relative to the baseline (R/B). Fig. 3.5 shows that for a given experiment, immediately following HFS, the PS amplitude typically decreased to ~20% of the baseline amplitude. During the subsequent 30 minute recovery period, the PS either returned substantially back to baseline (designated as short-term depression (STD)) or remained attenuated

(designated as long-term depression (LTD)) as illustrated in Fig. 3.5. Cluster analysis, as described below, was used to designate which results were classified as STD or LTD. Cluster analysis also provided the mean and standard error of the mean for the 30 minute recovery values of the PS amplitude as a function of the baseline levels for the STD, LTD, and total clusters.

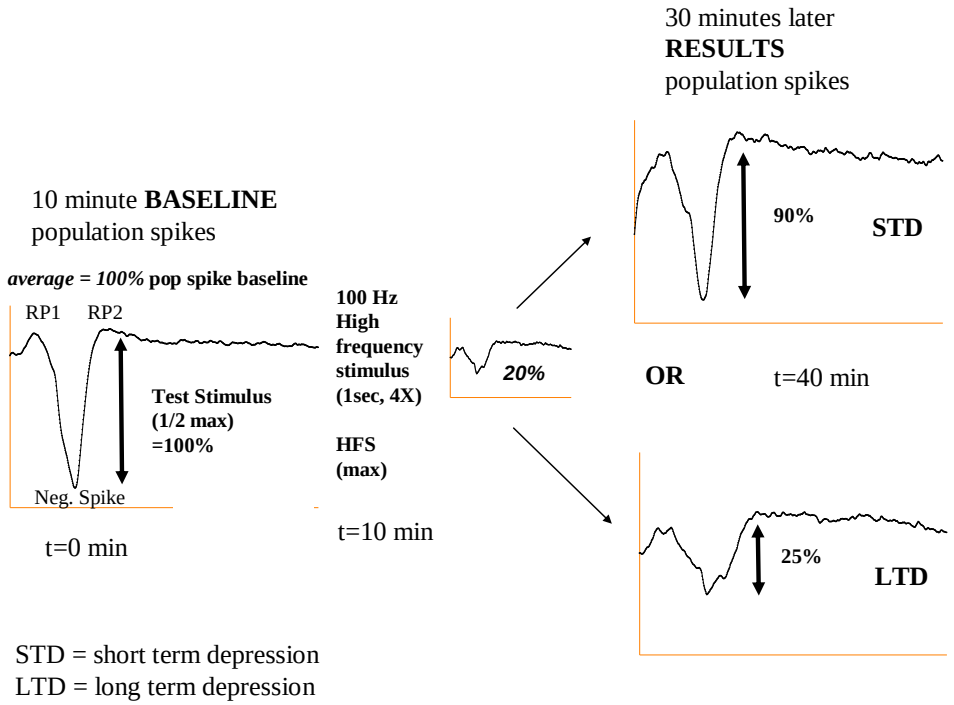

Fig. 3.5: Illustration of the HFS paradigm used in electrophysiology recordings and distinction between STD and LTD as determined by cluster analysis.

As described above, each electrophysiology experiment involved recordings of PSs in response to paired pulses at 50 ms interpulse interval recorded during the baseline (B), HFS, and during the results (R) following HFS. This allowed a comparison of the paired pulse ratio (PPR) calculated as the ratio of the second population spike (R2) amplitude to the first population spike (R1) amplitude. When the R2 PS amplitude is greater than the R1 PS amplitude this is designated as paired pulse facilitation (PPF). When the R2 PS amplitude is less than the R1 PS amplitude, this is designated as paired pulse depression (PPD). Example population spikes showing PPF and PPD are shown in Fig. 3.6. Because the PPR has been used as a measure of the probability of pre-synaptic

release, these measurements provide potentially useful information about pre-synaptic effects of the HFS protocol.

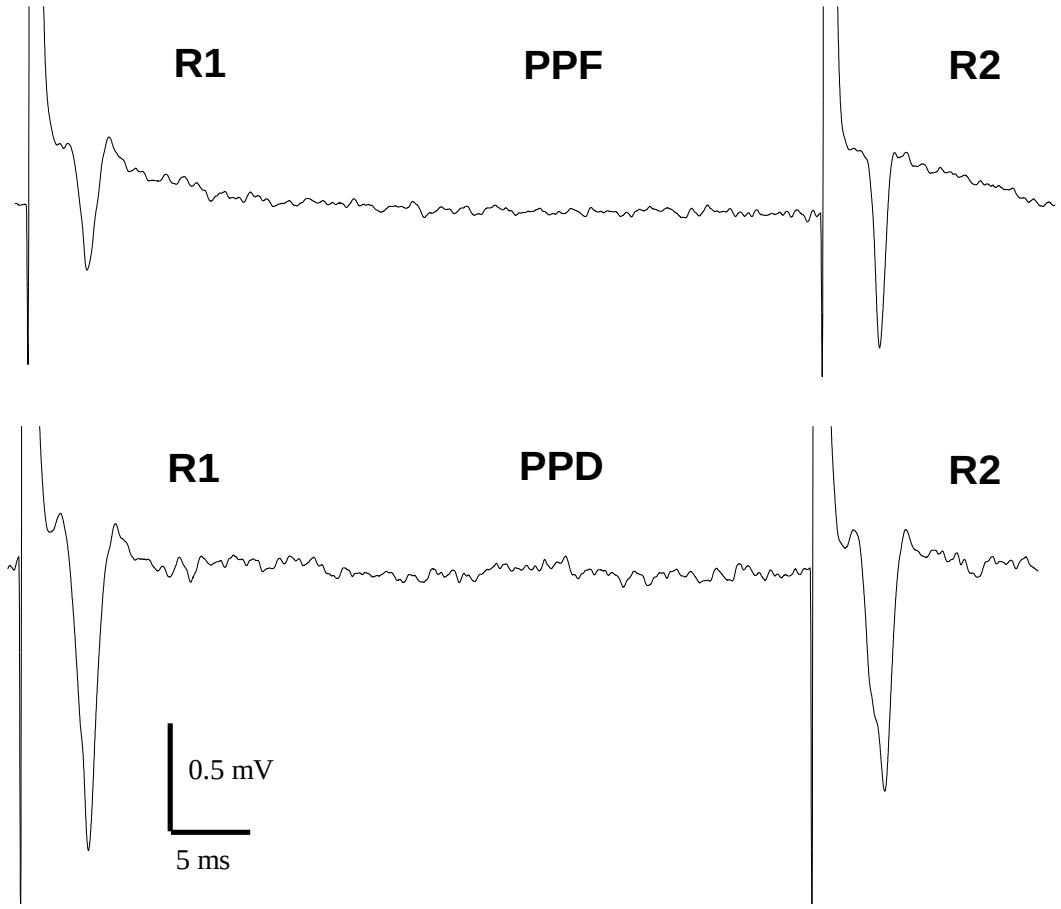

Fig. 3.6: Example of 50 ms interpulse interval recordings showing PPF (top) and PPD (bottom).

For each of the four experimental groups, receptor antagonist experiments were carried out in which the D2 receptor antagonist 10 μM sulpiride or the CB1 receptor antagonist 2 μM AM251 were added to the ACSF bath in order to examine the contribution these receptors to the establishment or maintenance of long-term synaptic depression. Slices were pretreated in the drug for 20 minutes prior to the start of each experiment and for the duration of each experiment. Other than the addition of receptor antagonists, the same field recordings and HFS paradigm were used for each experimental group as the experiments without receptor antagonists. A minimum of 6 slices was recorded in the experiment for each condition both for drug and non-drug perfused experiments.

The time course of recovery was determined for the STD populations, as well as for experiments in the presence of a CB1R and D2R antagonists for all experimental groups. First, from the average values of each set of experiments, an exponential least squares regression fit was made from the initial ~20% depression of the PS to the final value of the PS after 30 minutes. The data were then fit with a least squares regression to the equation:

Where: Y = value of the PS as a percentage of the baseline PS (normalized to 100%); B = initial value of PS after HFS; A= final value of PS 30 minutes after HFS; t = time (minutes); τ = time constant representing time necessary to decay to 1/e of final value of PS

This equation models an exponential decay to a final recovered value following HFS. The time constant (τ) measures the relative rate of recovery in minutes for STD, allowing comparison of recovery rates among the experimental groups. After fitting, the data were inverted by subtracting the final estimated value A (estimated recovery after 30 minutes) from each point so that the initial PS following HFS becomes the largest value and the final value after 30 minutes becomes the smallest. Finally the y axis representing the inverse of the PS value (recovery - PS) at each time point is plotted in a logarithmic scale to display regression plots as linear where the time constant is now -1/slope of each curve.

Dopamine agonist stimulated [^{35}S]-GTP-γ-S binding assay

[^{35}S]-GTP-γ-S binding assays were conducted by a method described previously (Martinez et al., 2008). Brains were removed from 35-50 day old male mice from each of the four experimental groups and immediately immersed in isopentane at -35 °C, chilled in a dry ice/methanol bath and then stored in airtight containers at −80 °C until sectioning. Coronal sections (10 μm) that included the striatum (approximately from Bregma 0.98 to -0.94) were cut and the level of sectioning in each plane was verified by

examination of Nissl-stained sections. Sections were thaw-mounted onto pre-cleaned Superfrost- Plus® microscope slides (VWR Scientific, West Chester, PA) and stored at −80 °C in airtight containers until assays were performed.

Slides were pre-incubated in assay buffer (50 mM Tris-HCl, 100 mM NaCl, 5 mM $MgCl_2$, pH 7.4 at 25 °C) containing 1 mM DL dithiothreitol, 0.2 mM EGTA and 2 mM GDP at 25 °C for 10 min. Sections were then incubated with 100 pM [^{35}S]-GTPγS (specific activity = 1250 Ci/mmole; Perkin Elmer Life Sciences, Boston, MA) for 90 minutes in the absence or presence of 10 μM unlabeled GTPγS and D2R agonist, quinelorane. After incubation, sections were rinsed twice for 15 seconds each in fresh incubation buffer at 4 °C, dipped for one second in 4 °C distilled water, dried under a stream of cool air, and then vacuum desiccated overnight. Autoradiograms (Biomax MR Film) were produced with a set of ^{14}C standards following a 4 day exposure. Microdensitometry of ligand binding in the striatum was performed using Media Cybernetics Image Pro Plus® (Silver Spring, MD) on an Olympus BH-2 microscope at a total image magnification of 3.125×. In each assay, an optical density standard curve, expressed in picoCuries/10^5 μm^2, was established based on the autoradiograms of the standards.

The approximate EC_{50} determined for quinelorane-stimulated [^{35}S]-GTPγS binding was 20 μM and the EC_{100} was 200 μM based upon preliminary experiments carried out across a range of agonist values in WT/Sac control mice as presented in the Results. As a control, 50 μM sulpiride was used as an antagonist to a 100 μM quinelorane concentration and found to fully block the response as described in the Results.

Total [^{35}S]-GTPγS binding in the left and right paired sections from each brain region of interest was measured in quadruplicate sections incubated with varying levels of quinelorane. Non-specific [^{35}S]-GTPγS binding was measured in duplicate sections incubated with the addition of 10 μM excess unlabeled GTPγS with varying levels of quinelorane. Total binding and non-specific binding were both determined by subtracting the background binding from each autoradiogram. The specific binding was then determined by subtracting total binding (average of quadruplicate sections for each n) from non-specific binding (average of duplicate sections for each n). This is illustrated in

Fig 3.7, which shows an example of total binding in an autoradiogram of a coronal slice in the presence of a saturating concentration of agonist. Not shown is an autoradiograph of a non-specific binding slice, which is subtracted from total binding to determine specific binding.

The preliminary results for WT/Sac controls were fitted to a Hill equation (Goutelle et al., 2008; Heck, 1971) as shown below to obtain the dissociation constant K_d associated with the EC_{50} agonist binding levels for a half maximum response to the agonist. The dissociation constant K_d was used to calibrate the EC_{50} agonist level selected for the experiment. Values close to maximum responses in the preliminary experiments were used to calibrate the EC_{100} agonist level selected for the experiment.

Hill Equation:

Where: [B] = concentration of ligand (agonist) bound to the receptor (µM); [L] = concentration of free ligand (agonist) (µM); B_{max} = maximum response to agonist (femtomoles/ 10^5 μm^2); K_d = dissociation constant (µM), n = Hill coefficient

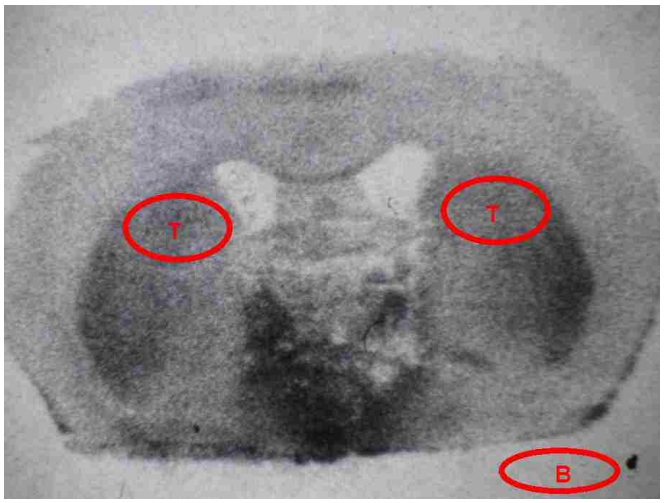

Specific binding = (total binding – non specific binding)

total - background non-spec - background

Fig. 3.7: Example autoradiogram of a coronal striatal brain slice illustrating how specific binding levels are calculated. Averages of total binding (in quadruplicate sections) with background binding subtracted (shown) are subtracted from averages of non-specific binding slices (in duplicate sections) with background binding subtracted (non-shown).

Quinelorane-stimulated [^{35}S]-GTPγS binding was measured to compare basal binding (without quinelorane), and net binding for both the EC_{50} (20 μM) and EC_{100} (200 μM) quinelorane concentrations as determined by preliminary experiments with WT/Sac controls. The net binding was determined by subtracting the basal binding values from the EC_{50} (20 μM) and EC_{100} (200 μM) binding values to obtain net binding values for the EC_{50} (20 μM) and EC_{100} (200 μM) quinelorane concentrations. The use of net binding permitted quantification of quinelorane binding at each agonist concentration (EC_{50} and EC_{100}) in order to determine the differential effects of the agonist-stimulated responses on GTP binding. Each n for each experimental group included quadruplicate coronal sections each for basal, EC_{50}, and EC_{100} quinelorane levels as well as duplicate coronal sections for non-specific binding including 10 μM unlabeled GTPγS. A total of n = 6 was used for each experimental group.

[^{3}H]-Quinpirole dopamine agonist radioligand saturation binding assay

Saturation binding assays were conducted by methods described previously (Levant et al., 1992). Brains were removed from 35 – 50 day old mice and immediately immersed in isopentane at -35 °C, chilled in a dry ice/methanol bath and then stored in airtight containers at -80 °C until homogenation. Each brain homogenate consisted of 4 total brains (2 male and 2 female) in order to obtain sufficient tissue. Brain tissue was homogenized in 20 volumes of assay buffer (50 mM Tris-HCl, 5 mM KCl, 2 mM $MgCl_2$, and 2 mM $CaCl_2$, pH 7.4) at 23 °C using fitted spherical glass homogenizers. The crude homogenate was centrifuged twice for 30 and 15 minutes respectively at 13,000 × g, to yield a final tissue concentration of 1.5 - 2.5 mg per ml buffer. Brain protein levels were quantified by Bradford assays and refrozen until binding assays were performed.

Saturation binding assays were performed in triplicate polystyrene tubes in a final volume of 0.3 ml of assay buffer as described (Levant et al., 1992). The dopamine agonist, [^{3}H]-quinpirole, was included at 6 concentrations ~0.2 nM to ~9 nM as determined from preliminary binding studies as presented in the Results (Levant et al., 1992). Binding was initiated by the addition of membrane homogenate at room temperature and maintained for 5 hours to allow saturation to occur. Non-specific binding was defined in the presence of 50 μM spiperone. The reaction was terminated by

the separation of the free from bound radioligand by rapid filtration over Whatman GF/B filters using a Brandel cell harvester. Filters were washed twice with 3 ml of ice-cold 50 mM tris-HCl, pH 8.0 and punched into mini-vials. After the addition of the scintillation cocktail (Packard Ultima Gold), vials were shaken, allowed to equilibrate for at least 5 hours, and counted in a Packard model 2000 liquid scintillation counter. K_d and B_{max} were determined for [^{3}H]-quinpirole from least squares fits to Scatchard plots of triplicate samples using data from the specific and non-specific binding from 5 samples (brain homogenates) of the four experimental groups as presented in the Results as well as Appendix 1.

Drugs

The following drugs were stored frozen in aliquots and diluted to the appropriate concentration in ACSF for electrophysiology or pharmacological assay on the day of the experiment. S-sulpiride, AM251, quinelorane, dithiothreitol and spiperone were obtained from Tocris (Ellisville, MO, USA); GDP and GTPγS from Sigma-Aldrich (St Louis, MO, USA); [^{35}S]-GTPγS and [^{3}H]-quinpirole from Perkin-Elmer (Waltham, MA, USA). Aliquots of S-sulpiride were made in DMSO as required.

Data analysis

SPSS 16.0 (SPSS, Inc., Chicago, IL) was used for statistical analysis of data. Numerical values for data measurements are expressed as the mean ± standard error unless otherwise specified. Statistical *p* values were represented as follows: * $p < 0.05$; ** $p < 0.01$ and *** $p<0.001$. The paradigm used for the electrophysiology and binding experiments was designed as a 2 × 2 analysis to compare effects of genotype and environment. Comparisons were made with a two-way ANOVA two genotype (HET v WT) × two prenatal treatment (PNE v Sac) groups and all post-hoc tests were Tukey's HSD unless otherwise noted.

A two-step cluster analysis with no pre-determined number of clusters (SPSS 16.0) was used to group the field potential experiments into STD and LTD clusters for each experimental group (Fig. 3.5). The two-step cluster analysis utilizes a Student's t-test with a Bonferroni adjustment applied to statistically discriminate clusters. An

example of the cluster analysis is shown in the Results. This analysis seeks to identify clusters within a data set that minimize within-group variation and maximize between-group variation. The result of the cluster analysis is the identification of either a single cluster or several (2 or more) clusters within the data set as well as the mean and standard deviation for each identified cluster.

Chapter 4 - Results

Overall hypothesis and approach

To reiterate, the hypothesis of this research is that G × E factors and interactions from the *Snap25* haplodeficiency and prenatal nicotine exposure lead to long term impairments in D2 receptor functionality in striatal medium spiny neurons. This occurs as a result of impairments of D2 receptor affinity and signaling leading to impairments of the process of striatal LTD induction. *Snap25* heterozygote knockout male mice (HET) were bred with wild type C57BL/6J female mice (WT) under either saccharine or prenatal nicotine exposure (PNE) bottle fed conditions during pregnancy to produce four experimental groups of mice representing genotype (HET) × environmental (PNE) interactions designated as: WT/Sac, WT/PNE, HET/Sac and HET/PNE as further described in the Methods. Changes in synaptic plasticity were explored by comparing the induction of LTD in these four G × E experimental groups as described below. The results related both to the electrophysiology and binding studies presented here have been recently published (Baca et al., 2013). All methods used including the statistics described below for cluster analysis, ANOVA, and post-hoc tests, unless noted otherwise, are presented in the Methods. The results of this research are presented in order of the specific aims as outlined in the Hypothesis chapter:

Aim 1-To characterize G × E *factors and interactions in long-term synaptic depression using a high frequency stimulus (HFS) LTD induction paradigm.*

Aim 2-To characterize G × E *factors and interactions in striatal D2Rs using a dopamine agonist-stimulated [^{35}S]-GTP-γ-S binding assay.*

Aim 3- To characterize G × E *factors and interactions in striatal D2Rs using a [^{3}H]-quinpirole dopamine agonist radioligand saturation binding assay.*

D2R-dependent induction of long-term synaptic depression (LTD) in the striatum is affected by HET genotype and PNE treatment and their interactions

To characterize use-dependent plasticity in these preparations, I used a high frequency stimulus (HFS) paradigm to elicit synaptic depression of cortical inputs to the dorsal striatum in coronal slices of the WT/Sac control group (Calabresi et al., 1992; Lovinger et al., 1993). This paradigm was selected because it is the most common paradigm used in the literature to elucidate the mechanisms involved in the induction of LTD thereby allowing the results to be compared with a body of existing literature (Kreitzer and Malenka, 2008; Lovinger, 2010; Surmeier et al., 2007). A series of preliminary experiments independent of this research were performed to explore how different frequency paradigms may affect the induction of LTD. A summary of these results are presented in Appendix 2. As described in more detail in the Methods, for each slice I determined the input stimulus intensity necessary to produce a half maximum amplitude PS for use during baseline and recovery periods and maximum amplitude PS for the HFS induction protocol. The amplitude of the PS 30 minutes after HFS was then compared to the average amplitude during the 10 minute baseline period to determine the percentage recovery to baseline for each slice following HFS (see Methods; Figure 3.5).

Following the HFS stimulus, all slices exhibited an initial depression in the PS amplitude to ~20% of baseline (post-tetanic depression, PTD). For some slices, the PS returned to near baseline within a few minutes, while for other slices the PS remained depressed for the full 30 minute recording period. I used a cluster analysis (see Methods) to make an unbiased differentiation between the two populations of responses that were then defined operationally as short-term depression (STD) and long-term depression (LTD) based on the percent of PS recovery at 30 minutes. Fig. 4.1A shows representative PS records from slices of the designated STD and LTD clusters that were measured during baseline recording and then 30 minutes after HFS. Fig 4.1B provides a comparison of the PS recoveries of the STD and LTD populations as well as the combined data for all slices recorded in the WT/Sac group. Fig 4.1C shows the time course for the STD, LTD, and combined populations and includes the 10 minute baseline and 30 minute recovery period following HFS for each population. Further analysis of the data of the percent PS amplitude recovery following HFS for LTD and STD populations

(Fig 4.1B and 4.1C) indicate that ~40% (6/15) of the slices were included in the LTD cluster and the remaining ~60% (9/15) of the slices were included the STD cluster. The observation that the HFS paradigm can result in STD, as well as LTD, has been reported previously (Lovinger et al., 1993; Sung et al., 2001) and suggests that, since both processes can result from HFS, they may be interrelated. One possible relationship is that PTD induces STD, which in turn can be transformed into LTD. The relationship between STD and LTD will be explored further in the Discussion.

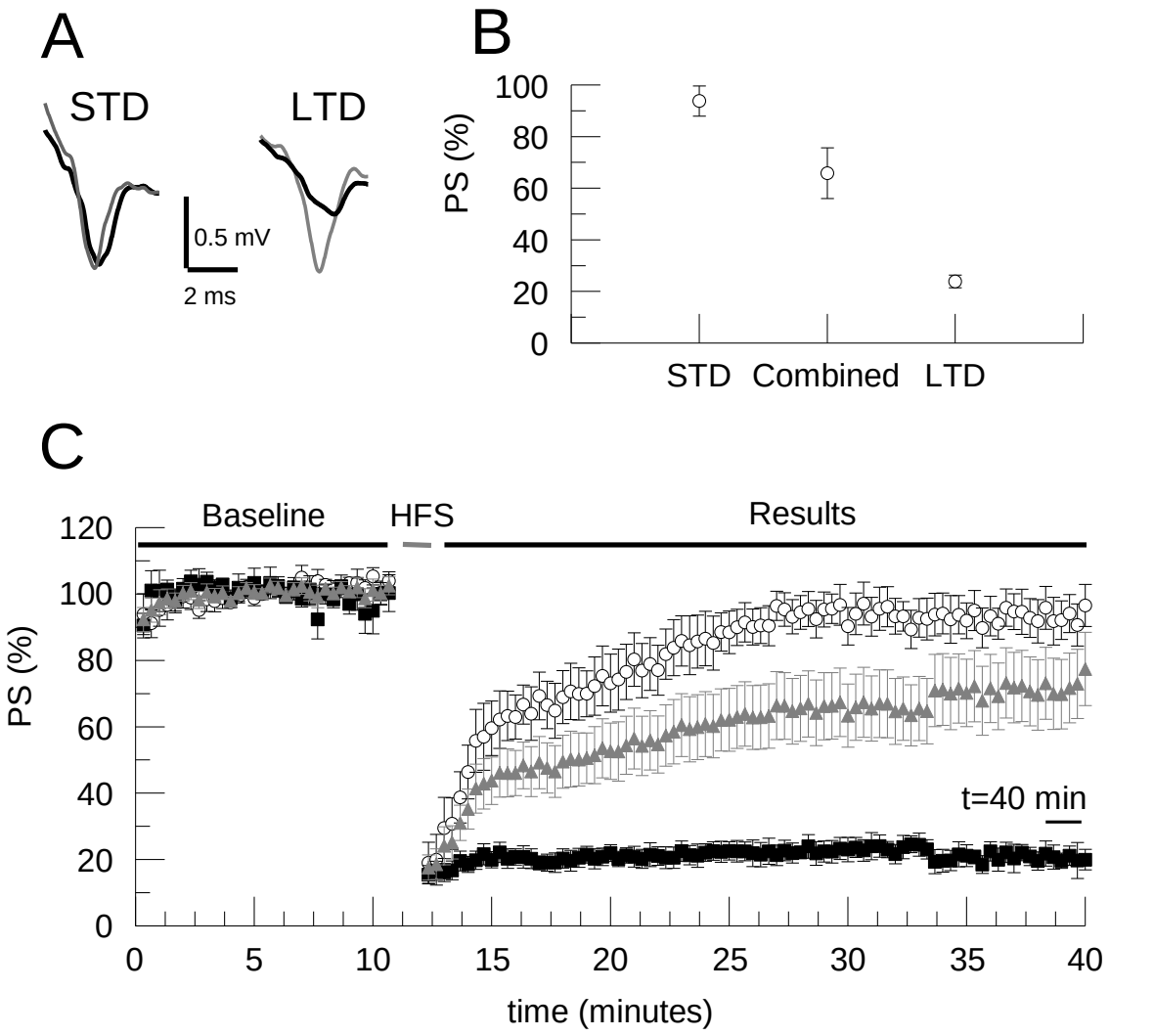

Fig. 4.1: Cluster analysis determination of STD and LTD populations in WT/Sac control group. **A** Representative population spike (PS) traces of STD and LTD for baseline (gray) and 30 minutes after HFS (black). **B** Comparison of percent recovery of PS at 30 minutes after HFS for LTD and STD clusters as well as the combined results without clustering showed significantly distinct STD and LTD clusters, (p<0.01). **C** Long-term synaptic plasticity in WT/Sac control group was induced with HFS (4 × 100 Hz, 1 s) producing either LTD (<30% recovery at 40 min, black □) or STD (>70% recovery at 40 min, white ○) as determined by cluster analysis. Combined results (gray Δ**)** before cluster analysis are also shown. PS amplitude was normalized to initial 10 minute baseline preceding HFS. STD samples n = 9 slices; LTD samples n= 6 slices; values shown as mean ± SEM.

As described above, I utilized a HFS paradigm in which the test stimulus applied during the 10 minute baseline and 30 minute recovery periods was adjusted to produce a half maximum PS amplitude while that during the HFS stimulus was set to produce a maximum PS amplitude. I next tested whether varying the test stimulus intensity had any

effect on the propensity to produce STD or LTD in the WT/Sac group. Varying this intensity from ~0.35 to 0.70 of the maximum, tended to produce an increase in the final PS amplitude at 30 minutes of recovery (Fig. 4.2). However, the correlation was weak (r^2 = 0.1007; n=13) and the 95% confidence interval was between -78% and 238%, indicating no clear effect of test stimulus amplitude on the induction of LTD or STD. For this reason, I maintained the baseline and recovery period stimulus amplitude at the value necessary to generate ½ maximum PS amplitude for the remaining experiments including those involving the other experimental groups (WT/PNE, HET/Sac, and HET/PNE).

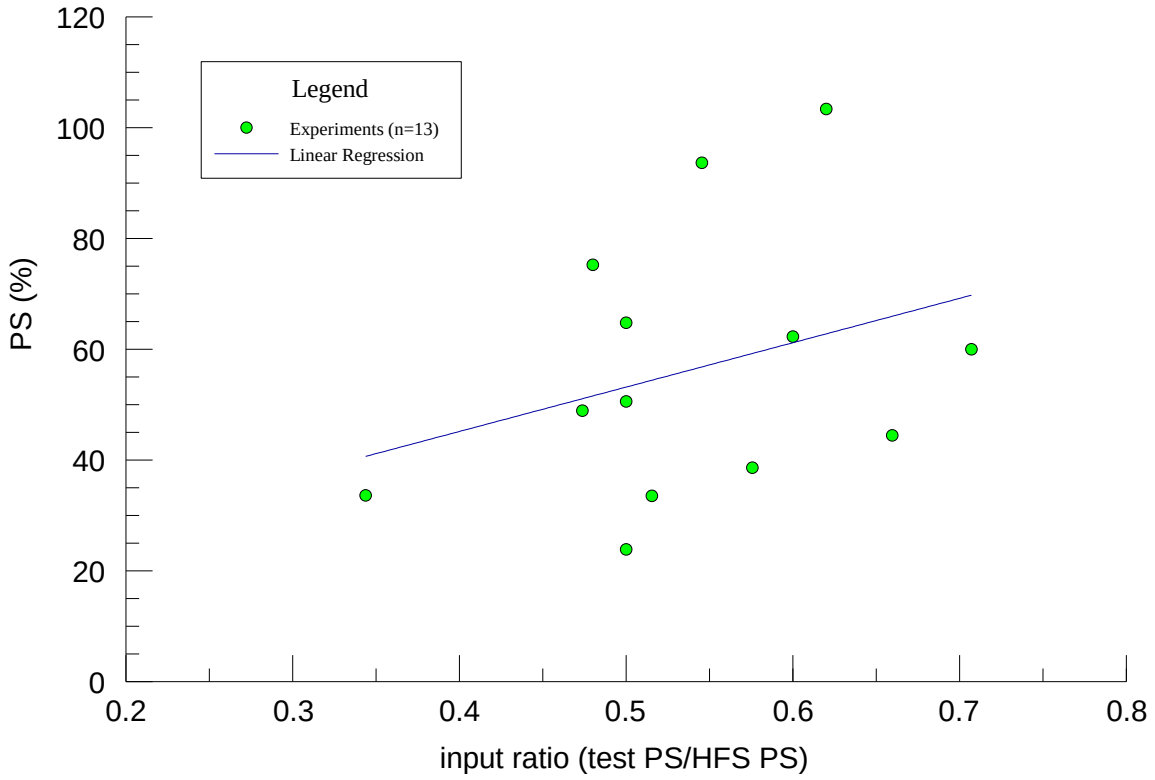

Fig. 4.2: Effect of variation of the ratio of test and HFS input stimulus on final population spike magnitudes in WT/Sac control group. Using the same HFS paradigm, the ratio of the test stimulus PS applied during the baseline and 30 minute post-HFS versus the HFS PS was varied from ~0.3 – 0.7 (nominally set at ~0.5). There was a weak positive correlation for a linear regression of %PS amplitude vs. test stimulus amplitude (r^2 = 0.1007) with increased test/HFS input ratio to final pop spike amplitude.

I next assessed whether the induction of these two forms of synaptic plasticity differed among the remaining experimental groups (WT/PNE, HET/Sac, and HET/PNE). HFS in slices prepared from each of these three groups produced responses that were

qualitatively similar to those seen in the WT/Sac control group and could be resolved by cluster analysis into LTD (Fig. 4.3A, B) or STD (Fig. 4.3C, D) clusters that were significantly different from each other (Fig. 4.4 A, B, C & D, $p < 0.01$).

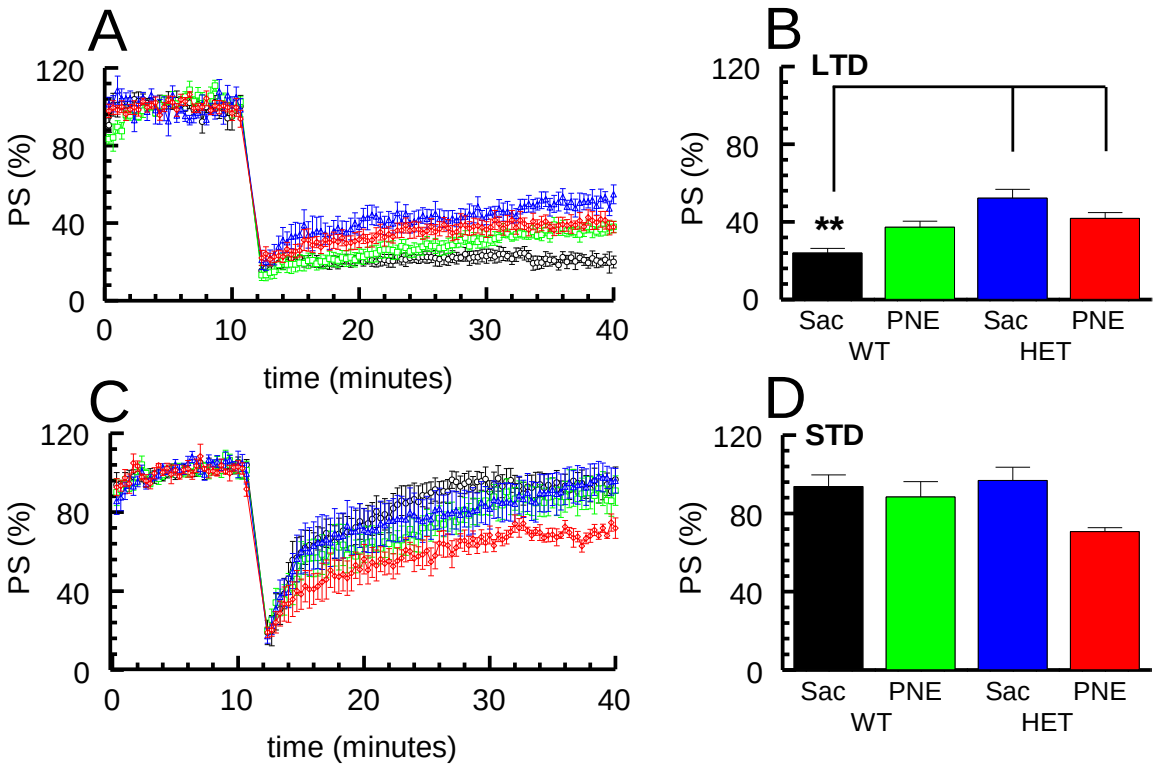

Fig. 4.3: Comparison of STD and LTD between the four G × E groups. A, C Time course of PS amplitude normalized to initial 10 minute baseline following HFS in LTD (A) and STD (C) populations of the four G × E experimental groups. (mean ± SEM, STD n = 5- 9 slices; LTD n= 6- 8 slices) (WT/Sac, black ○; WT/PNE, green □; HET/Sac, blue Δ; HET/PNE, red ◊). **B, D** Percent recovery of PS at 30 minutes following HFS in LTD (B) and STD (D) clusters shown in A and C for the four G× E experimental groups. Post-hoc tests for LTD group revealed that WT/Sac group showed significantly greater maintained depression than HET/Sac and HET/PNE groups ($p < 0.01$).

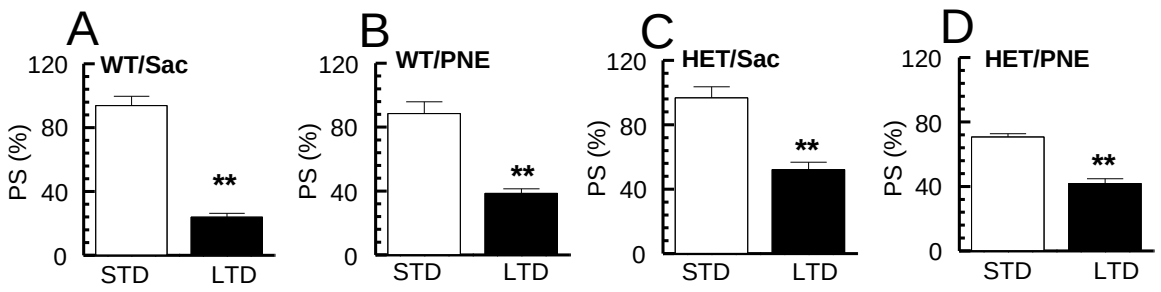

Fig. 4.4: Comparison of STD and LTD in each of the four G × E groups. A - D
Comparison of percent recovery of PS 30 minutes after HFS for STD and LTD clusters in WT/Sac, WT/PNE, HET/Sac and HET/PNE groups respectively (p<0.01).

A two-way ANOVA comparing the levels of LTD revealed a significant effect of genotype ($F_{(1,22)}$=23.81, $p < 0.001$), as well as a significant interaction of genotype × treatment ($F_{(1,22)}$=12.42, $p < 0.01$), but not of treatment alone ($F_{(1,22)}$=0.20, p=0.66). A post-hoc test of the comparisons between LTD populations showed that the HET/PNE and HET/Sac groups exhibited less robust LTD (~1.7 – 2.2 fold larger PS after 30 minutes) compared to the WT/Sac control group (Fig. 4.3A, B; p<0.01) indicating reduced LTD in the HET mice regardless of prenatal exposure. The WT/PNE group also displayed less robust LTD approaching significance in comparison to the WT/Sac group (p=0.057).

In contrast, two-way ANOVA of the levels of STD (% PS recovered after 30 minutes) revealed a significant effect of treatment ($F_{(1,27)}$=5.16, $p < 0.05$), but not genotype ($F_{(1,27)}$=1.13, $p = 0.30$), or genotype × treatment ($F_{(1,27)}$=2.26, $p = 0.14$). While the STD obtained from slices of the HET/PNE group showed less recovery to baseline, ~0.7 – 0.8 fold compared to the other groups, this decrease was not significant after post-hoc analysis (Fig. 4.3C, D).

A further comparison of the relative level of LTD to that of STD obtained for each group (% PS_{STD} / % PS_{LTD}) revealed that the ~1.7 fold difference between STD and LTD in the HET/PNE group (Fig. 4.4D) was less; than that found for the other groups (WT/Sac ~3.9 fold, Fig. 4.4A; WT/PNE ~2.4 fold, Fig. 4.4B; HET/Sac ~1.9 fold; Fig. 4.4C). Additionally, a larger percentage of slices in the HET/PNE group underwent LTD rather than STD (~62%, 8/13) (WT/Sac ~40%, 6/15; WT/PNE ~40%, 6/15; HET/Sac

~43%; 6/14). These results indicate a selective alteration in the mechanisms responsible for initiating the transition from STD to LTD in the HET/PNE group.

I made an additional assessment of the differences in the stimulus intensity necessary to evoke similar PS amplitudes in the four groups to determine whether there were differences in intrinsic excitability between groups. Comparisons were made of the ratio of the amplitudes of the PS produced to the half maximum input stimulus for each group during baseline recordings prior to HFS inputs (Fig. 3.4, Methods; PS output in mV divided by test input stimulus (1/2 maximum) in mA). The values found for each group were WT/Sac 1.096 ± 0.136; WT/PNE 1.044 ± 0.145; HET/Sac 1.102 ± 0.093; HET/PNE 1.132 ± 0.109 (magnitude (mV/mA) ± SE; n=7 slices per group). A two-way ANOVA comparing the responses between these groups showed no significant effects for genotype ($F_{(1,24)}$= 0.15, p =0.71), treatment ($F_{(1,24)}$=0.08, p =0.93), or interaction of genotype × treatment ($F_{(1,24)}$=0.11, p =0.74). This indicates that the differences in relative amounts of LTD and STD were not due to changes in excitability of afferent inputs to MSNs, since the relative size of PS produced for each was not significantly different.

Both CB1 and D2 receptors, along with other receptors including metabotropic glutamate receptors (mGluRs), have been shown to be critical in the process of induction of LTD in cortico-striatal synapses (Kreitzer and Malenka, 2005; Surmeier et al., 2007). Therefore, because of the differences that were found between the HET/PNE and other groups, both in terms of eliciting either LTD or STD and in the levels of recovery of LTD and STD, I tested whether the mechanisms responsible for induction of LTD were affected by either the *Snap25* genotype or PNE treatment. For these experiments, I used the antagonists AM251 (2 μM) to block cannabinoid CB1Rs and sulpiride (10 μM) to block dopamine D2Rs in each of the four G × E groups, using the same HFS paradigm that produced distinct STD and LTD clusters (Fig. 4.3). As shown in Fig. 4.5A, cluster analysis of data obtained for the WT/Sac control group in the presence of both CB1R and D2R antagonists yielded only a single population that was similar in time course and final value 30 minutes after HFS stimulus to our previously defined STD population, consistent with previous studies suggesting that the transition from STD to LTD requires both CB1Rs and D2Rs (Lovinger, 2010). Similarly, when I applied CB1R or D2R antagonists in the WT/PNE, HET/Sac, and HET/PNE groups, I again observed a single

cluster that was similar to the STD population (Fig. 4.5B, C, & D). Fig. 4.6 shows a comparison of responses to CB1 and D2R antagonists within each group instead of between groups as shown in Fig. 4.5 B and D. This suggests that activation of CB1R and D2R pathways remain important for induction of LTD in WT/PNE, HET/Sac, and HET/PNE groups.

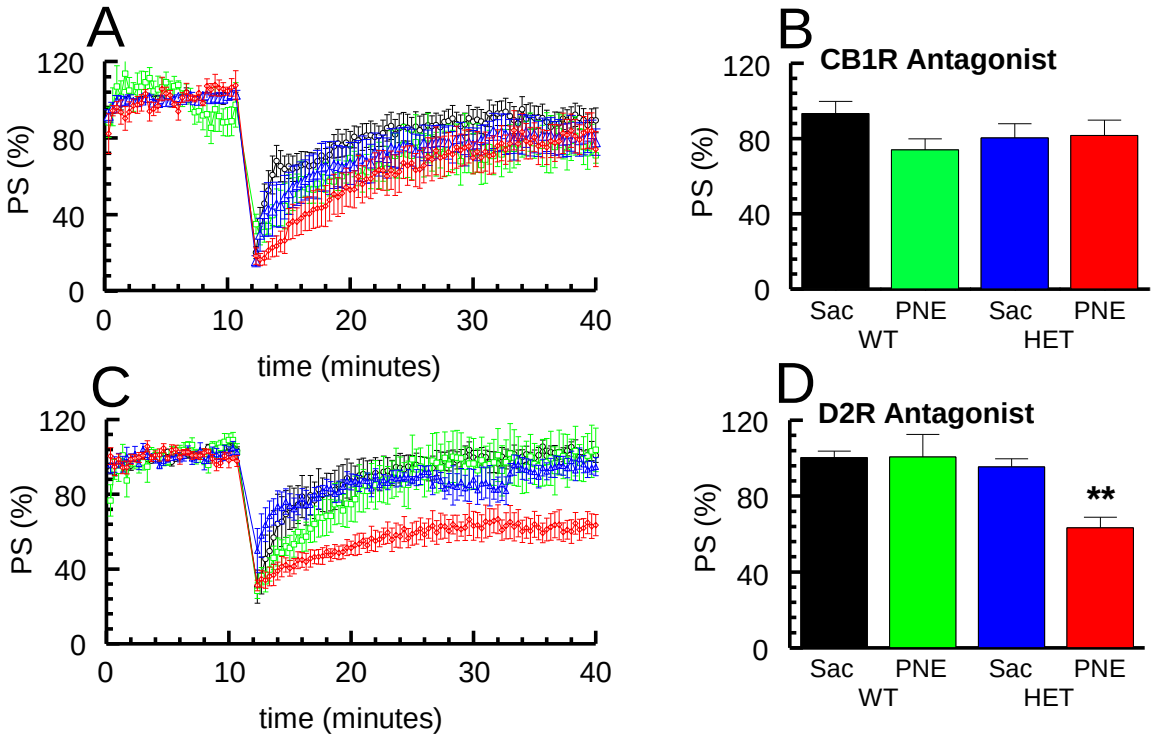

Fig. 4.5: Comparison of effects of D2R and CB1R antagonists on LTD induction between the four G × E groups. A, C Time course of PS amplitude normalized to initial 10 minute baseline following HFS in the presence of CB1R antagonist, AM251, (2 μM) (A) and D2R antagonist, sulpiride, (10 μM) (C) for the four G × E experimental groups. D2R antagonist n = 6- 8 slices; CB1 antagonist n = 6- 7 slices; values shown are mean ± SEM. (WT/Sac, black ○; WT/PNE, green □; HET/Sac, blue Δ; HET/PNE, red ◊). **B, D** Percent recovery of PS at 30 minutes following HFS in the presence of AM251 (B) and sulpiride (D) shown in A and C for the four G× E experimental groups. Post-hoc tests for D2R antagonists revealed HET/PNE group significantly less recovery than other groups ($p < 0.01$).

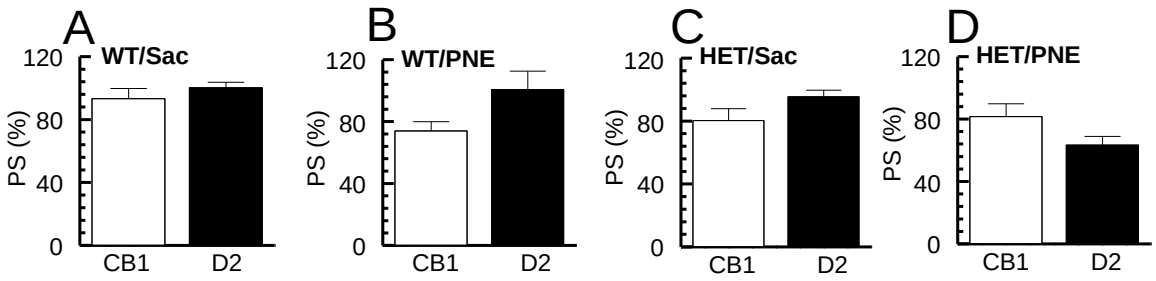

Fig. 4.6: Comparison of effects of D2R and CB1R antagonists on LTD induction in each of the four G × E groups. A - D Effect of AM251 (CB1) or sulpiride (D2) on percent recovery of PS at 30 minutes following HFS in WT/Sac, WT/PNE, HET/Sac and HET/PNE groups respectively.

I next compared the response of the four G × E groups to HFS in the presence of a CB1R antagonist. A two-way ANOVA comparing the response to HFS between these groups in the presence of the CB1R antagonist did not reveal any significant differences (Fig. 4.5 A, B), in keeping with the well-established central role of endocannabinoid feedback in the induction of LTD (Adermark et al., 2009; Lovinger, 2010). This finding suggests that the CB1R-dependent signaling pathway responsible for initiating LTD induction is not impaired in HET mice exposed to prenatal nicotine.

I next compared the response of the four G × E groups to HFS in the presence of the D2R antagonist. In contrast to the CB1R antagonist, a two-way ANOVA comparing the response between these groups in the presence of the D2R antagonist revealed a significant effect of genotype ($F_{(1,23)}$=10.07, $p < 0.01$), treatment ($F_{(1,23)}$=5.71, $p < 0.05$), as well as a significant interaction of genotype × treatment ($F_{(1,23)}$=5.97, $p < 0.05$). Post-hoc analysis showed that the response of the HET/PNE group in the presence of the D2R antagonist was significantly different from that of the other groups exhibiting decreased recovery (~0.6 – 0.7 fold) (Fig. 5.5 C, D; $p < 0.01$). This finding strongly suggests that the D2R-dependent signaling involved in LTD induction is selectively impaired in HET mice exposed to prenatal nicotine.

Differences in recovery rates of STD between groups with CB1R and D2R antagonists

As discussed above, I found that following the HFS stimulus, the PS amplitude in all slices exhibited an initial depression to ~20% of baseline (post-tetanic depression, PTD). With the STD population, but not the LTD population, as determined by cluster analysis, the PS amplitude returned to near baseline within a few minutes for all four G × E groups. Similarly, application of CB1R or D2R antagonists in the four G × E groups, produced a single response that was similar to the STD population response. I performed additional analysis to compare the relative rates of recovery during STD between groups, and in the presence of CB1R and D2R antagonists using the data shown in Fig. 4.3C for STD and in Fig 4.5A & C for CB1R and D2R antagonists. I measured the recovery rate by determining the least squares fit for the exponential recovery during STD following the ~20% depression during PTD in the presence of CB1R and D2R antagonists for the four G × E groups, and using the time constant (τ) as a measure of the relative recovery rate for each group. Fig. 4.7A illustrates the method for determining the time constant for STD for the WT/Sac group (see Methods for details) and the same procedure was repeated for the other groups, and in the presence of CB1R and D2R antagonists. Briefly the time constant of recovery was determined as the negative slope of a least squares regression fit to a plot of the 30 minute recovery period. The data was transformed to display the difference between the maximum recovery fit of the PS after 30 minutes and the value of each point, shown as a semilog plot versus time so the plots would be linear. The time constant represents the time required for 1/e (37.8%) recovery to its final value. I initially attempted to determine τ values from individual experiments and then determine the mean and standard error in order compare groups. Unfortunately the decay in some experiments did not follow a clear exponential and there was high variation in many of the other experiments, and thus statistical analysis of these results could not be performed. So I compared the average responses from each experiment for each group (data taken from plots for STD; Fig. 4.3C; CB1 antagonist, Fig. 4.5A, D2 Antagonist, Fig. 4.5 C). By using averaged responses, however, I was able to obtain exponential decays from averaged values for each set of experiments for each of the groups.

The WT/Sac group had a shorter time constant for STD than the other groups (Fig. 4.7B: WT/Sac τ = 5.4 min, WT/PNE τ = 9.7 min, HET/Sac τ = 8.4 min, HET/PNE τ = 9.1 min), showing that, although there may not be significant differences in the fraction of slices in the STD cluster between groups, there was a small increase in the time course of recovery as a result of the G × E factors and interactions. In the presence of D2R antagonists there were no distinct differences between groups (Fig. 4.7C: WT/Sac τ = 6.3 min, WT/PNE τ = 6.4 min, HET/Sac τ = 7.1 min, HET/PNE τ = 6.6 min), so although D2R antagonists affect the magnitude of the final recovery after 30 minutes in the HET/PNE group (Fig. 4.5D), they appear not to alter the time course of recovery. In the presence of CB1 antagonists, there was a surprising increase in the time course of recovery for the HET/PNE group compared to other groups (Fig. 4.7C: WT/Sac τ = 5.3 min, WT/PNE τ = 5.3 min, HET/Sac τ = 5.1 min, HET/PNE τ = 16.3 min), although, as discussed previously, this did not manifest in any effects in the final recovery after 30 minutes in the HET/PNE group (Fig. 4.5B). The possible implications of these findings are explored in the Discussion.

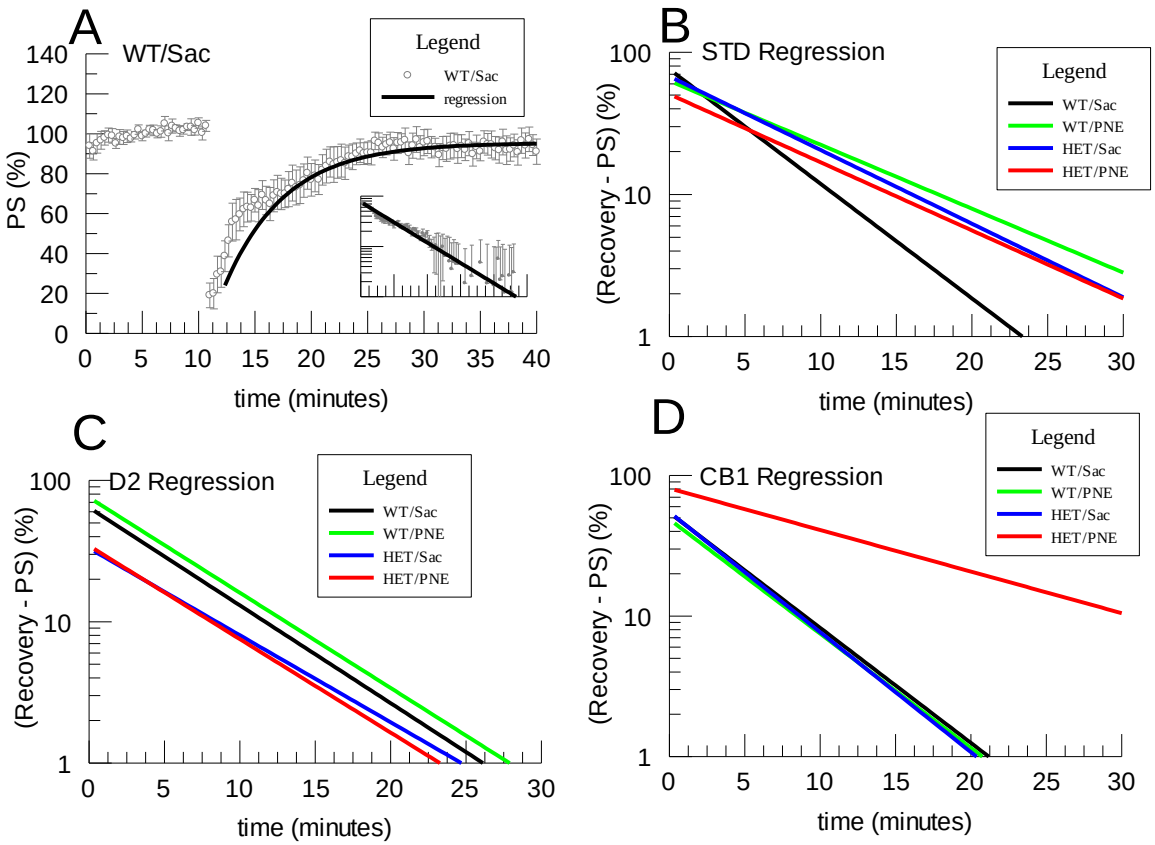

Fig. 4.7: Least square regression analysis of recovery rates in the four G × E groups for LTD induction paradigm for STD, or in the presence of a D2 antagonist and CB1 antagonist. A Example least squares regression analysis of the average time course for WT/Sac group (normalized to initial 10 minute baseline) for the 30 minute recovery of the STD cluster following HFS (mean ± SEM, gray ○, n= 9 slices; regression black line). Inset shows the least squares fit of the same data transformed with final fit value for recovery (e.g. 95%) subtracted from each point, plotted over time in order to obtain a linear plot with the slope represented as $-1/\tau$, plotted as a semilog (final recovered value subtracted from each point) versus time. Tau (τ) represents the exponential time constant necessary for 37.8% (1/e) of the final recovery after 30 minutes from the initial drop following HFS. **B-D** Least square regression fits for LTD induction experiments for the STD cluster, and in the presence of a D2 antagonist, and CB1 antagonist in the four G × E groups. As with the inset in Fig 4.7A, regression fit is redrawn to show data with a negative slope (final fit recovery value subtracted from each data point plotted over time). (Legend shows colors associated with each G × E group).The WT/Sac group had a shorter time constant than other groups in STD regression. All groups had similar time constants in the presence of a D2 antagonist. The HET/PNE group had a longer time constant than other groups in the presence of a CB1 antagonist.

Induction of long-term synaptic depression (LTD) in the striatum does not affect paired pulse facilitation (PPF)

All of the above experiments were carried out with a pair of stimulus pulses separated by a 50 ms interpulse interval (see Methods for details). As discussed in the introduction, the paired pulse ratio (PPR), defined as the ratio of the PS amplitude of the second pulse (R2) to that of the first (R1), is often used as an indication of pre-synaptic contributions to a process. A ratio greater than 1 indicates paired pulse facilitation (PPF) and less than 1 indicates paired pulse depression (PPD). PPF, in particular, is generally considered to be a pre-synaptic process. I measured the PPR during the 10 minute baseline period for each experiment as well as 30 minutes after the recovery period for the four G × E groups and these results are displayed in Fig. 4.8. For the WT/Sac group, the PPR did not change significantly between the baseline and recovery periods in the STD and LTD populations, or in the presence of D2R or CB1R antagonists. Similarly comparison of baseline and recovery periods for the other G × E groups did not reveal significant differences in PPR between the STD and LTD populations, nor was it affected by the presence of D2R or CB1R antagonists. A two-way ANOVA comparing PPR between the G × E groups, between STD and LTD or in the presence of a CB1R or D2R antagonist did not show a significant effect of genotype, treatment, or a significant interaction of genotype × treatment. These results indicate that neither the HFS protocol nor the various conditions that alter D2R signaling significantly alter the PPR. A net increase in PPR (PPF) would imply a relative decrease in the probability of release of pre-synaptic vesicles from cortical afferents onto MSNs. This suggests that these effects on D2R signaling may not involve primarily a change in pre-synaptic glutamate release, but rather that of post-synaptic changes in how D2Rs affect the induction of LTD. Interestingly, these G × E changes appear not to involve the well-established pre-synaptic role of long-term decreases in glutamate release involved in LTD induction (Choi and Lovinger, 1997b). These implications will are explored further in the Discussion.

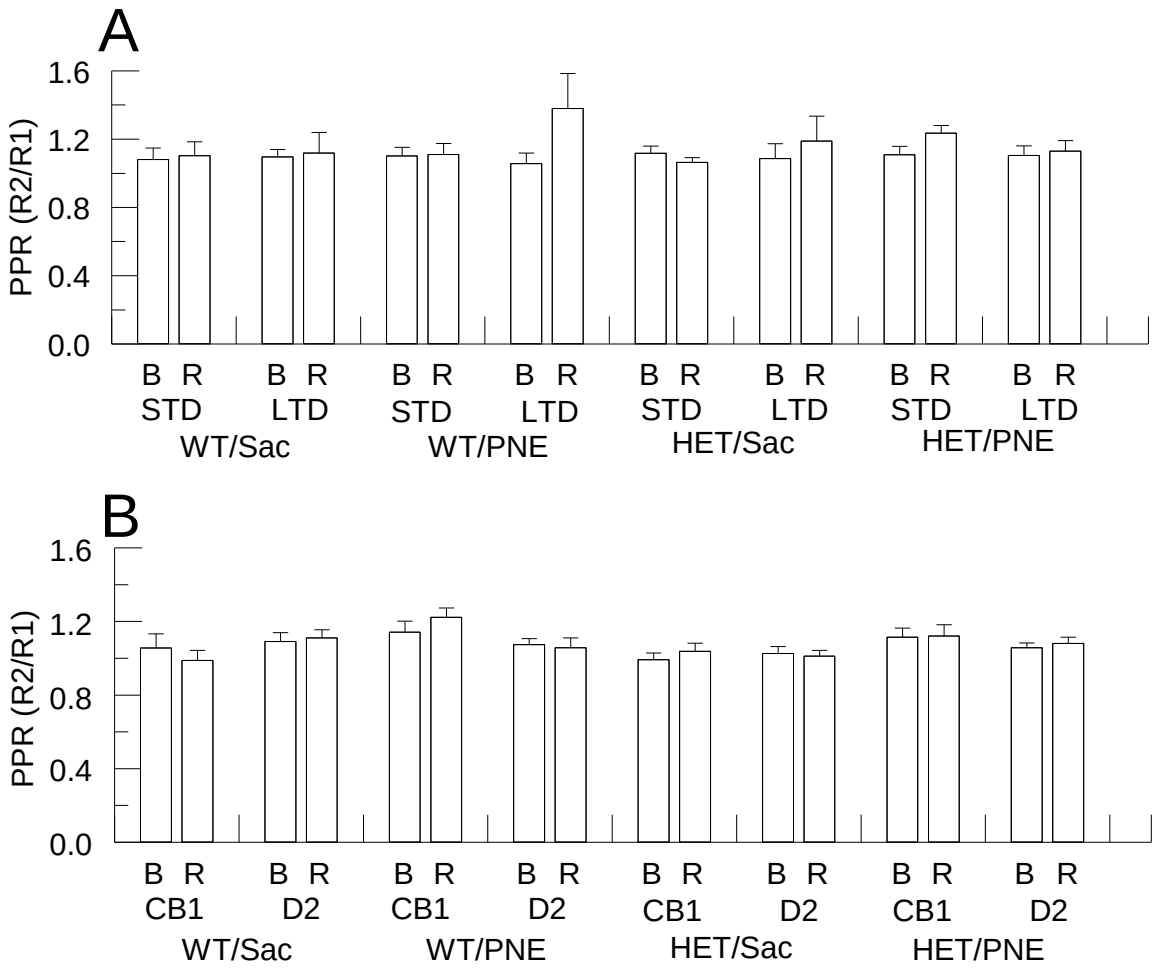

Fig. 4.8: Comparison of effects of the paired pulse ratio on LTD induction in the four G × E groups for STD and LTD clusters and in the presence of a CB1 or D2 antagonist. Paired pulses with a 50ms interpulse interval were recorded during the 10 minute baseline and for 30 minutes following HFS for each experiment. The paired pulse ratio (PPR) of the PS amplitude associated with the second stimulus (R2) divided by the PS amplitude associated with the first stimulus (R1) or (R2/R1) was determined for the average of the 10 minute baseline period (B) and results 30 minutes after HFS (R). **A** Comparison of PPRs of baseline (B) and 30 minute after HFS results (R) for LTD and STD clusters for the four G × E groups revealed no differences in PPR between B and R within each group or comparisons between groups (students t-test). **B** Comparison of PPRs of baseline (B) and 30 minute after HFS results (R) for experiments in the presence of a CB1 or D2 antagonist for the four G × E groups revealed no differences in PPR between B and R within each group or between groups (students t-test).

I next examined PPR during the baseline period for each of the four G × E groups for all experiments regardless of whether the HFS eventually produced LTD or STD or whether the experiments were performed in the presence of a D2R or CB1R antagonist. I

reasoned that these initial PPRs would not be a function of whether HFS led to LTD or STD or the eventual effect of D2R or CB1R antagonists. The latter is justified by published accounts, which indicate that CB1R and D2R antagonists primarily function in the LTD induction process rather than during basal stimulus of MSNs (Centonze et al., 2001; Singla et al., 2007). I performed cluster analysis on the baseline responses for each of the four G × E groups and discovered that baseline PPR led to two clusters of slices: ~1/3 of the slices (WT/Sac 6/28; WT/PNE 9/26; HET/Sac 10/25; HET/PNE 10/28; ratio of slices), which produced a significant PPF of ~1.2-1.3 and ~2/3 of the slices, which produced no short-term plasticity (PPR ~1.0) as shown in Fig. 4.9. For each of the four G × E groups, I quantified the changes in PPR for the 30 minutes after the recovery period as well. Comparison of baseline and recovery for the four G × E groups did not reveal significant differences in PPR before and after HFS for the PPF or no short-term plasticity clusters. A two-way ANOVA comparing the baseline responses between these groups for both the PPF and no short-term plasticity clusters, did not show a significant effect of genotype, treatment, or a significant interaction of genotype × treatment between groups with one exception. The no short-term plasticity cluster was significantly larger in the HET/PNE group than the HET/Sac group. These results reveal that for each of the four G × E groups, approximately 1/3 of slices exhibit short-term facilitation (PPF) and approximately 2/3 of slices did not exhibit short-term plasticity. Importantly, with the one exception mentioned above, there were no alterations in PPRs in the PPF or no short-term plasticity clusters as a result of HFS.

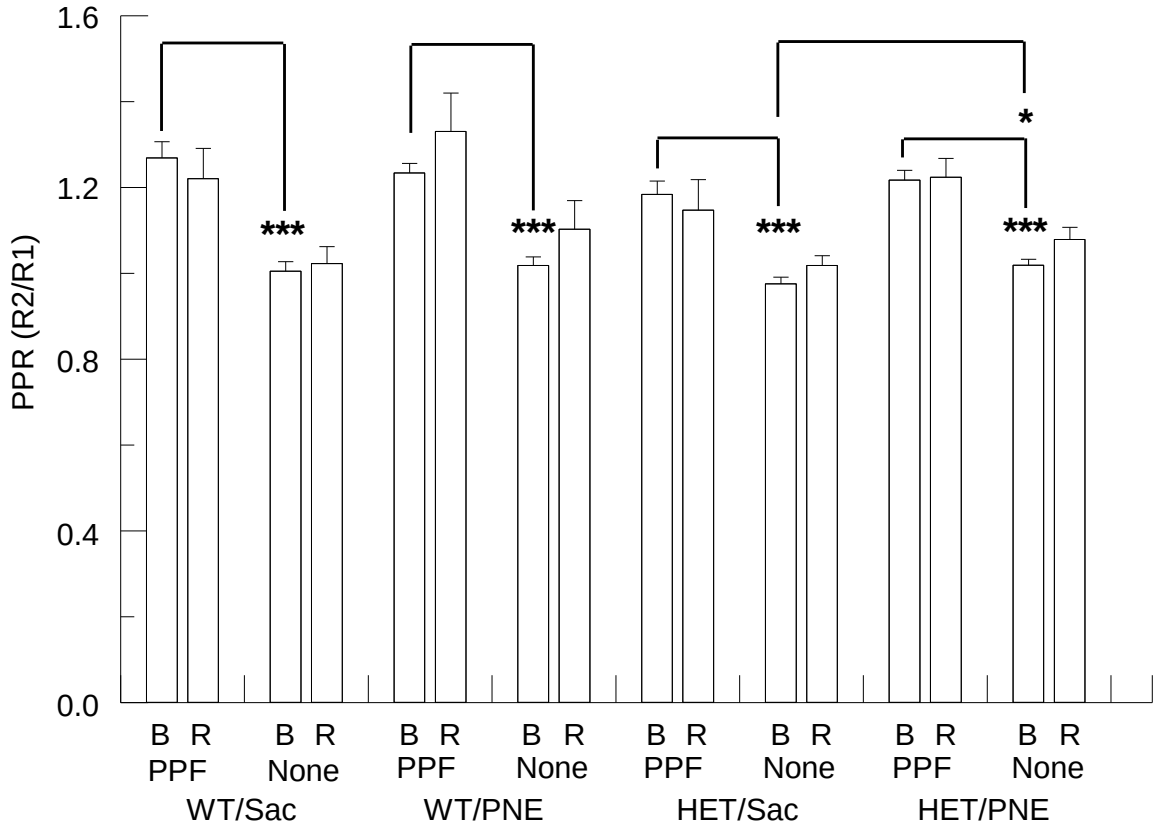

Fig. 4.9: Comparison of effects of PPF or no short-term plasticity on LTD induction in the four G × E groups. Cluster analysis was performed on the baseline paired pulse ratios (PPRs) for experiments grouped for all conditions (STD, LTD, in presence of CB1, or D2 antagonists). Each G × E group clustered into significant ($p < 0.001$) groups with either PPF or no short-term plasticity (None). Comparison of baseline (B) PPRs to results 30 minutes after HFS (R) do not reveal differences within groups for PPF and no short-term plasticity (None) clusters. Comparison across groups revealed a significantly larger baseline no short-term plasticity cluster for the HET/PNE group compared to the equivalent cluster in the HET/Sac group, but no other group comparisons showed significance.

D2R agonist affinity and/or receptor coupling is altered in *Snap25* heterozygotes prenatally exposed to nicotine

To investigate further the role of D2R signaling in striatal synaptic depression, I first performed [^{35}S]-GTPγS binding experiments to measure the agonist-stimulated response of G-protein-coupled receptors (GPCRs) using the D2R/D3R-specific agonist quinelorane (Sovago et al., 2001) in coronal sections of P35-50 mice of the four G × E experimental groups. [^{35}S]-GTPγS binding is a common method to determine the effect of an agonist on receptor affinity, downstream signaling, and/or number of receptors. The

assay is based on agonist binding of the GPCR that leads to conformational changes in the GPCR, enabling interaction with a G protein. GDP is released from the α subunit and is replaced by [^{35}S]-GTPγS which is resistant to hydrolysis so remains bound to the α subunit, so the radioactivity is a measure of agonist binding. The agonist binding, reflected in accumulation of [^{35}S]-GTPγS, can measure changes in receptor number, affinity, and/or receptor-effector coupling.

I measured the intensity of the signal over the dorsal striatum as previously described (Martinez et al., 2008) to obtain both the basal level of GTP binding and binding following half maximal and maximal agonist stimulation. As expected, preliminary experiments demonstrated a concentration-dependent increase in response to increasing quinelorane concentration over a range of 1 nM to 1000 μM that resulted in an EC_{50} of approximately 20 μM and EC_{100} of approximately 200 μM in WT/Sac controls (Fig. 4.10). The specificity of the binding was tested by co-incubating slices with 100 μM quinelorane and a saturating level of the D2R/D3R-specific antagonist sulpiride (50 μM), which fully blocked the agonist-stimulated GTP binding in the same WT/Sac controls (Fig. 4.10). Also shown in Fig. 4.10 are fits of the data to a Hill equation (see Methods for details) from which the K_d was found to be 18.88 μM, close to the 20 μM used for the EC_{50} value. The inset in Fig. 4.10 shows the hyperbolic relationship for increased agonist binding as a function of concentration as is typical for Michaelis-Menten kinetics where a ligand saturates a receptor with increasing binding. Interestingly, the Hill equation fit for the WT/Sac group had a Hill coefficient of 0.314 indicating negative cooperative binding (Goutelle et al., 2008). Since only one replicate was done only for the WT/Sac group, it is not possible to draw general conclusions about this result. However the ramifications for this finding are discussed as a possible future direction for further research in the Discussion.

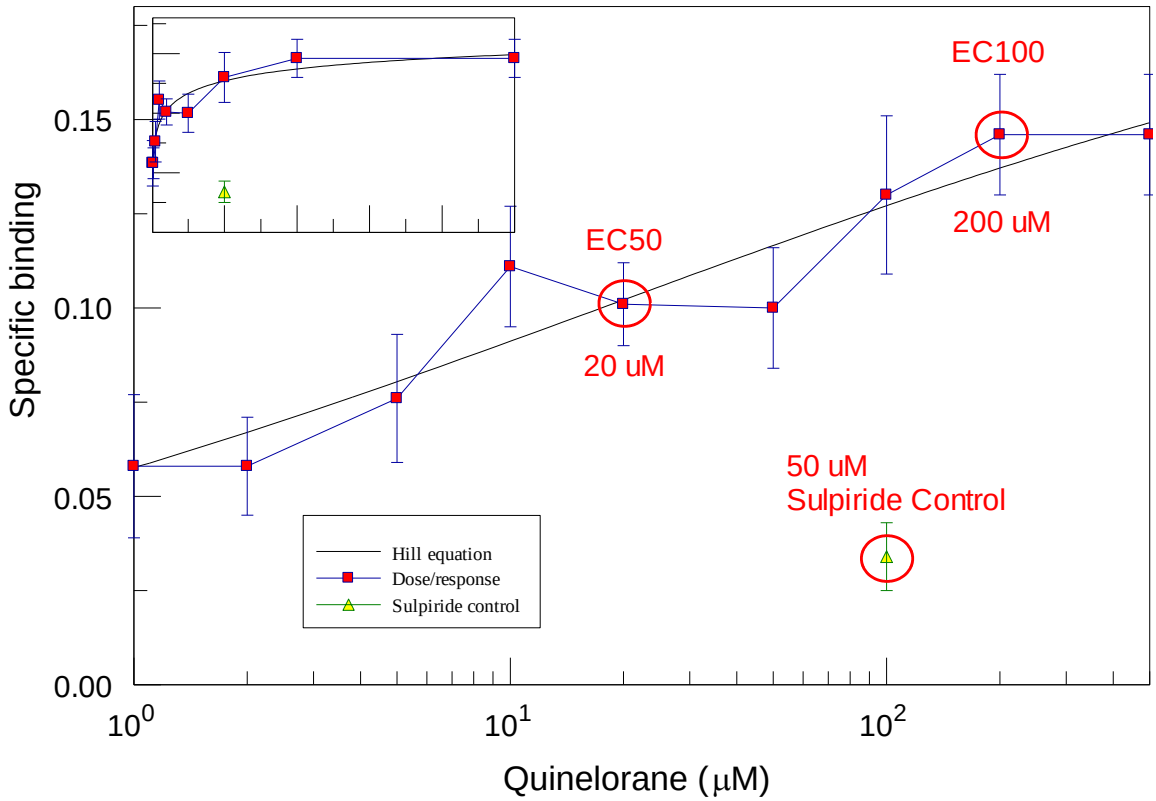

Fig. 4.10: Preliminary EC_{50} and EC_{100} binding. The total binding for each slide was subtracted from the nonspecific slides incubated in the presence of 10 μM unlabelled GTPγS (each in turn determined by subtracting regions in the striatum from background as with total binding) to determine specific binding for each data point. Binding from both the left and right side of the striatum was used in the analysis. This figure shows a dose response curve for quinelorane binding between 200 nM and 1000 μM. Inset shows same plotted with a linear. The units are femtomoles/ 10^5 μm^2. Values (mean ± SE) for specific binding at 100 μM was 0.146 ± 0.006; at 100 μM with 50 μM sulpiride was 0.039 ± 0.042, which compares with specific binding at 200 nM quinelorane, which was 0.042 ± 0.005 indicating that quinelorane is specific for D2R/D3Rs. The Hill equation fit indicated a K_d value of 18.88 μM, close to the 20 μM used for the EC_{50} value, and a Hill coefficient n=0.314.

The results of these agonist-stimulated GTP binding experiments in the four G × E groups are summarized in Table 4.1. Under basal conditions without quinelorane, a two-way ANOVA revealed a significant effect of genotype on GTP binding ($F_{(1,20)}$=5.89, $p < 0.05$), although a post-hoc test failed to show any significance difference between the groups. At half maximal stimulation with the agonist quinelorane (EC_{50}; 20 μM), a two-way ANOVA revealed decreased [^{35}S]-GTPγS binding compared to the WT/Sac control with significant effects of both genotype ($F_{(1,20)}$=9.49, $p < 0.01$) and treatment ($F_{(1,20)}$=7.78, $p < 0.05$), although no significant interaction of genotype × treatment was detected ($F_{(1,20)}$=0.02, p =0.90). Post-hoc analysis of these data demonstrated that the

stimulated receptor binding of GTP at the EC_{50} for quinelorane was significantly decreased in the HET/PNE group compared to WT/Sac controls (~0.6 fold; $p < 0.01$), indicating reduced activation of D2R signaling in the dorsal striatum of HET mice exposed to prenatal nicotine. In contrast to the effects obtained at the EC_{50} concentration, a two-way ANOVA of the data obtained at maximal stimulation (EC_{100}; 200 µM) revealed a significant effect of genotype ($F_{(1,20)}=7.20$, $p <0.05$), but no significant effects for treatment ($F_{(1,20)}=0.30$, $p =0.59$), or for a genotype × treatment interaction ($F_{(1,20)}=0.29$, $p =0.59$). Moreover, post-hoc analysis of the EC_{100} data did not reveal any significant differences between these groups. These results suggest that the synaptic plasticity differences seen in the HET/PNE group may be due to changes in D2R signaling, which is revealed only under limited agonist concentrations and might result from either a decrease in receptor affinity and/or G-protein receptor-effector coupling.

Group	Basal Binding	EC_{50} (20 µM quinelorane)	EC_{100} (200 µM quinelorane)
WT/Sac	0.049 ± 0.005	0.104 ± 0.007	0.245 ± 0.011
WT/PNE	0.042 ± 0.006	0.085 ± 0.010	0.254 ± 0.018
HET/Sac	0.035 ± 0.005	0.083 ± 0.004	0.207 ± 0.011
HET/PNE	0.031 ± 0.004	0.066 ± 0.002**	0.223 ± 0.016

Table 4.1: Dopamine agonist, quinelorane simulated [^{35}S]-GTP-γ-S binding. Comparative values of the four G × E experimental groups for basal [^{35}S]-GTP-γ-S binding without quinelorane, net EC_{50} [^{35}S]-GTP-γ-S binding with quinelorane at 20 µM, and net EC_{100} [^{35}S]-GTP-γ-S with quinelorane at 200 µM respectively. All samples in quadruplicate and binding is given in femtomoles/10^5 μm^2. (mean ± SEM, n = 6 animals from which quadruplicate sections were obtained). The net EC_{50} and EC_{100} binding represent net binding with basal binding subtracted prior to analysis. Post-hoc tests for EC_{50} revealed HET/PNE group had significantly less binding than other groups ($p < 0.01$).

Decreased [^{3}H]-Quinpirole agonist saturation binding kinetics indicates decreases in D2R affinity in *Snap25* heterozygotes prenatally exposed to nicotine

To distinguish between a reduced affinity and number of expressed D2Rs, I next performed agonist saturation binding experiments with the D2R selective radioligand [^{3}H]-quinpirole in striatal tissue homogenates (Levant et al., 1992) in order to determine the K_d and B_{max} for the four G × E groups. Saturation binding is a well established method for quantifying the affinity of an agonist as well as the number of receptors

present, and is complementary to the [^{35}S]-GTPγS binding assay for determining changes in agonist affinity and number of receptors. For each experiment, specific binding was determined at six agonist concentrations from 0.2 nM to 9 nM and the values of the K_d and B_{max} were determined by least-squares fits of data from replicate experiments (see Experimental procedures). Fig. 4.11 shows a representative saturation isotherm obtained from one of the WT/Sac striatal homogenate experiments. Fig 4.11A shows the total and non-specific binding obtained over the range of agonist concentrations from which the specific binding was obtained (total binding minus non-specific binding). Fig 4.11B shows the plot of the ratio of the bound /free ligand as a function of the free ligand from which the K_d can be determined from the slope (-1/slope) and B_{max} values from the X-intercept according to Scatchard analysis. The isotherms as well as data associated with samples used for all groups are presented in Appendix 1.

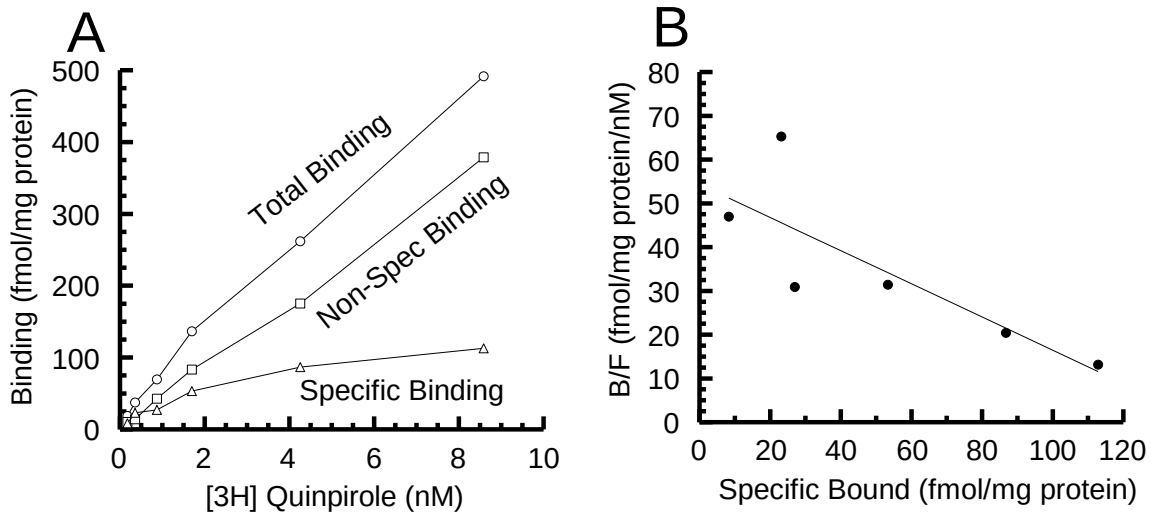

Fig. 4.11: Representative saturation isotherm and Scatchard plot for [^{3}H]-Quinpirole D2R agonist saturation binding in WT/Sac striatal homogenates. Striatal membranes were incubated with 6 concentrations of [^{3}H]-Quinpirole (~0.2 – 9nM) at 23^o C. K_d and B_{max} were estimated with least square fits to Scatchard plots of triplicate samples. **A** Plot of total, non-specific and specific binding as a function of [^{3}H]-Quinpirole concentration. **B** Scatchard plot of ratio of bound/free ligand versus specific bound ligand fraction for the same example.

Table 4.2 is a summary of the saturation binding kinetics obtained for the four G × E groups. The K_d obtained for the HET/PNE group was markedly greater than the

comparable values obtained for the other three groups. A two-way ANOVA of the K_d obtained from each of the four experimental groups revealed a significant effect of genotype ($F_{(1,16)}$=20.01, $p < 0.001$), treatment ($F_{(1,16)}$=5.36, $p <0.05$), as well as an interaction of genotype × treatment ($F_{(1,16)}$=5.15, $p <0.05$). Importantly, post-hoc analysis demonstrated that the K_d for D2R receptor agonist binding of HET/PNE group was significantly higher (~1.6 -2.1 fold; versus WT/Sac and WT/PNE, $p < 0.01$; versus HET/Sac, $p < 0.05$) than the other groups (Table 4.2), indicating a reduced agonist affinity for D2Rs in HET mice exposed to prenatal nicotine. In contrast to the K_d results, no significant difference was found between the B_{max} values determined for the four G × E groups indicating that the number of receptors remained unchanged. Taken together with the data obtained from the agonist stimulated GTP binding experiments, these results suggest that G × E interactions affecting synaptic plasticity in the striatum, which are reflected by impaired dopamine-dependent induction of LTD, are mediated through changes in agonist affinity and possibly G-protein receptor-effector coupling as indicated by the [^{35}S]-GTPγS results with subsequent effects on downstream G-protein signaling by these D2 receptors.

Group	K_d (nM ± SEM)	B_{max} (fmol/mg protein ± SEM)
WT/Sac	3.322 ± 0.458	117.7 ± 15.5
WT/PNE	3.348 ± 0.599	128.0 ± 15.2
HET/Sac	4.562 ± 0.565	127.8 ± 15.7
HET/PNE	7.128 ± 0.606*,**	119.5 ± 9.3

Table 4.2: [^{3}H]-Quinpirole D2R agonist saturation binding kinetics.
Comparative values of K_d and B_{max} for the four G × E experimental groups. All samples in triplicate and values (mean ± SEM, n = 5, each n represents dissected striatal homogenates from 2 male and 2 female brains). Post-hoc tests for the K_d revealed HET/PNE group significantly greater than **WT/Sac and WT/PNE ($p < 0.01$) and *HET/Sac ($p < 0.05$).

Chapter 5 - Discussion

Summary of findings

Table 5.1 below, which includes F-values and significance for main gene, environmental as well as gene-environmental effects, summarizes the major findings of this research. The table also presents significant post-hoc effects measured when gene, environmental or gene-environmental effects were found. The electrophysiological results showed that the induction of LTD in the dorsal striatum by the HFS paradigm resulted in distinct populations of responses in all four G × E groups, which I have designated as STD and LTD. Additional experiments were performed with the WT/Sac control group to confirm that the production of STD or LTD was not a function of the test and HFS input ratios (nominally set at ~0.5 for all experiments). Between-group comparisons of LTD populations revealed that LTD was less robust in the HET/PNE and HET/Sac groups compared to WT/Sac controls due to a main gene effect and gene-environmental interaction. Between-group comparisons of STD populations did not reveal significant differences between groups, although the HET/PNE group showed less recovery to baseline compared to other groups and there was a main effect of environment. In the presence of a D2R antagonist, the HET/PNE group exhibited significantly less recovery to baseline following HFS than the other groups indicating that the induction of LTD is impaired by a process involving D2Rs. However, a CB1R antagonist did not produce a significant difference between groups, confirming that the alterations in LTD induction does not affect the endocannabinoid feedback control of cortical glutamatergic input to medium spiny neurons (MSNs) that has previously been shown to be responsible for LTD induction in the striatum (Lovinger, 2010). Additional findings were that, although a greater percentage of slices from the HET/PNE mice resulted in LTD than in STD, the ratio of LTD to STD responses (% $fEPSP_{STD}$ / % $fEPSP_{LTD}$) was less for the HET/PNE group than that observed for the other groups. The differences found for the HET/PNE group cannot be due to differences in intrinsic excitability, since comparisons of half maximum stimulus intensities between the groups showed no significant differences. Overall, these differences observed for STD and LTD

are consistent with G × E interactions leading to pronounced impairments in the induction of LTD in the HET/PNE group compared to other groups.

All electrophysiology experiments were carried out with a pair of stimulus pulses separated by a 50 ms interpulse interval (IPI) in order to allow assessment of changes in PPR before and after HFS. Comparisons of PPR within each group did not reveal significant changes in any group for the STD and LTD populations or in experiments done in the presence of a D2R or CB1R antagonist. Similarly, comparison between groups also did not reveal significant differences in PPR before or after HFS for STD and LTD populations, or in the presence of a D2R or CB1R antagonist.

These results suggest that the electrophysiology findings of an impaired induction of LTD in animals with a combination of HET genotype and PNE treatment, could result from changes in D2R affinity and/or changes in the number of D2R receptors, since in the presence of a D2R antagonist, the induction of LTD was impaired. This was initially tested using a [^{35}S]-GTPγS binding assay to measure the agonist-stimulated response of G-protein-coupled D2R receptors. The agonist-stimulated response was reduced in the HET/PNE group when compared to the WT/Sac control group, consistent with the reduction in agonist affinity for the D2R receptor, and/or reduced GPCR – trimeric G protein coupling, which would reduce downstream signaling from the GPCRs (since this assay measures G-protein activation from agonist-stimulated GPCR response, this response could be due to changes in affinity, receptor-effector coupling, or both). Moreover, the decreased agonist-simulated response, observed at the EC_{50}, but not at the EC_{100}, in the gene and environmental, but not gene-environmental groups, supports the conclusion that the receptor number was not altered by this G × E interaction. Next, a D2R agonist saturation binding assay, using [^{3}H]-quinpirole (a D2R selective agonist) followed by Scatchard analysis, showed that the HET/PNE group exhibited significantly lower affinity (higher K_d) for D2R binding without a significant change in B_{max} that would reflect a change in the number of receptors.

Collectively, these results argue strongly that the combination of the HET genotype and prenatal nicotine exposure (G × E interaction) leads to an impaired D2R GPCR signaling resulting from decreased agonist affinity and possibly receptor-effector coupling of the D2R receptors. These receptor binding observations are consistent with

the electrophysiological results showing that, in the presence of a D2R antagonist, cortico-striatal circuits in HET/PNE mice exhibit significantly less recovery following HFS than the other groups indicating that the induction of LTD is impaired. Importantly, the finding that CB1Rs are not similarly affected confirms that the deficit in synaptic plasticity precedes the endocannabinoid feedback control of cortical glutamatergic input to medium spiny neurons (MSNs) that is responsible for inducing LTD in the striatum (Lovinger, 2010).

Experiment	Main Effect		Interaction	Post-Hoc
	Gene	Environment	G x E	
	Snap25	PNE		
HFS induction of LTD				
LTD	F=23.8***	F=0.2	F=12.4**	WT/Sac**[1]
STD	F=1.1	F=5.2*	F=2.3	
D2R Antagonist	F=10.1**	F=5.7*	F=6.0*	HET/PNE**[3]
CB1R Antagonist	F=0.1	F=1.6	F=2.1	
Quinelorane simulated [^{35}S]-GTP-γ-S binding				
Basal	F=5.9*	F=1.2	F=0.1	
Net EC_{50}	F=9.5**	F=7.8*	F=0.02	HET/PNE**[2]
Net EC_{100}	F=7.2*	F=0.3	F=0.3	
[^{3}H]-Quinpirole dopamine agonist saturation binding kinetics				
K_d	F=20.0***	F=5.36*	F=5.2*	HET/PNE**[3]
B_{max}	F=0.0	F=0.0	F=0.4	

Table 5.1: Summary of overall results. Table shows F values and significance of two-way ANOVAs carried out for each experiment for main G × E effects as well as G × E interaction effects. For experiments with main effects, the table indicates significant post hoc effects. Notes: 1. WT/Sac was significantly different from HET/Sac and HET/PNE only. 2. HET/PNE was significantly different from WT/Sac only. 3. HET/PNE was significantly different from WT/Sac and WT/PNE and HET/Sac. (* *p<0.05*; ** *p<0.01*; *** *p<0.001*)

Relationship between STD and LTD

Cluster analyses of my data indicated that the HFS paradigm produces STD as well as LTD in all four G × E groups. Two distinct, but related, questions arise concerning these results. First, what accounts for the variability in the production of STD

and LTD for a given experiment (brain slice), and second what is the relationship between STD and LTD. Although these questions are incidental to the hypothesis, they address interesting aspects of the mechanisms of long-term synaptic plasticity and field potential summation.

As noted, experiments were performed with WT/Sac controls to determine whether the production of STD or LTD was not a function of the test to HFS stimulus intensity ratio. Although varying this ratio between ~0.3 and ~0.7 did produce a slight increase in the final PS amplitude, the correlation was extremely weak (see Results; Fig. 4.2). To minimize any possible contribution from the test to HFS stimulus intensity ratio, this ratio was set at 0.5 and was always within a range of ~0.4 to ~0.6.

Experiments were done with hemislices, and there were cases where, for example, the left hemislice produced LTD while the right hemislice produced STD or both produced LTD or STD. So the production of LTD or STD does not seem to be slice dependent.

It is possible that there are regional differences in the expression of STD and LTD within the striatum. Lovinger and colleagues (Partridge et al., 2000) found in voltage-clamped neurons from P16- P34 Sprague Dawley rats that HFS of the dorsomedial (DM) striatum was more likely to produce LTP whereas HFS of the dorsolateral (DL) striatum was more likely to produce LTD. My results were all from field potential recordings from P35-P50 mice and were predominantly in the DL striatum. There was considerable difference in developmental stage between these two studies with the mice used in my experiments being at a much later developmental stage than the rats in the previously published experiment (Partridge et al., 2000). Also, it is difficult to compare results obtained from single cells from whole-cell voltage-clamping to the mixed populations of cells that contribute to the field potentials in my research.

Another possibility is that the differences between STD and LTD could reflect differences in proportions of cortical and thalamic inputs to MSNs. It has been previously demonstrated that the glutamatergic input to MSNs is ~60% cortical and ~40% thalamic (Surmeier et al., 2007). Using an slightly oblique (~20 degree) horizontal slice, which permitted stimulating selectively cortical or thalamic inputs to individual voltage-clamped MSNs, Surmeier and colleagues found that cortical inputs had a PPR (50 ms

IPI) of ~1.2 and thalamic input cells had a PPR of ~0.8 (Ding et al., 2008). These researchers also found that repeated stimulus trains resulted in short-term enhancement of EPSCs for cortical inputs and depression of EPSCs for thalamic inputs. I found that the PPR of the PSs for all G × E groups was ~1.1 (Fig. 5.8) and, when these groups were further separated into populations using cluster analysis, I found one population with a PPR of ~1.2 (~1/3) and another with a PPR of ~1.0 (2/3) (Fig. 5.9). This indicates that while the inputs in my experiments are certainly a mixture of cortical and thalamic fibers, they are likely to be predominantly cortical, since the PPRs are closer to those found for cortical inputs. Importantly, I did not find a correlation between the PPR and the likelihood of producing LTD or STD in a given experiment. It seems unlikely that the differences between LTD and STD could be accounted for by differences between cortical and thalamic inputs.

As discussed in Appendix 2, the distribution of STD and LTD clusters is affected by the HFS paradigm used to induce long-term plasticity. Importantly, all of the experiments reported here used the same HFS paradigm and that paradigm is the most commonly used in previously published reports. It would be interesting to investigate in the future whether further distinctions among the G × E groups are revealed by using other HFS paradigms.

As stated in the introduction, MSNs make up ~90% of all neurons in the striatum and they are roughly evenly divided between those expressing D1Rs (direct pathway) and those expressing D2Rs (indirect pathway). Using whole-cell voltage-clamped neurons from transgenic mice labeled with bacteria artificial chromosome (BAC) either for direct or indirect MSNs, it was shown that only D2-type indirect neurons undergo endocannabinoid-dependant LTD following HFS (Kreitzer and Malenka, 2007). One possibility is that individual field potential experiments selectively target sub-populations of MSNs, which consist predominantly of D1R-or D2R-expressing neurons. Field potentials that included predominately D1R neurons would undergo STD and those including predominately D2R neurons would undergo LTD. However immunoreactive staining of 1 mm^2 sections to differentiate D1R and D2R expressing MSNs revealed a fairly homogenous distribution both types of MSN (Penny et al., 1986). Given that field

potentials sum responses of a large population of individual neurons, it is unlikely that selective STD or LTD responses could be due to sub-populations of D1R or D2R MSNs.

Another issue, which may be relevant to the relationship between STD and LTD, is the relative thresholds of glutamatergic and dopaminergic inputs necessary to obtain STD and LTD. As described in the introduction, striatal MSNs receive convergent glutamatergic input that depolarizes them and activates mGluRs as well as dopaminergic input that activates D2Rs. This convergent input is necessary to produce endocannabinoids that act pre-synaptically on CB1Rs, in order to initiate the induction of LTD. Lack of either sufficient glutamatergic or dopaminergic input would not allow sufficient production of endocannabinoids for the induction of LTD. According to this hypothesis, populations of cells, which lack sufficient glutamatergic or dopaminergic input, would undergo STD, but not LTD. For a given field potential experiment, the fEPSP depends on the location of the stimulating electrode and hence the population of MSNs whose potentials are summed. It is conceivable that some summed populations of MSNs may receive sufficient input to produce a population spike, but not sufficient input to induce LTD after HFS. Given that other options considered seem less likely, this seems to be the most promising possibility.

All experiments in all four G × E groups, exhibited an initial depression in the PS amplitude to ~20% of baseline (post-tetanic depression; PTD) whether the amplitude subsequently returned to baseline after 30 minutes (STD) or remained attenuated at near the level of the initial PTD (LTD). This suggests that STD and LTD may be causally related. The PTD is most likely due to short-term depletion of vesicles in the readily releasable pool (RRP) following HFS (Citri and Malenka, 2008). Pre-synaptically, it has been estimated that individual vesicle recycling can occur in as little as 30s (Ryan et al., 1993). Recycling a pool of vesicles following HFS may take longer, but it unlikely to take the 15-20 minutes that would be necessary to account for the recovery dynamics associated with STD. Post-synaptically, activity-dependent clathrin-mediated AMPA internalization and reinsertion has been extensively investigated (van der Sluijs and Hoogenraad, 2011). For example, in hippocampal cell cultures using fluorescent imaging, AMPA receptors were observed to rapidly internalize (<30s) followed by a slow return to baseline levels (~600s) when the stimulus was terminated (Ashby et al., 2004). There has

been little research on AMPA trafficking in MSNs to determine whether the same dynamics exist in this cell type. However we can speculate, given the fact that AMPA recycling following a stimulus takes ~10 minutes, that this may be a key mechanism involved in the dynamics of STD, since the recovery dynamics most closely align with those seen in STD in the four G × E groups. LTD has been shown to have a significant pre-synaptic component and could be superimposed on STD when sufficient glutamatergic and dopaminergic input leads to the production of endocannabinoids, which bind retrogradely to activate pre-synaptic CB1 receptors to suppress glutamate release. The model of the relationship of LTD and STD based on these considerations is illustrated in Fig. 5.1 below.

As noted in the Results, the WT/Sac group had a shorter time constant for STD than the other groups. This may indicate that as a result of the G × E factors and interactions, the rate of AMPA trafficking in MSNs has increased (Fig 4.7B). In the presence of D2R antagonists there were no distinct differences between groups (Fig. 4.7C), so although D2R antagonists affect LTD induction, they do not appear to alter the rate of AMPA trafficking. Interestingly, in the presence of CB1 antagonists, there was a surprising ~3 fold increase in the time constant for the HET/PNE group compared to other groups (Fig. 4.7D). The PS did recover to baseline 30 minutes after HFS, so CB1 antagonists were able to block LTD induction, but with a longer time constant. Binding of endocannabinoids on pre-synaptic CB1 receptors is considered the last step of the process which occurs in LTD induction. The fact that the HET/PNE group showed increased time constant could indicate that the rate of AMPA trafficking is slowed due to G × E factors and interactions, complementing the more modest time constant increases found for STD.

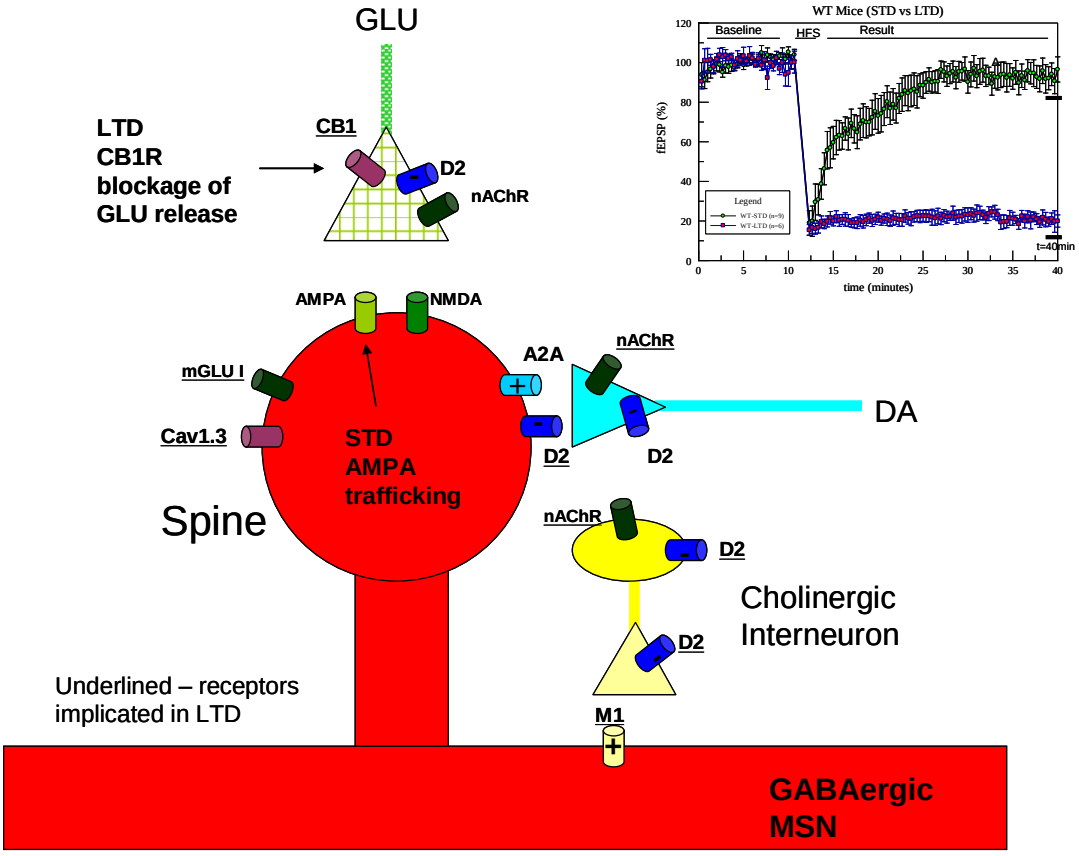

Figure 5.1: Model of relationship of STD and LTD. Following HFS, glutamate vesicles in the pre-synaptic RRP are depleted causing initial PTP. At the same time the HFS leads to activity dependent AMPA receptor internalization. STD is proposed to be due to the dynamics of AMPA internalization and membrane reinsertion. LTD is proposed to undergo the same PTP and AMPA internalization associated with STD. However, with sufficient glutamatergic and dopaminergic input, post-synaptic endocannabinoid production occurs with subsequent retrograde transmission to the pre-synaptic terminal where it binds to CB1 receptors causing a long-term decrease in glutamate release associated with LTD.

Changes in PPR for STD and LTD

Changes in PPR are often used as a measure of changes in the probability of transmitter release (P_R) in the presynaptic terminal in response to the second stimulus compared to the first stimulus (Citri and Malenka, 2008). Synapses with a high initial P_R, will be dominated by depletion of the RRP of vesicles resulting in PPD (Zucker and Regehr, 2002). By contrast, in synapses with a low initial P_R, the remaining residual Ca^{2+} from the influx of first stimulus will combine with the Ca^{2+} influx due to the second stimulus resulting in PPF (Zucker and Regehr, 2002). I compared changes in PPR before and after HFS, but did not find differences between STD and LTD populations in any of the G × E groups. This may indicate that PPR is not a sensitive enough marker of pre-

synaptic contributions to distinguish between STD and LTD. An increase in PPR has been found in striatal MSNs using a similar HFS protocol in whole-cell voltage-clamp recordings indicating a decrease in probability of release of glutamate in presynaptic terminals (Choi and Lovinger, 1997b). These researchers did not examine changes in PPR during STD. The fact that I did not observe similar changes using field recordings in the G × E groups could indicate that PPR may vary considerably within a population of neurons and this may obscure changes in PPR that occur at individual neurons. Regardless, my observation that CB1 antagonists depress LTD induction in WT/Sac controls, supports the consensus (Lovinger, 2010) that LTD induction in my experimental conditions results from a long-term decrease in presynaptic glutamate release due to retrograde transport of endocannabinoids to presynaptic terminals.

G × E factors and interactions impair induction of LTD in the striatum and decrease D2R affinity and/or receptor-effector coupling

I have shown that the combination of the HET genotype and prenatal nicotine exposure (G × E interaction) leads to an impaired D2R GPCR signaling resulting from decreased agonist affinity and possibly receptor-effector coupling of the D2R receptors. Impairment of D2Rs has also been implicated by the impaired ability to block LTD in the presence of D2R antagonists.

As outlined in the Introduction, the current understanding is that HFS-dependent LTD induction in the striatum is due to convergence of glutamatergic activation of MSNs, which depolarizes them causing the transition from the resting DOWN state with a membrane potential of ~-85 mV to an active UP state with a membrane potential of ~-55 mV with simultaneous dopaminergic input. Because blockade of either D2Rs or metabotropic glutamate receptors (mGluRs) prevents LTD induction in the striatum with the HFS paradigm, activation of both receptor types post-synaptically is necessary for this process to occur (Lovinger, 2010). The glutamate activation of mGluRs and dopamine activation of D2Rs independently contribute to the opening of $Ca_V1.3$ L-type Ca^{2+} channels and the subsequent production of endocannabinoids by the MSNs (Surmeier et al., 2007; Wang et al., 2006). These endocannabinoids diffuse retrogradely

to act on pre-synaptic CB1 receptors on glutamatergic terminals leading to long-term depression of glutamate release (Lovinger, 2010).

This role of D2Rs in striatal LTD is underscored by my findings that the combination of the HET genotype and prenatal nicotine exposure leads to a decreased affinity and signaling in one or more populations of D2Rs, and this appears to both impair the induction of striatal LTD and to reduce the relative magnitudes of both LTD and STD.

These observations raise two broad sets of questions. First, how do G × E factors mechanistically contribute to the changes in D2R affinity and/or receptor coupling? Since D2Rs are expressed in MSNs as well as dopaminergic and glutamatergic terminals and on cholinergic interneurons, we need to consider whether changes in D2R affinity and/or receptor coupling affect all or only a subset of these receptors. Second, how can changes in D2R affinity and/or receptor coupling as a result of G × E factors and interactions impair LTD induction? The two questions are addressed in consecutive sections below, which also include future directions that address and resolve distinct possibilities for each.

G × E factors and interactions decrease D2R affinity and/or receptor-effector coupling

I will consider here how these G × E factors and interactions could potentially alter D2R affinity and/or receptor-effector coupling, which in turn could lead to impairments of downstream signaling. As summarized in Figure 5.2, our results suggest that there is decrease in both D2R GPCR affinity and G-protein receptor-effector coupling ([^{35}S]-GTPγS binding assay results), but the number of receptors have not been significantly altered by the combination of HET genotype and prenatal nicotine exposure.

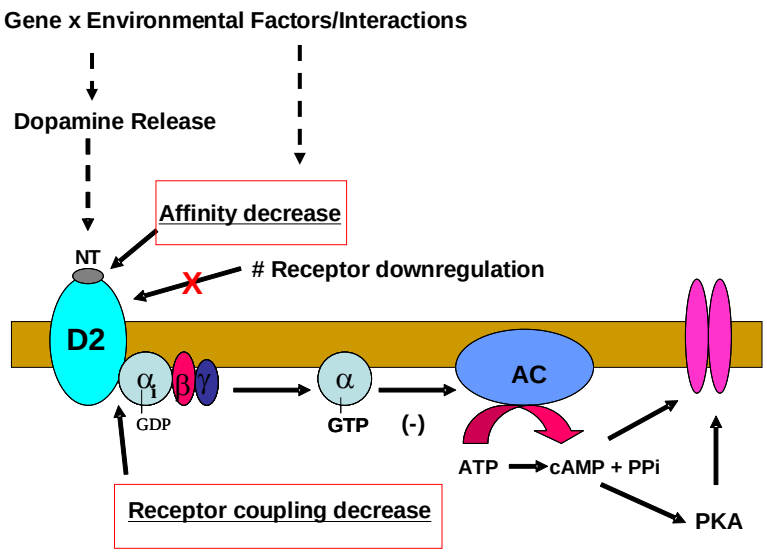

Figure 5.2: G × E factors and interactions alter D2R affinity and possibly receptor-effector coupling. The figure shows the basic layout of the D2R GPCR and coupled G proteins and downstream effectors to show that D2R affinity and/or receptor coupling has been decreased by G × E factors and interactions in the HET/PNE group compared to the WT/Sac group. These G × E conditions may alter dopamine release as well as alter other neurotransmitters and receptors to effect the changes in a developmental and/or use dependent manner.

One consideration is the role of the HET genotype in changes in D2R affinity. Preliminary evidence from *in vivo* microdialysis assays as discussed in the Introduction indicates that heterozygous *Snap25* null mutants (equivalent to HET/Sac group) have increased evoked extrasynaptic dopamine in the striatum compared to their wild type littermates (equivalent to WT/Sac group) (Fan, Wilson, Hess, unpublished observations). This suggests that the decreased expression of SNAP-25 in the HET/Sac group may result in enhanced dopamine release and this might act as a precondition for the decreased D2R agonist affinity/receptor-effector coupling and subsequent down-regulation of receptor signaling that is responsible for modulating striatal activity. These mice have decreased evoked extrasynaptic glutamate in the striatum compared to their wild-type littermates, which could also factor into the decrease in D2R agonist affinity, since NMDA, AMPA, and mGluR receptors are expressed on glutamatergic inputs to MSNs, and striatal dopamine release has been shown to be altered by changes in

glutamate release (David et al., 2005). Beyond these preliminary results, little is known about how developmental and/or use dependent changes, which occur with *Snap25* haploinsufficiency can effect glutamate and dopamine release in the striatum (Washbourne et al., 2002).

Another consideration is the role of prenatal nicotine exposure in changes in D2R affinity. As discussed in the Introduction, various subtypes of the nicotinic acetylcholine receptor (nAChR) are expressed in striatal glutamate and dopamine terminals, as well as on MSNs and cholinergic interneurons (Fig. 5.1) (Quik et al., 2007). Activation of these receptors can alter dopamine release onto MSNs (Threlfell et al., 2012). Nicotine-stimulated release of dopamine has been shown to be decreased in synaptosomes prepared from the striatum of adolescent rats prenatally exposed to nicotine (Gold et al., 2009). By down-regulating the nAChR modulation of dopaminergic terminals, the persistent effect of early nicotine exposure might be expected to lead to a down-regulation of dopamine release onto striatal MSNs. Importantly, nAChR antagonists have been shown to block LTD induction (Partridge et al., 2002) suggesting that prenatal nicotine may act on these nAChRs to additionally impact the induction of LTD through its effects on dopamine release leading to alterations in D2R affinity and/or receptor-effector coupling.

Deficiencies of SNAP-25 and persistent effects of prenatal nicotine exposure may, therefore, converge on dopaminergic transmission in the striatum. Preliminary microdialysis measurement suggest that the HET/Sac genotype leads to increases in dopamine release and decreases in glutamate release, while prenatal nicotine exposure leads to decreases in dopamine release. The results presented here indicate that neither the HET genotype (HET/Sac group) nor prenatal nicotine exposure (WT/PNE group) are associated with distinct differences in D2R affinity and/or receptor-effector coupling compared to controls. Only combined G × E factors and interactions produced reductions in affinity and/or receptor coupling. Thus, while the HET genotype and prenatal exposure to nicotine could have distinct effects on dopamine as well as glutamate release through different mechanisms, the interaction between these two conditions must affect the homeostatic regulation of dopaminergic signaling to result in a reduced affinity and/or receptor-effector coupling, which in turn can reduce downstream signaling of D2Rs.

Further research needs to be undertaken to determine how the combination of HET genotype and prenatal exposure to nicotine alters dopamine release and effects D2R affinity. A first step could be to perform *in vivo* microdialysis measurements in the four G × E groups to determine whether dopamine and glutamate efflux are enhanced or reduced in the HET/PNE group relative to the HET/Sac group.

Another important question regards the types of D2R receptors that are affected by the G × E interaction. The [^{3}H]-Quinpirole agonist saturation assay may indicated changes in the affinity of all D2-class receptors expressed in the striatum. Quinpirole, used to determine the K_d and B_{max} values, is a selective D2-class receptor agonist with affinity for all three D2-class receptor types: D2, D3, and D4 receptors (Seeman and Van Tol, 1994). Quinelorane used in the [^{35}S]-GTPγS binding assay is selective for D2Rs and D3Rs, but not D4Rs. As discussed in the Introduction, all D2-class receptors are expressed in MSNs in the dorsal striatum with D2Rs normally expressed ~2 fold higher than D3Rs and D4Rs combined (Surmeier et al., 1996). One interesting possibility is that our results reflect different changes in affinity or relative numbers of functional receptors for each of the D2-class receptor subtypes, so the K_d and B_{max} values determined represent values for the aggregate changes of the combination of all of these receptors, while the [^{35}S]-GTPγS binding assay represents possible alterations in D2Rs and D3Rs. These values are more likely due to changes in D2Rs, since they have the highest levels in expression, but a large change in affinity one of the other two subtypes could mask small changes in D2Rs. Some of the variability of the K_d and B_{max} values in individual experiments found in the Scatchard plots obtained from [^{3}H]-quinpirole saturation binding assays (see Appendix 2) could be reflective of different levels of individual D2-class receptor subtypes in striatal homogenates, which could alter these values in a given experiment if the changes predominantly occur in one subtype. In future experiments, specific D2R, D3R, and D4R agonists could be used in binding experiments to dissect this and determine if changes occur in all receptor subtypes or are predominant only in one type. S-sulpiride, used here as a D2R antagonist in the electrophysiology LTD induction experiments has a high affinity for D2R and D3R, but not D4R receptors (Seeman and Van Tol, 1994). So far, only D2Rs have been implicated as having a role in LTD induction, so impairment of LTD induction in the HET/PNE group relative to

controls seems to implicate D2Rs, and not D3Rs or D4Rs. This does not mean that D3Rs and D4Rs may not also be altered by these G × E factors and interactions.

As described in the Introduction, it is known that the D2 receptor can exist in either a state of low or high affinity for dopamine ($D2^{Low}$ or $D2^{High}$, respectively) and it is possible to determine the relative levels of each affinity state (Seeman et al., 2006). The $D2^{Low}$ state represents the condition where the D2R GPCR is uncoupled from the heterotrimeric protein ($G\alpha_{i/o},G_{\beta},G\gamma$) and the $D2^{High}$ state represents the condition where the D2R GPCR is coupled and this latter state is more readily able to bind dopamine and D2R agonists (van Wieringen et al., 2013). There are two alternative models that explain GPRC coupling interactions with G proteins prior to agonist binding (Hein and Bunemann, 2009). One model asserts that GPCRs and G proteins are not associated prior to agonist binding, only coupling upon agonist binding. An alternative model asserts that GPCRs and G proteins can stably associate with each other prior to agonist binding. There is evidence supporting both models, but no consensus on which if either is the predominate mode of coupling (Hein and Bunemann, 2009).

Using Scatchard analysis, I found K_d values for WT/Sac controls (K_d = 3.32 nM; Table 4.2) similar to those found in the literature using the same methods (Levant et al., 1992) and these were significantly decreased in the HET/PNE group (K_d = 7.13 nM; Table 4.2). A study using rat striatal homogenates using techniques that distinguish between dopamine binding to the $D2^{Low}$ and $D2^{High}$ affinity states found that about ~77% of D2Rs are in the $D2^{High}$ affinity state (K_d = 43 nM) versus the $D2^{Low}$ affinity state (K_d = 4.55 µM). The K_d values that I determined in the saturation assay most likely reflect values for $D2^{High}$ affinity states, since they are closest to those found for this state. One method to distinguish between $D2^{Low}$ and $D2^{High}$ affinity states involves using a competition binding assay for labeled D2 agonists [^{3}H]-raclopride or [^{3}H]-spiperone in the presence of a range of dopamine concentrations in either low or high NaCl tris-buffer (Seeman et al., 2005). The high affinity states are not detected in the presence of high NaCl, so the values and relative levels of low and high affinity states can be determined using this method. The D2R high affinity state is inhibited by Na^+, and promoted by Mg^{2+}, through their influence on the binding crevice associated with the D2R agonist binding site. Furthermore, the GPCR – G protein interaction is inhibited in the presence

of high levels of GTP (Hein and Bunemann, 2009) so the concentration of all of these factors must be taken into account when designing a binding assay. A shift towards a higher proportion of $D2^{Low}$ affinity states, as a result of the G × E interaction, could account for the results I observed, since the net effect would be an overall decrease in D2R affinity. The [^{3}H]-raclopride or [^{3}H]-spiperone competition assay could be performed to determine the relative amounts of $D2^{Low}$ and $D2^{High}$ affinity states in the four G × E experimental groups to determine whether there was a change in the relative levels of these states.

Finally, as described in the Introduction, it has been also shown that the D2 receptor has two isoforms, designated as the long D2L and short D2S isoforms, that are generated by alternative splicing., The former is differentiated by an additional 29 amino acids in the third intercellular loop (Usiello et al., 2000). The D2S is predominantly expressed pre-synaptically on glutamatergic, dopaminergic, and cholinergic terminals synapsing onto MSNs (Fig. 6.2) and D2L is expressed predominately post-synaptically on MSNs spines (Usiello et al., 2000). Additional experiments performed by cross breeding D2L null mice with the HET group, either exposed or not to prenatal nicotine, followed by repetition of the saturation binding assays that distinguish $D2^{Low}$ and $D2^{High}$ affinity states would distinguish changes in the D2 isoforms and thus indicate pre- vs. postsynaptic involvement.

Mechanisms of D2R activation, including desensitization in response to high levels of agonists, and subsequently resensitization when agonist exposure is reduced for (Beaulieu and Gainetdinov, 2011) have been extensively studied. A common mechanism for desensitization involves phosphorylation of an activated D2R by G protein-coupled receptor kinases (GRKs) followed by the recruitment of adapter proteins termed arrestins at specific sites on GPRC intracellular loops and COOH terminals. This leads to blockage of GPCR downstream signaling and/or receptor internalization (Beaulieu and Gainetdinov, 2011). One candidate kinase in the modulation of D2R signaling is GRK2, and GRK2 expression levels have been shown to be altered in animals with Parkinsonianism. In addition, cocaine treatment of GRK2 heterozygous mice produces hyperactivity that is associated with ADHD (Gainetdinov et al., 2004). Another important family of G protein modulators that play a role in D2R agonist binding are the regulators

of G protein signaling (RGSs), which help regulate the rate of G protein hydrolysis and thereby turn off G protein signaling,. RGS9-2 has been recently shown to be involved in regulating the responses to psychostimulants upon agonist binding to D2Rs (Beaulieu and Gainetdinov, 2011). However, although both ligand binding sites and potential residues involved in phosphorylation of both D2L and D2S GPCR isoforms particularly in the third intracellular loop are known, little is known about how binding of these sites either by ligands or phosphorylation by kinases is linked to changes in D2R affinity or receptor-effector coupling (Vallone et al., 2000). Protein kinase A (PKA) and protein kinase C (PKC) also have phosphorylation sites, which may be involved in desensitization of D2Rs (Beaulieu and Gainetdinov, 2011). There is evidence that D2Rs may expressed as either dimers or tetramers with the consequence that the binding of agonist to the first receptor leads to negative cooperativity and reduced binding of subsequent receptors (Seeman et al., 2006), The Hill coefficient of 0.314 that I found in the WT/Sac control experiment for the [^{35}S]-GTPγS binding assays (Results; Fig 4.10) may be indicative of this process and further follow-up experiments on the four G × E groups might reveal if this is the case. While I have demonstrated that these G × E factors and interactions can reduce affinity and/or receptor-effector coupling in D2Rs, and it is recognized that GRK/arrestin signaling may play a role in alterations in these processes, it still remains to be determined which signaling pathways are linked to alterations in affinity and/or receptor-effector coupling. Primary research, which links changes in affinity of D2Rs to the phosphorylation of specific D2R sites, would contribute to a fuller understanding of this process.

G × E factors and interactions impair induction of LTD in the striatum

As a result of genetic, environmental and gene-environmental interactions, the HET/PNE group showed a significant decrease in the ability of D2R antagonists to impair LTD induction and this effect was not observed in the presence of a CB1 antagonist (Table 5.1). As discussed, reductions in D2R affinity and/or receptor-effector coupling were revealed by the [^{3}H]-quinpirole agonist binding and [^{35}S]-GTP-γ-S binding experiments, although it cannot be ruled out that there were parallel changes in D3Rs or D4Rs affinity (though the [^{35}S]-GTP-γ-S results using quinelorane don't implicate D4Rs

since it is not specific for D4Rs). As noted, S-sulpiride, used as a D2R antagonist in the electrophysiology experiments is a selective D2-class receptor antagonist with affinity for two of the three D2-class receptor types: D2R and D3R, but not D4 receptors (Seeman and Van Tol, 1994). Since only D2Rs have been implicated in the LTD induction process, the significant decrease in the ability of the antagonist S-sulpiride to impair LTD must be primarily through its effects on D2Rs, although it may also have effects on D3Rs. However, I will limit the remaining discussion to effects on D2Rs.

As discussed in the Introduction, the precise role D2Rs in the induction of LTD in the striatum has not been fully established, because the D2Rs involved in the induction process may be found alternatively on MSN spines (Fig. 5.3; path1) or associated with cholinergic interneurons (Fig 5.3; path2). Since MSNs are the predominant neuron in the striatum the changes in affinity and possibly receptor-effector coupling for D2Rs, associated with the impairment of the induction of LTD, most probably reflects D2Rs associated with MSN spines (Fig 5.3; red M). However, this does not preclude the involvement of D2Rs associated with cholinergic interneurons (Fig 5.3; red C) or glutamatergic and dopaminergic inputs (Fig. 5.3; red *) which could also undergo changes in affinity and receptor-effector coupling.

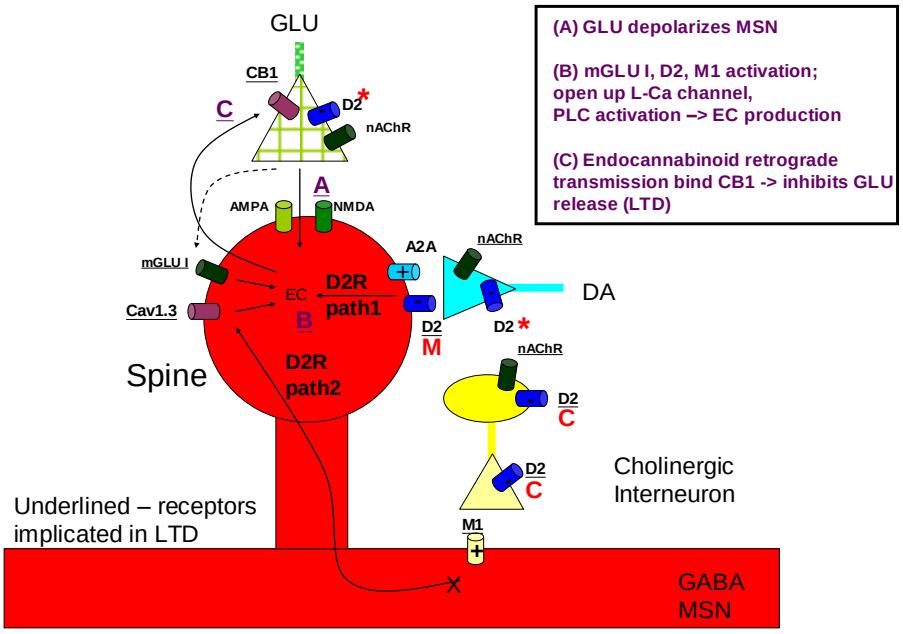

Figure 5.3: D2Rs involved in LTD induction of Striatal MSNs. The figure illustrates the circuit on a MSN spine associated with induction of LTD (glutamatergic and dopaminergic inputs to MSNs) along with cholinergic interneurons. Potential pathways for LTD induction are shown and described in the inset. The two paths in which D2Rs may be involved in LTD induction are shown. Locations of D2Rs associated with MSNs (red M), cholinergic interneurons (red C) as well as glutamatergic and dopaminergic inputs (red *) in the LTD induction pathway are shown.

Impairment of the induction of LTD in the striatum in the HET/PNE group and coincident alterations in D2R affinity and possibly receptor-effector coupling suggests that the role of D2Rs in the induction process has been altered. In the presence of saturating levels of D2R antagonist, available D2Rs should be blocked thereby preventing dopamine-dependent endocannabinoid production associated with LTD. In the presence of a D2R antagonist the HET/PNE group only recovered by ~0.6 – 0.7 fold compared to the other groups. The attenuation in recovery when D2R binding is blocked suggests that endocannabinoids are produced in HET/PNE mice independent of the D2R-dependent pathway. This demonstrates that the G × E interaction during brain development selectively affects the D2R-mediated, but not the CB1-mediated response to HFS in the HET/PNE group suggesting that endocannabinoid release has been decoupled from D2R involvement in LTD induction these animals. This implies that the reduction in

D2R affinity and possibly receptor-effector coupling has impaired the signaling pathway downstream from D2Rs that culminates in the production of endocannabinoids (Introduction; Fig. 1.4). Downstream signaling from both mGluRs and D2Rs have been implicated in the production of endocannabinoids. One possibility is that mGluRs in the HET/PNE group are able to induce LTD independent of D2R input, due to the developmental or used-dependent changes introduced by these G × E factors and interactions. Bath application of mGluR agonists has been shown to induce LTD in MSNs and this LTD was enhanced in the presence of a sufficient concentration of D2R agonists (Kreitzer and Malenka, 2005) suggesting that the inputs to these receptors work synergistically in the induction of LTD. An important follow-up experiment would be to test how the four G × E groups respond to the application of an mGluR agonist in the presence or absence of a D2R antagonist. If both mGluR and D2R receptors work synergistically, we would expect induction of LTD to occur selectively in the HET/PNE group in the presence of a D2R antagonist.

Implications for neuropsychiatric disorders

As discussed in the Introduction, the *SNAP25* gene is a candidate susceptibility gene for both ADHD and schizophrenia, and prenatal exposure to nicotine has been shown to be a significant risk factor for ADHD. Recently behavioral research to assess spontaneous locomotor activity and social interaction using the same G × E experimental groups were published in conjunction with the main findings presented here (Baca et al., 2013). A major behavioral finding of that research is that the HET/PNE group, but not the HET/Sac group, showed hyperactivity with respect to WT/Sac controls indicating that G × E factors and interactions are critical to this hyperactivity. Another finding of that study was that the HET/PNE group showed impairments in social interaction, which may be relevant to mouse models associated with schizophrenia. The SNAP-25 haplodeficient *coloboma* mouse mutant is a well established model of ADHD, since it displays hyperactivity, ameliorated by amphetamine, as well as inattention and impulsivity (Fan et al., 2012) and our previous study was in part aimed at extending the *coloboma* model by showing that both *Snap25* haploinsufficiency and prenatal nicotine exposure are necessary for this hyperactivity. Importantly the amphetamine responsiveness was shown

to be ameliorated through D2Rs and not D3Rs and D4Rs (Fan et al., 2010). The *coloboma* mouse mutant microdeletion contains *Snap25* plus 10 or more additional genes (Hess et al., 1994), indicating that these other genes may contribute to the underlying behavioral endophenotype. Together, these studies might provide a genetically defined mouse model that may contribute further to our understanding of the crucial role played by gene-environmental interactions in neuropsychiatric illnesses, such as depressive disorders, ADHD, schizophrenia, obesity, and substance abuse (Wermter et al., 2010).

Given that the *SNAP25* gene is a candidate susceptibility gene for both the neuropsychiatric disorders ADHD and schizophrenia, and that prenatal nicotine has been shown to be a significant risk factor for ADHD, a natural follow-up is to explore the implications of these G × E factors in synaptic plasticity that is associated with known brain regions and receptors associated with these disorders. As discussed in the Introduction, there is growing evidence for the influence of long-term synaptic depression in the striatum being linked to learning and behavior (Lovinger, 2010; Yin et al., 2009) with possible links to these disorders. The electrophysiological and affinity findings reported here may align with the hyperactivity and impairments in social interaction, which have been found to be associated with the same G × E factors and interactions. An interesting follow-up would be to determine if *coloboma* mouse mutants show similar reductions in D2R affinity and impairments in LTD induction in the striatum.

Significant genetic association has been reported between ADHD and single nucleotide polymorphic (SNP) variants of *SNAP25* (Faraone et al., 2005). The involvement of both the protein and gene for SNAP25 in dopaminergic transmission suggests that alterations in *SNAP25* gene regulation and expression along with environmental factors may confer susceptibility to these disorders by affecting synaptic plasticity in the striatum may underlie the aberrations of behavior seen in ADHD and other psychiatric disorders such as schizophrenia. Follow up work to this research could examine whether other identified G × E factors in ADHD and other neuropsychiatric disorders are associated with similar reductions in D2R affinity and impairments of LTD induction. As shown in this research, the use of targeted mutations as well as challenges with identified environmental factors can be an important tool to dissecting the

mechanisms that may underlie specific behaviors associated with neurocognitive disorders.

Future directions

The results of this study support the overall hypothesis that G × E factors and interactions, which result from *Snap25* haplodeficiency and prenatal nicotine exposure in mice, lead to long-term impairments in D2 receptor affinity and possibly receptor-effector coupling in striatal MSNs with resultant impairments in the process of striatal LTD induction. The Discussion includes consideration of several important questions that should be addressed in future studies. The following section highlights three additional issues that are central to the interpretation of the results of this study, but were not previously considered. I have proposed specific hypotheses that address these issues, which are consistent with the findings in this research, and finally outline experiments that could be carried out to test them.

One of my central findings was that cluster analysis following application of the 100 Hz HFS induction paradigm yielded distinct STD and LTD clusters in all four G × E groups (Fig 4.3). Generation of these two clusters was not unique to this induction paradigm, since alternative induction paradigms, such as the 10 Hz and 30 Hz paradigms reported in Appendix 2, also resulted in distinct STD and LTD clusters. Importantly, field potential recordings sum the extracellular fields from a population of neurons so the observation of STD or LTD indicates that the majority of neurons at the recording site in each hemi-slice expressed one or the other of these distinct forms of long-term plasticity. I considered that there could be regional differences in the potential to induce STD and LTD stemming from a preponderance of cortical over thalamic inputs or the distribution of D1R or D2R expressing MSNs and that these regional differences could account for the observed clusters, but as I have already discussed there are inconsistencies with each of these explanations when applied to the observed data. Another possibility is that the distinct STD and LTD clusters may be due to a threshold effect in which a simultaneous convergence of glutamatergic and dopaminergic inputs onto a population of MSNs is necessary to produce sufficient endocannabinoid feedback to allow the transition from

STD to LTD to occur. Given that glutamatergic input is a necessary precondition to depolarize MSNs from the DOWN state to the UP state and that this is a necessary requisite for PTD, which was consistently observed, it appears that sufficient glutamatergic input exists in the majority of slices. However, Lovinger and colleagues, using high-speed chronoamperometry measurements of dopamine release in striatal slices, found that a one second 100 Hz paradigm produced highly variable dopamine outputs of 42.8 ± 21.3 μM (Partridge et al., 2002). Thus I hypothesize that: *the HFS paradigm will induce a transition from STD to LTD when a sufficient amount of dopamine release converges with the glutamate-driven depolarization of MSNs in order generate endocannabinoid production that exceeds a critical threshold.*

To test this hypothesis, I suggest performing the 100 Hz HFS paradigm in field potential slice recordings on WT mice while simultaneously using chronoamperometry to measure dopamine release. I predict that LTD induction will correlate with higher tissue dopamine concentrations and STD with lower dopamine concentrations in a given slice. If these preliminary findings prove to be consistent with my hypothesis, a follow-up experiment would be to perform the LTD induction experiments in the presence of various concentrations of a dopamine agonist to determine if a particular agonist level leads exclusively to the production of LTD. These findings would be strong support for the hypothesis of an endocannabinoid threshold as the basis of the STD to LTD transition.

As I showed in Fig. 4.5, in the presence of a D2R antagonist, all G × E groups exhibited only a single cluster that recovered to baseline within 40 minutes. However, the HET/PNE group, but not the HET/Sac group, exhibited significantly less recovery to baseline following HFS than the WT/Sac control group. Additionally, I showed in Fig. 4.3 that the HET/PNE showed a less robust LTD than the WT/Sac control group. This indicates that in the G × E condition, the induction of LTD is impaired by a process involving D2Rs. As was previously discussed, the nicotine-stimulated release of dopamine is decreased in synaptosomes prepared from the striatum of adolescent rats prenatally exposed to nicotine (Gold et al., 2009). Using an adenovirus carrying a cre-inducible channelrhodopsin gene targeted to cholinergic interneurons, Cragg and

colleagues (Threlfell et al., 2012) were able to demonstrate that cholinergic interneurons can directly activate dopamine release through nAChRs expressed on dopaminergic terminals. Additionally, nAChR antagonists have been shown to block LTD induction (Partridge et al., 2002) suggesting that prenatal nicotine may act on nAChRs to impact the induction of LTD by altering dopamine release with compensatory alterations in D2R affinity. Through epigenetic factors, the prenatal action of nicotine on nAChRs on dopaminergic terminals could lead to persistent down-regulation of dopamine release onto adult striatal MSNs. Thus I hypothesize that: *prenatal nicotine exposure combines with the HET genotype to account for the impairments found in LTD induction through a reduction in nAChR stimulated dopamine release from nAChRs expressed on dopamine terminals that synapse onto MSNs.*

To test this hypothesis, I propose measuring nAChR-dependent dopamine release in striatal homogenates in response to a nAChR agonist by measuring [^{3}H]-dopamine in the four G × E groups as has previously been described (Gold et al., 2009). Briefly, striatal homogenates from each G × E group are incubated in [^{3}H]-dopamine, and then separate samples are perfused with different concentrations of nAChR agonists including ACh as well as agonists specific for α4β2 and α6β2 type nAChR receptors, and then dopamine release is measured in terms of scintillation counts. A follow-up nAChR agonist stimulated ^{86}Rb efflux assay could also be undertaken on the same set of tissue samples to determine changes in agonist binding of the nAChR receptor for the four G × E conditions (Gold et al., 2009). I would expect reduced nAChR binding to be associated with reduced nAChR agonist induced dopamine release. Additionally I propose to perform the LTD induction paradigm in the presence of a nAChR agonist. I would expect that, if nAChR activation facilitated dopamine release, then LTD induction would be partially restored in the presence of the nAChR agonist in the HET/PNE group toward that which was found with WT/Sac controls. The caveat of course being that the reduced D2R affinity in the HET/PNE group might preclude full restoration of LTD. These experiments would support the specific hypothesis that prenatal nicotine exposure alters nAChR-dependent dopamine release in the adult striatum. Testing specific epigenetic factors that might be involved would be an important extension of these findings.

My single [^{35}S]-GTPγS binding assay, performed on WT/Sac controls over a range of agonist levels (fig 4.10), produced a Hill coefficient of 0.314, which is indicative of a negative cooperativity in the binding of dopamine to D2Rs. Negative cooperativity is consistent with D2Rs making receptor-receptor interactions such as dimers or tetramers that allow for steric interactions between agonist binding sites. In some models of D2R activity, this form of negative cooperativity is thought to be a normal process in D2R agonist activation (Seeman et al., 2006). Thus I hypothesize that: *binding of dopamine to striatal D2Rs is characterized by negative cooperativity, and G × E factors and interactions can alter the degree of this negative cooperativity.* This hypothesis explains my observation that D2Rs in the HET/PNE group had reduced affinity to be a result of an interaction of adjacent binding sites rather than a change of affinity of individual sites.

To test this hypothesis, I propose undertaking [^{35}S]-GTPγS binding assays on the four G × E groups across a range of agonist levels to obtain more complete specific binding data in order to generate Hill plots and associated Hill coefficients for the four G × E groups. If a negative Hill coefficient is found in all four groups, it would be consistent with this negative cooperatively model of reduced agonist binding of the receptors as would be anticipated for a dimerized (or multireceptor complex). In comparing the four G × E groups, I would expect a greater reduction in the Hill coefficient in the HET/PNE group relative to controls, which would be consistent with the reduction in affinity found in the HET/PNE group that I observed by Scatchard analysis of the [^{3}H]-quinpirole saturation binding assays (Table 4.2).

Appendix 1- Saturation Isotherms and Scatchard Plots for [^{3}H]-Quinpirole D2R agonist saturation experiments in four G × E experimental groups

A series of Bradford assays were performed on striatal brain homogenates (two male and two female striata) for each sample in the four G × E experimental groups as described in the methods section. Protein quantification of these samples is shown below in Table A1.1.

Sample	WT/Sac	WT/PNE	HET/Sac	HET/PNE
#1	2.0675	1.8889	2.5437	1.8889
#2	1.6508	2.0080	1.5913	2.5437
#3	1.5318	1.8294	1.8294	1.7699
#4	1.7104	1.4127	1.7699	2.1865
#5	1.5318	1.7104	1.5913	2.1270
Mean	1.698	1.770	1.865	2.103
SEM	0.099	0.101	0.176	0.134

Table A1.1: Protein quantification of each sample in four G × E experimental groups using Bradford assays measured in (µg protein /µl)

The [^{3}H]-Quinpirole D2R agonist saturation binding experiments were carried out as described in the Methods in which Scatchard analysis was used to determine the K_d and B_{max} values for the four G × E experimental groups as described in the Results. In order to perform the Scatchard analysis, a series of saturation isotherms were developed from the data. Specific binding was determined by subtracting the non-specific binding at a particular agonist concentration in the presence of a D2 specific antagonist spiperone (50 µM) from the total binding at a particular agonist concentration in triplicate. Saturation isotherms were developed by converting specific binding scintillation counts for specific agonist levels (total binding minus non-specific binding as described) as well as total and non-specific binding from scintillation counts. Radioligand concentrations were also converted from scintillation count measurements. The formulas used to

calculate specific binding (total and non-specific also) and the radioligand concentrations is shown below. These calculations use standard methods determining binding and ligand concentrations from scintillation counts. I utilized the Perkin-Elmer technical resource associated with the [^{3}H]-Quinpirole to perform the calculations listed below (http://www.perkinelmer.com/Resources/TechnicalResources/ApplicationSupportKnowledgebase/radiometric/calculations.xhtml).

Specific binding is calculated as:

(This equation was also used to convert total and non-specific binding from scintillation counts)

Where: Specific Binding (as well as total & non-specific binding) = converted scintillation counts measured in fM/mg protein; RLC = radioligand concentration = converted scintillation counts of ligand concentration measured in nM; SA = specific activity of the [^{3}H]-Quinpirole as measured by manufacturer (Perkin Elmer)= 41,900 Ci/M (Ci = curie = $2.2*10^{12}$ scintillation counts); Incubation volume = 300 µl = 0.0003 l; mg protein in sample = values obtained for each sample from Bradford assay (Table A1.1)

Next, Scatchard plots are made by plotting the ratio of specifically bound ligand to free ligand as a function of the ligand concentration based upon the specific binding and radioligand concentrations calculated as shown above.

Bound/Free = Specific Binding/RLC

The Scatchard plot allows a linear regression to be made for the data using the Michaelis-Menten equation:

Where: [B] = Bound ligand (specific binding as calculated above); [F] = Free ligand (radioligand concentration as calculated above); B_{max} = Estimated maximum binding of ligand for receptor (fmol/mg protein); K_d = Dissociation constant, estimated ligand concentration where binding of receptor is ½ of maximum value (nM)

Transforming this equation yields a linear equation:

Thus: B_{max} = X intercept ([B]/[F] =0); K_d = -1/slope of the line

Linear regression was used to produce Scatchard plots based on the plots of the ratio of bound/free ligand versus specific bound ligand fraction in order to obtain the K_d and B_{max} values for each sample in the four G × E experimental groups.

Sample	WT/Sac	WT/PNE	HET/Sac	HET/PNE
#1	4.947	3.956	5.841	6.166
#2	2.639	1.973	2.565	7.591
#3	3.589	5.371	4.251	5.775
#4	2.343	2.603	4.821	6.901
#5	3.092	2.836	5.331	9.205
Mean	3.322	3.348	4.562	7.128
SEM	0.458	0.599	0.565	0.606

Table A1.2: K_d values of each sample in the four G × E experimental groups using Scatchard analysis measured in (nM).

Sample	WT/Sac	WT/PNE	HET/Sac	HET/PNE
#1	163.6	150.8	161.1	114.2
#2	143.4	83.3	70.6	129.4
#3	105.1	159.1	120.9	85.2
#4	80.5	146.8	143.8	134.4
#5	95.7	100.0	142.7	134.1
Mean	117.7	128.0	127.8	119.5
SEM	15.5	15.2	15.7	9.3

Table A1.3: B_{max} values of each sample in the four G × E experimental groups using Scatchard analysis measured in (fmol/mg protein).

Below are presented plots of total, non-specific and specific binding as a function of [^{3}H]-Quinpirole concentration (left) and plots of the ratio of bound/free ligand versus specific bound ligand fraction (right) for each sample in the four G × E experimental groups consecutively, by which the K_d and B_{max} values were calculated.

Since linear regression was used to produce the Scatchard plots based on the plots of the ratio of bound/free ligand versus specific bound ligand fraction, the linear regression R^2 fitting parameters are listed below for each sample in the four G × E experimental groups.

Sample	WT/Sac	WT/PNE	HET/Sac	HET/PNE
#1	0.53	0.51	0.74	0.66
#2	0.67	0.70	0.63	0.55
#3	0.60	0.70	0.54	0.63
#4	0.69	0.73	0.68	0.60
#5	0.61	0.58	0.52	0.68
Mean	0.62	0.64	0.62	0.62
SEM	0.06	0.10	0.09	0.05

Table A1.4: Linear regression fit R squared values of each sample in the four G × E experimental groups.

WT/Sac Sample #1

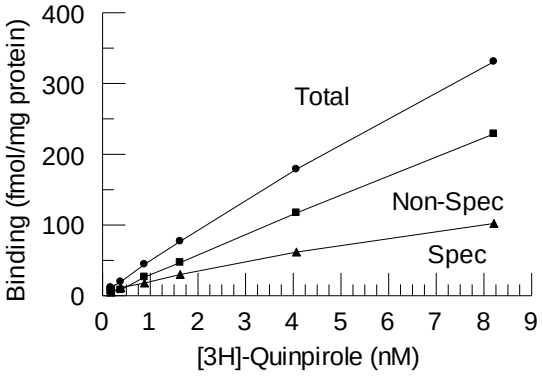

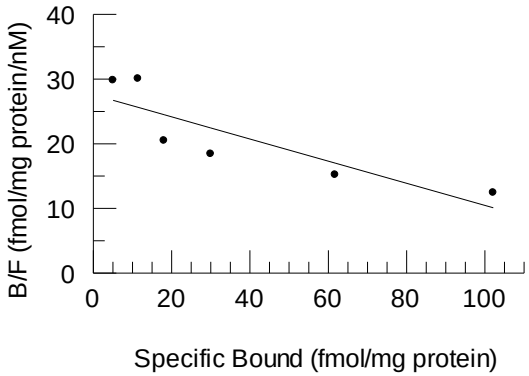

WT/Sac Sample #2

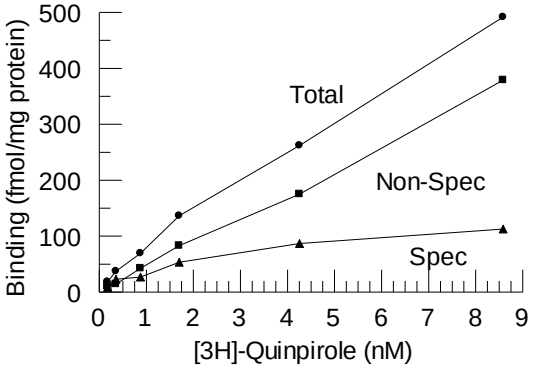

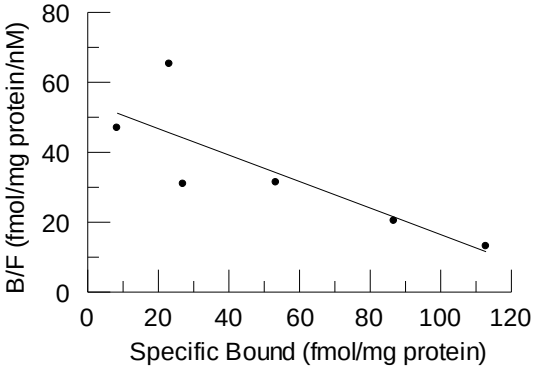

WT/Sac Sample #3

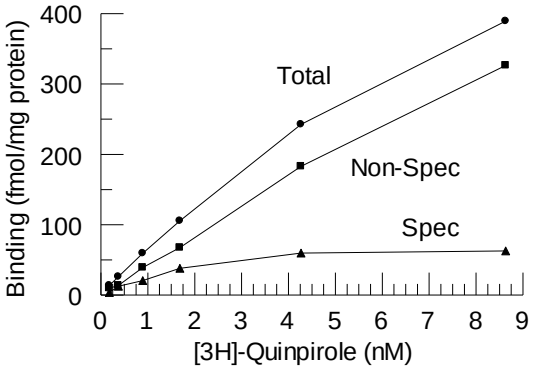

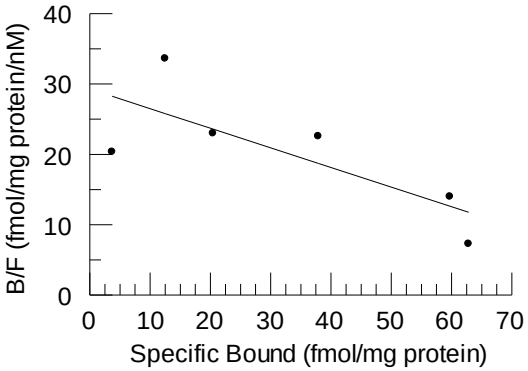

WT/Sac Sample #4

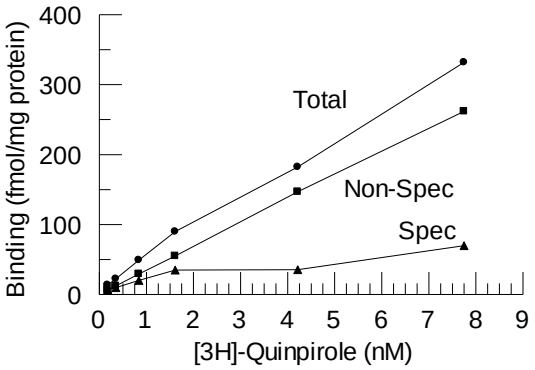

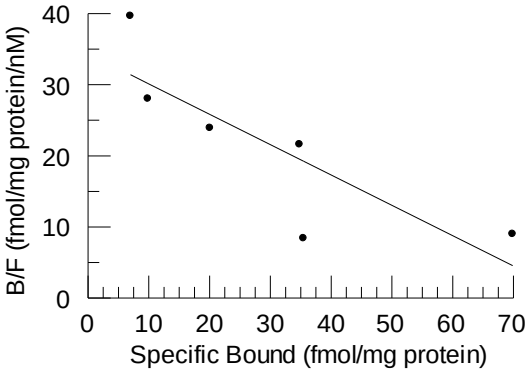

WT/Sac Sample #5

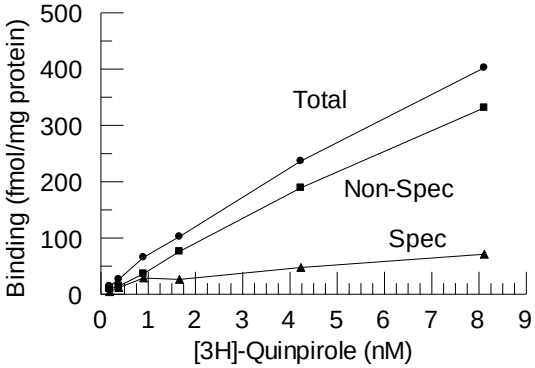

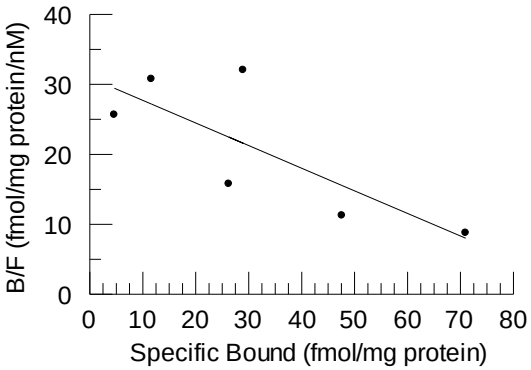

WT/PNE Sample #1

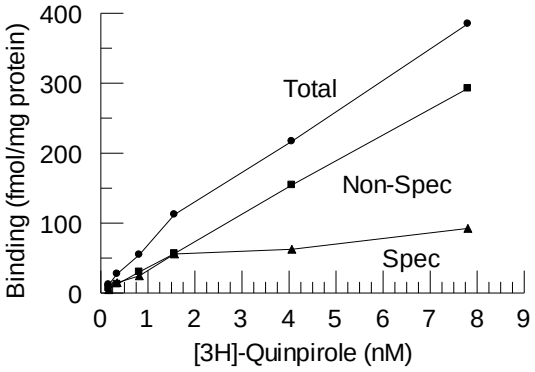

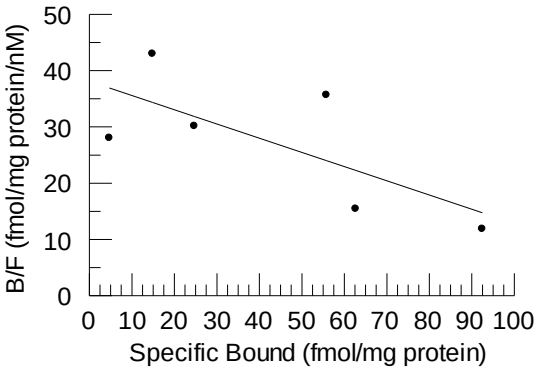

WT/PNE Sample #2

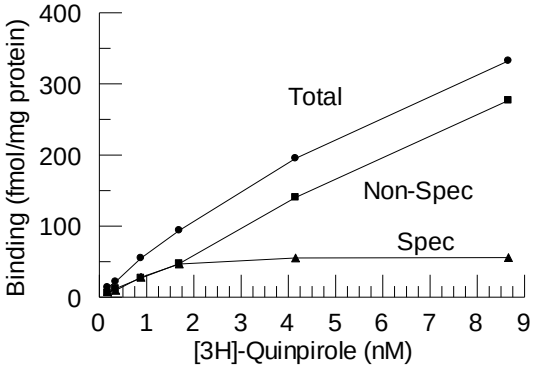

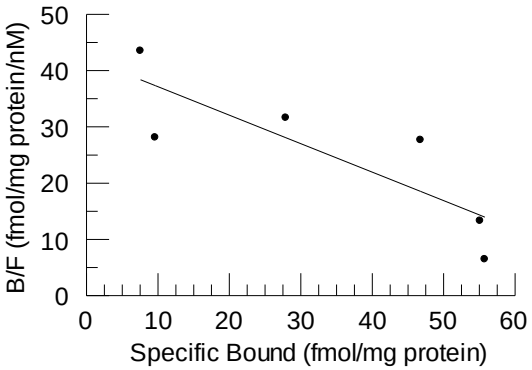

WT/PNE Sample #3

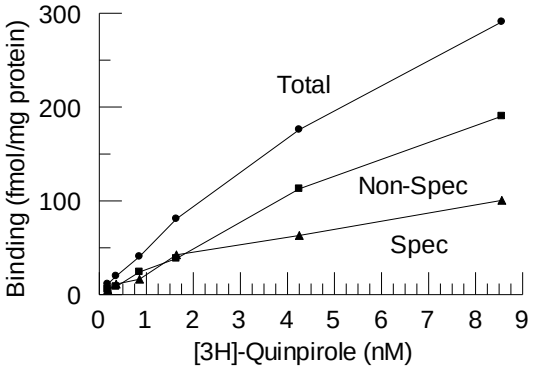

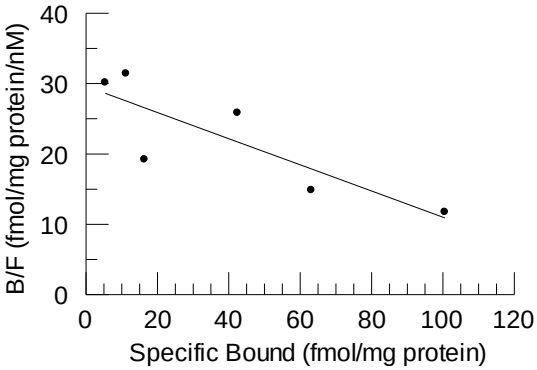

WT/PNE Sample #4

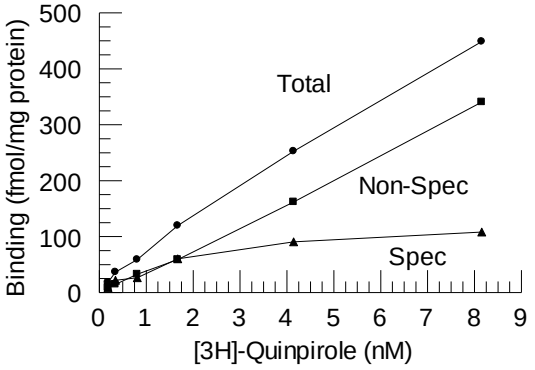

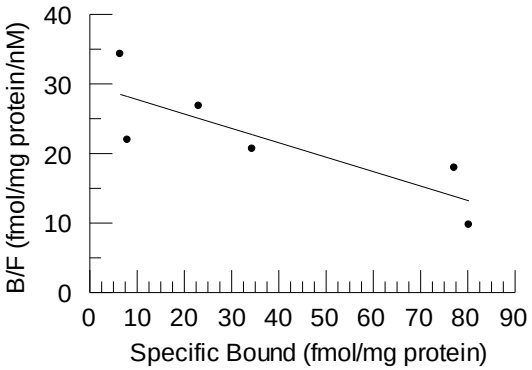

WT/PNE Sample #5

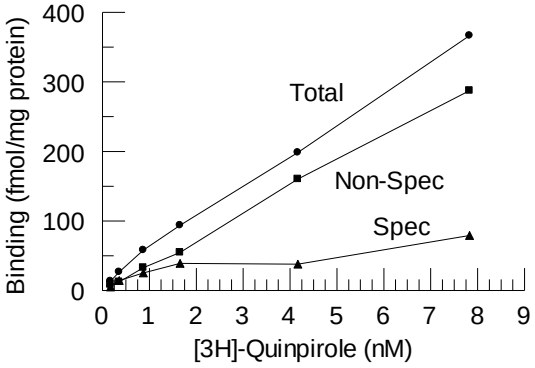

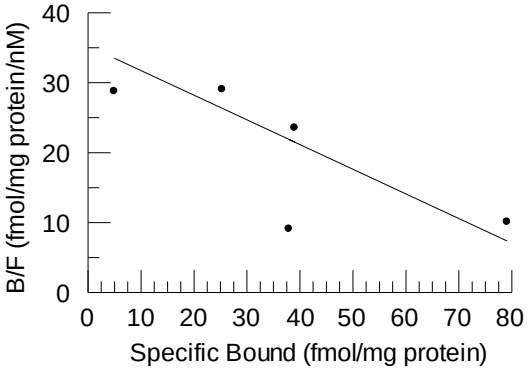

HET/Sac Sample #1

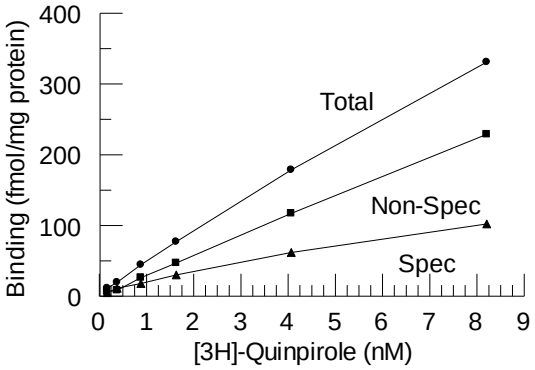

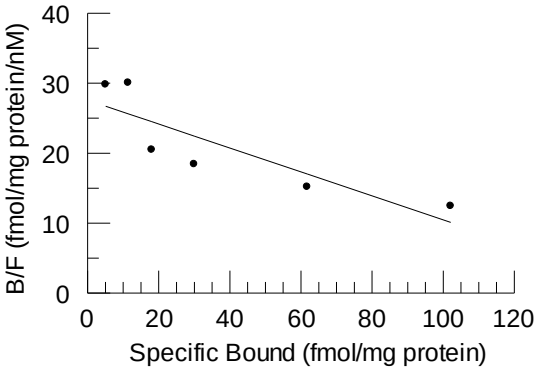

HET/Sac Sample #2

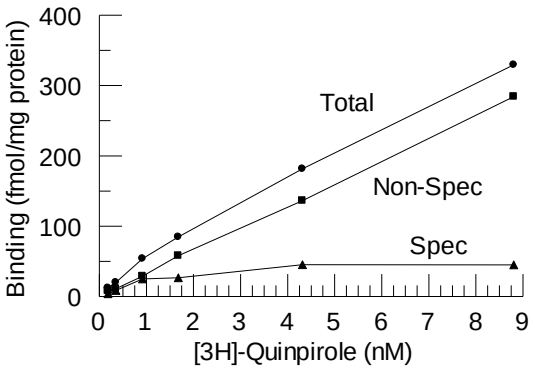

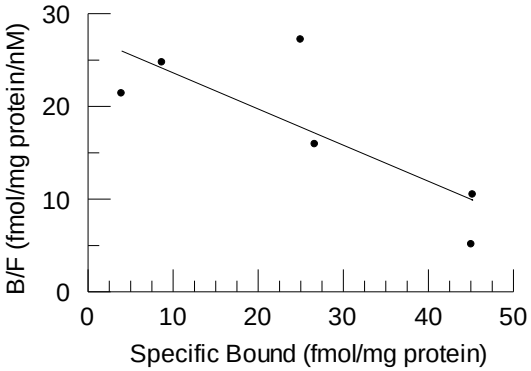

HET/Sac Sample #3

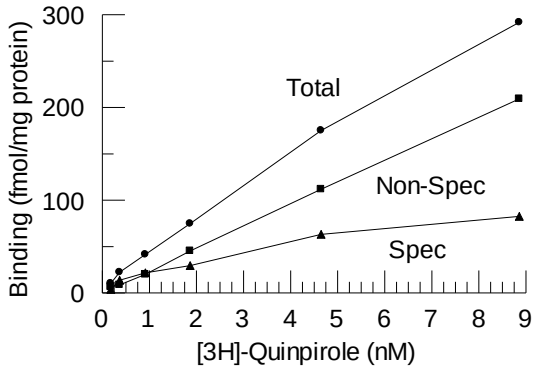

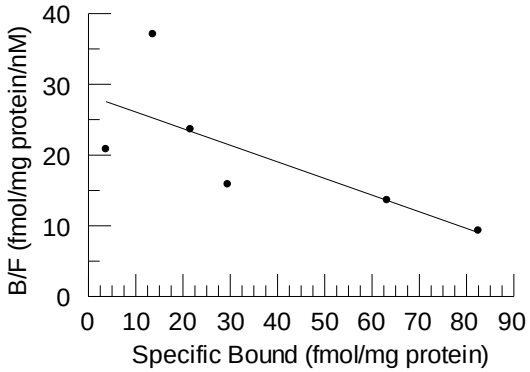

HET/Sac Sample #4

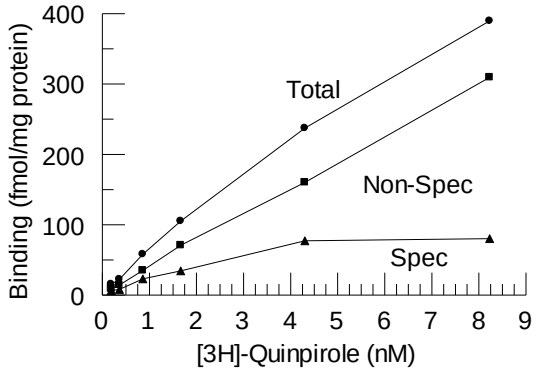

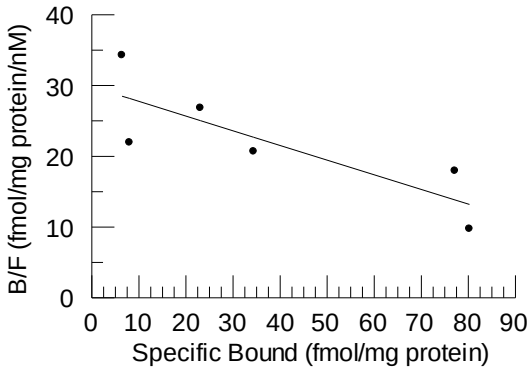

HET/Sac Sample #5

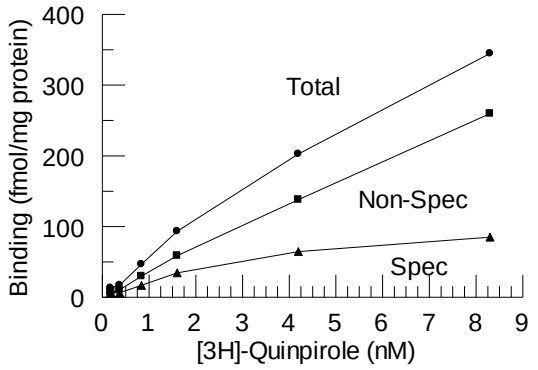

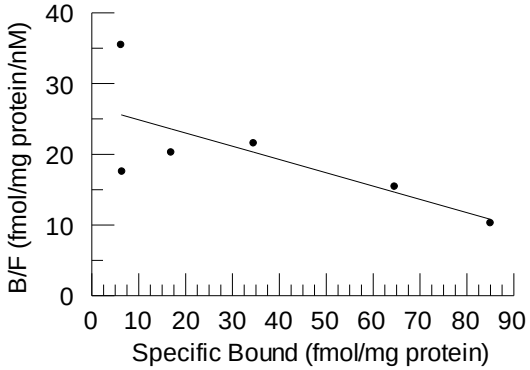

HET/PNE Sample #1

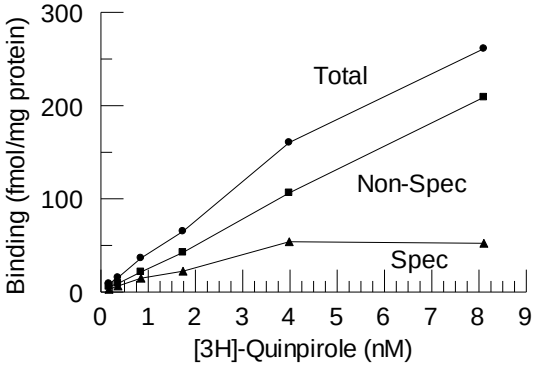

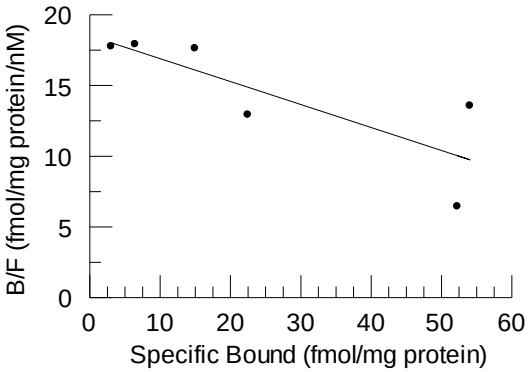

HET/PNE Sample #2

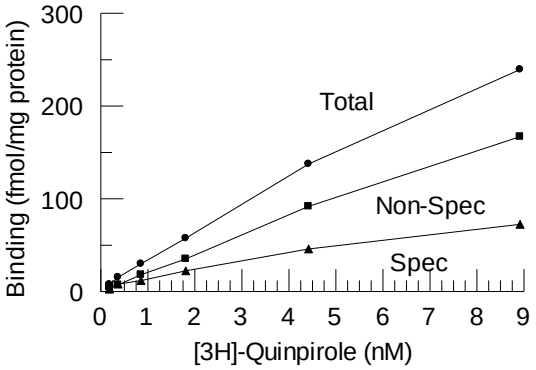

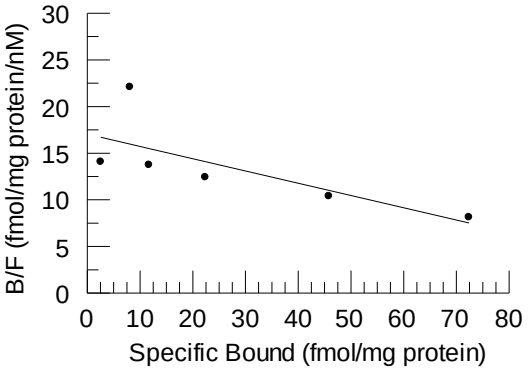

HET/PNE Sample #3

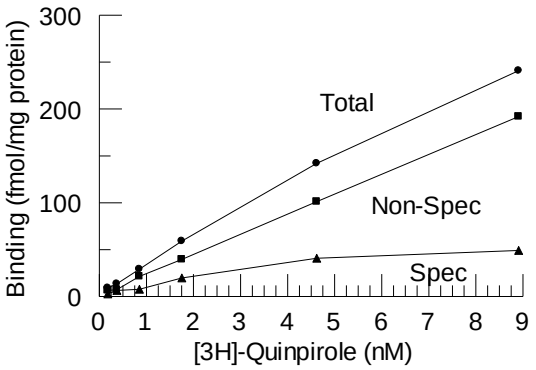

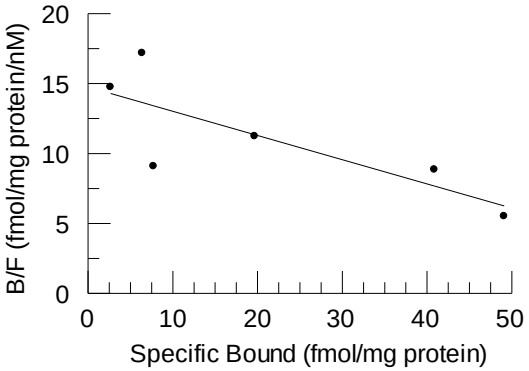

HET/PNE Sample #4

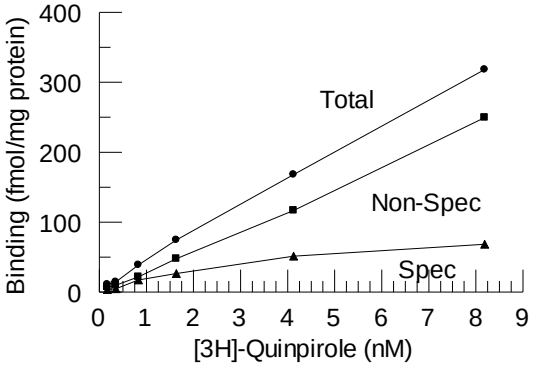

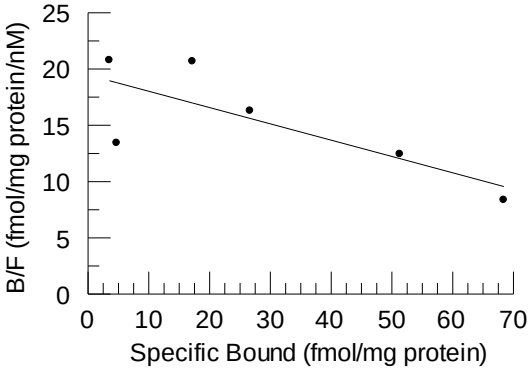

HET/PNE Sample #5

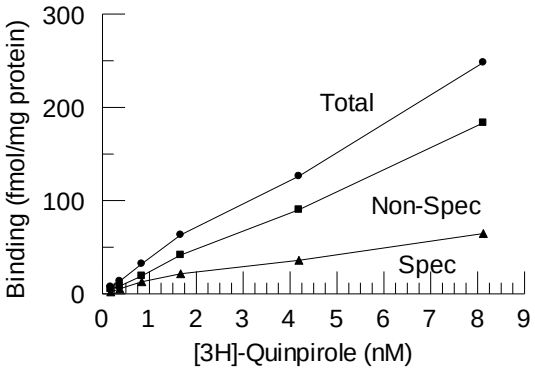

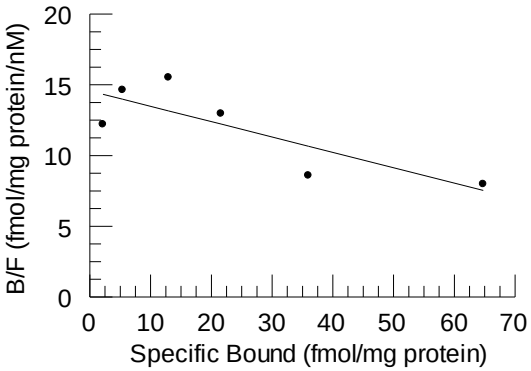

Appendix 2 – Alterations in STD and LTD occur with different frequency paradigms and STD and LTD affects cortico-striatal frequency filtering

Introduction

Synaptic plasticity underlies nervous system functions from signal processing to learning and memory. Short-term changes occurring in presynaptic neurons and in feedback circuits underlie the frequency dependency and instantaneous efficacy of transmission of action potentials through neuronal networks. Long-term changes in both the pre- and post-synaptic regions are thought to be the basis of learning and memory. The glutamatergic synapse between Layer V cortical projection neurons and medium spiny neurons in the dorsal striatum exhibits both of these forms of plasticity. Importantly, the cortico-striatal circuit plays an important role in various forms of associative learning and in modulation of motor behavior (Balleine et al., 2007).

The induction of long-term synaptic depression in the cortico-striatal synaptic field is initiated by convergent glutamatergic (layer V) and dopaminergic (substantia nigra) inputs onto medium spiny neurons (MSNs) leading to their depolarization and activation of post-synaptic metabotropic glutamate receptors (mGluRs) and dopamine type-2 receptors (D2Rs). Simultaneous depolarization of MSNs and activation of these receptors leads to production of endocannabinoids by MSNs, which retrogradely bind pre-synaptic CB1 receptors leading to long-term decreases in the probability of glutamate release characterized as long-term depression (LTD) (Surmeier et al., 2007). The vast majority of the investigations of LTD are based upon an induction paradigm using 3 to 4 trains of 100 Hz high frequency stimuli at maximum stimulus intensity along with antagonists to probe the role of various receptors in the induction of LTD (Calabresi et al., 1992). This induction through repetitive firing of glutamatergic fibers with coincident dopaminergic input, produces an initial post tetanic depression (PTD) followed by a process, which we have called short-term depression (STD), that lasts for about 10 minutes. In some instances, a longer lasting, LTD is induced, which is maintained for an excess of 30 minutes (Lovinger et al., 1993).

We have previously investigated the role of D2 and CB1 receptors in the induction of both LTD and STD following a 100 Hz high frequency stimulus paradigm (Baca et al., 2013), which confirms the occurrence of both forms of plasticity in MSNs, and the role of both receptors in the LTD induction process. However it is less well known if the induction of STD and LTD depend upon the frequency and magnitude of the induction stimulus. One of the few published studies, which examined how the induction of LTD in the striatum may be influenced by induction frequency, used a 10 Hz 5 minute HFS train as an induction paradigm (Ronesi and Lovinger, 2005) instead of a 100 Hz frequency commonly employed. This form of LTD, unlike that induced with the 100 Hz paradigm, does not seem to depend on post-synaptic depolarization or activation of mGluRs. We therefore explored whether there are differences in the magnitude or occurrence of STD and LTD as a result of the frequency and magnitude of the input stimulus when delivered at frequencies between 10 Hz and 100 Hz.

In addition, GABAergic feedback mechanisms responsible for the low-pass filter characteristics in MSNs in the striatum have been previously characterized (Jelinek and Partridge, 2012). In this study, we have extended this research to probe the effect of HFS induction of LTD or STD on these low-pass filter characteristics. This effort was funded under LDRD Project Number 151347 and Title "A Comprehensive Approach to Decipher Biological Computation to Achieve Next Generation High-performance Exascale Computing".

Results

To characterize use-dependent plasticity in these slices, a set of distinct high frequency stimulus (HFS) paradigms are used to elicit synaptic depression of cortical inputs measured by extracellular field excitatory postsynaptic potential (fEPSP) population spike (PS) amplitude recordings in the medial portion of the dorsal striatum in coronal slices of P21 – P28 C57/Bl6 mice.

To characterize the role of the HFS paradigm on the induction of synaptic depression, we used the following paradigms:

- 10 Hz; 5 minute train at half maximum or maximum stimulus intensity (3000 stimuli)

- 10 Hz; 4 sets of trains separated by 1 minute at maximum stimulus intensity (400 stimuli)
- 30 Hz; 4 sets of trains separated by 1 minute at maximum stimulus intensity (400 stimuli)
- 100 Hz; 4 sets of trains separated by 1 minute half maximum or maximum stimulus intensity (400 stimuli)

The paradigms that utilized four sets of trains were designed so that each would include 400 stimuli, so each is referred to as a 400 stimuli HFS paradigm with a half maximum or maximum input stimulus magnitude, except one of the 10 Hz paradigms which had 3000 stimuli. Two 10 Hz paradigms were used, one with a 5 minute continuous train of pulses (3000 stimuli) and another with 4 sets of trains of pulses (400 stimuli). The former was included in order to make comparisons with previous data (Ronesi and Lovinger, 2005), which suggest that there may be different mechanisms involved in the induction of LTD at this frequency. The latter 10 Hz, along with the 30 Hz and 100 Hz HFS paradigms were included in order to assess the influence of the frequency of a fixed number of stimulus pulses. We also included both half maximum and maximum stimulus intensities during the HFS for some of the paradigms in order to compare and contrast how the magnitude of the stimulus might affect the induction of LTD.

In all of the HFS paradigms used, PSs exhibited an initial depression to ~20-30% of baseline (post-tetanic depression, PTD). For some slices, the PS returned back to near baseline levels within a few minutes, while for other slices it remained depressed for the full 30 minute recording period (Fig. A2.1A). We used a cluster analysis (see experimental procedures) to differentiate between two distinct populations, which were operationally defined as short-term depression (STD) and long-term depression (LTD) based on the percent of PS recovery after 30 minutes. Fig. A2.1B shows summary data of the percent PS recovery following HFS for the 10 Hz 400 stimuli maximum input HFS paradigm for the STD and LTD populations determined by cluster analysis as well as the combined data from experiments with all HFS paradigms. Fig. A2.1C shows representative PSs for the 10 minute baseline period and for the 30 minute period

following HFS for slices that were assigned to STD and LTD populations by cluster analysis. We found that each of the other HFS paradigm generated plasticity that could be differentiated into distinct STD and LTD populations as was found with the 10 Hz HFS paradigm shown in Fig A2.1.

We also performed a set of control experiments without HFS, to compare PSs at 30 minutes with PSs after an initial 10 minute baseline. In these control experiments, the PS magnitudes did not vary significantly during the 40 minute recording period and were found to be at ~95% of the baseline levels, at the end of the 40 minute period. Additionally cluster analysis did not reveal significantly distinct populations in these control data. The magnitude of PSs of control slices were used to compare changes in PS recovery of the various HFS paradigms used in these experiments.

An initial comparison PS amplitudes following each of the HFS paradigms was performed on the total population before cluster analyses were undertaken . A multiple comparisons ANOVA ($F_{6,118}$=7.17, p<0.0001) showed significant effects between the different HFS paradigms examined (Fig. A2.2A). Interestingly, post-hoc analysis showed that all of the HFS paradigms demonstrated a greater percent recovery of PS following HFS than the 10 Hz 3000 stimuli maximum input HFS paradigm, which was also less than the control population with no HFS applied (Fig A2.2A). None of the other paradigms showed recovery of PS at 30 minutes after HFS that was distinct from the control population. These results indicate that independent of cluster analysis, the 10 Hz 3000 stimuli maximum input HFS paradigm shows differences from other HFS paradigms including others at 10 Hz.

We next assessed whether the induction of these two forms of synaptic plasticity (LTD and STD) as determined by cluster analysis differed among the various HFS paradigms examined. A multiple comparisons ANOVA ($F_{6,53}$=28.53, p<0.0001) showed significant effects between the LTD populations of the different HFS paradigms examined (Fig. A2.2B). Post-hoc analysis of all of the LTD clusters showed significantly less recovery to baseline of the PS amplitude 30 minutes after HFS compared to controls (Fig. A2.2B). Additionally, post-hoc analysis showed that 4 HFS paradigms generated LTD populations with significantly greater recovery to baseline than the 10 Hz 3000 stimuli maximum intensity HFS paradigm (Fig. A2.2B; note iii). A multiple comparisons

ANOVA ($F_{6,60}$=3.09, p<0.01) showed significant differences among the different HFS paradigms in their ability to generate STD (Fig. A2.2C). However, post-hoc analysis did not show significant differences between any of the HFS paradigms and controls.

We next compared the responses to HFS for the STD and LTD populations for the 10 Hz, 30 Hz and 100 Hz 4 × 400 stimuli maximum input HFS paradigms, since they both included the same number of pulses and were delivered at maximum input. A multiple comparisons ANOVA (F=29.20, p<0.0001) showed significant effects between the LTD and STD populations with the different HFS paradigms (Fig. A2.3). Post-hoc tests indicated that each HFS paradigm generated significant STD and LTD populations, but there were no differences between STD or LTD populations for each of the HFS paradigms (Fig. A2.3). However there were differences among the HFS paradigms in their ability to elicit LTD. The 10 Hz 400 stimuli maximum intensity HFS paradigm elicited LTD rather than STD in 56% of slices, versus 41% for the 30 Hz paradigm, and 31% for the 100 Hz paradigm.

It has been demonstrated recently that low-pass filter characteristics of cortico-striatal circuits are dependent on GABAergic feedback, since use of a GABA inhibitor depresses the high frequency roll off to random stimulus frequencies between 2 and 100 Hz (Jelinek and Partridge, 2012). We decided to test if these low pass filtering characteristics of STD and LTD clusters change as a result of the HFS paradigm. We chose the 10 Hz 400 stimuli maximum intensity HFS paradigm for these experiments, since it was the most effective in eliciting LTD and it was a markedly different HFS paradigm from that used in the previous study (Fig. A2.3). As in the previous study (Jelinek and Partridge, 2012), a random stimulus paradigm was used in order to control for the possibilities that the ascending or descending frequencies of fixed frequency paradigms could affect the frequency dependence of the PS response.

Figure A2.4A shows the time course of PS responses for the STD and LTD populations for the 10 Hz 400 maximum stimulus HFS paradigm used in the experiments to test frequency responses before and after HFS. Figure A2.4A shows the sequence of: an initial 10 minute set of baseline stimulus recordings made at half maximum intensity (BL#1); then the first random stimulus paradigm (RS#1); then a second 10 minute set of baseline recordings at half maximum intensity (BL#2); then four trains of 10Hz stimuli at

maximum intensity (HFS; 400 stimuli total); then a 30 minute set of recordings (RESULT); and finally the second random stimulus paradigm (RS#2) for the STD and LTD populations as determined by cluster analysis.

As shown in Fig. A2.4C, there were STD and LTD cluster populations as expected following the HFS paradigm. As shown in Fig. A2.4D, the ratio of the PS amplitudes during BL#2 to that during BL#1 was close to unity for both the STD and LTD populations, which indicates that there was not a significant depression in the PSs due to the first random stimulus paradigm.

To determine the effect the induction of synaptic depression on the low pass filter properties, the responses to RS#1 were compared with the responses to RS#2. Analysis for RS#1 included both slices that received subsequent HFS and control slices that did not, since RS#1 occurs prior the HFS protocol. Analysis for RS#2 was performed separately on STD and LTD populations. Fig. A2.4B shows a log-log plot (Bode magnitude plot) of the normalized amplitudes of PS responses to frequencies between 2 to 60 Hz. A least squares regression fit of RS#1 data to a 3^{rd} order Butterworth low pass filter yielded a corner frequency (CoF) of 4.37 Hz and a stop band slope parameter (A) of 0.0185. A similar fit of the RS#2 STD cluster yielded a CoF of 14.20 and an A of 0.0370, indicating a prominent increase in the high frequency cut off frequency and slight shift in the stop band slope compared to RS#1. A least squares regression fit for the RS#2 LTD cluster yielded a CoF of 3.45 and an A of 0.0084, indicating a slight decrease in high frequency cut off frequency and a more prominent shift in the stop band slope compared to RS#1. We compared the frequency-dependent PS amplitudes for the RS#1 and RS#2 STD and LTD clusters at 20.8 Hz, 35.2 Hz and 57.5 Hz. As shown in Fig. A2.4E, at 20.8 Hz, no significant difference was found between RS#1 and RS#2 STD and LTD clusters. At 35.2 Hz, the RS#2 STD and LTD PS amplitudes of the clusters were both significantly greater than that of the RS#1 cluster. At 57.2 Hz, the RS#2 LTD the PS amplitude of the cluster was significantly greater than that of either the RS#2 STD cluster or the RS#1 cluster.

A set of control experiments was carried out using the same experimental paradigm as shown in Fig. A2.4A, but without imposition of the HFS paradigm. We found no significant differences in the magnitude of PSs representing the BL#1, BL#2,

and results after 30 minutes, (data not shown), indicating that there was no run down of PS magnitudes over this time period. A least squares regression of these data to a 3rd order Butterworth low pass filter gave a CoF of 5.15 Hz and a stop band slope parameter, A, of 0.0190 for the RS#1 controls, and a CoF of 5.68 Hz and a stop band slope parameter A of 0.0170 for the RS#2 controls. These values were comparable to those found for RS#1 in those experiments in which HFS was applied.

We next repeated the 10 Hz 400 maximum stimuli experiments in the presence of 20μM picrotoxin, a $GABA_A$ receptor antagonist. As before, cluster analysis identified distinct STD and LTD populations at the 30 minute time period following HFS. However We could not obtain significant least squares fit of the data to a 3rd order Butterworth low pass filter, in the RS#1, RS#2 STD, orRS#2 LTD cluster, indicating a major $GABA_A$-dependent component of the low pass filter characteristic previously shown (Jelinek and Partridge, 2012), both during RS#1, but also following HFS (data not shown).

Discussion

Long-term synaptic plasticity is generally accepted as a model of learning and memory. To be a valid model, this plasticity must be initiated by a physiologically-relevant neural signal. HFS stimuli that mimic theta activity are commonly used to initiate LTP, but a similar association with the EEG power spectrum has not been made for LTD induction.

In this study, the 10 Hz 400 stimuli maximum input HFS paradigm was found to have a higher likelihood of producing LTD than the 30 Hz and 100 Hz 400 maximum input stimuli paradigms (Fig. A2.3), though the resulting magnitudes for LTD and STD were similar. The 10 Hz 3000 stimuli HFS was found to produce a more robust level of LTD (less recovery after 30 minutes compared to baseline levels) compared to the 400 stimuli paradigms (Fig. A2.2). Thus, the 10 Hz HFS stimuli in the alpha range (8 – 13 Hz) was the most likely of those tested to produce LTD rather than STD and a longer train of stimuli (3000 versus 400) produced a more robust level of LTD.

Not much is currently known about how firing rates of striatal MSNs can vary *in vivo*. Intra-somatic current injection of between 100 – 400 pA into patch-clamped D1 or D2 expressing MSN reveals a firing rate of ~0 - ~15 Hz for D1 MSNs and ~0 - ~25 Hz

for D2 MSNs., This indicates that D2 MSNs are more excitable than D1 MSNs (Gertler et al., 2008). D2Rs expressed in MSNs have been associated with striatal LTD so perhaps frequencies between 5 - 25 Hz may be associated with striatal LTD *in vivo*. This is consistent with my observation that LTD is more robust at lower frequency levels.

Two of the HFS paradigms compared the use of ½ maximum stimulus intensity to maximum stimulus intensity during the HFS paradigm. No significant differences were found between the 100 Hz 400 stimuli HFS paradigm at ½ maximum input versus the same stimulus at maximum input (Fig. A2.2B). A more robust level of LTD was found for the 100 Hz 3000 stimuli HFS stimuli at maximum stimulus intensity compared to the same paradigm at ½ maximum stimulus, which was comparable to other stimulus paradigms (Fig. A2.2B).

Using a random stimulus paradigm (Jelinek and Partridge, 2012) before and after the 10 Hz 400 maximum input HFS paradigm we found that prior to the introduction of HFS, the previously characterized low-pass filter characteristics were confirmed (Fig. A2.4B; gray). Additionally we found the previously reported dependency of the low-pass filter characteristics on GABAergic feedback, since use of a GABA inhibitor greatly attenuated the low-pass filtering characteristics. Following the HFS stimulus, the STD population showed a distinct shift in the low-pass filter as characterized by an increase in the CoF from 4.4 Hz to 14.2 Hz (Fig. A2.4B; red). Interestingly, the CoF of the LTD population did not change significantly from its baseline value of 3.44 Hz, but the population did show a reduction in its stop band slop parameter A (Fig. A2.4B; green). These results show that low-pass filter characteristics are differentially affected between the STD and LTD populations. It would be interesting to determine whether this difference reflects a difference in the cortico-striatal synapses that precedes the induction of long-term plasticity or if it is more causally related to the induction paradigm. As was true prior to the introduction of HFS, both STD and LTD populations were found to depend on GABAergic feedback, since independent experiments performed in the presence of a $GABA_AR$ antagonist revealed that STD and LTD low-pass filtering was greatly attenuated or eliminated.

Methods

Animals

All experiments were approved by the Institutional Animal Care and Use Committee at the University of New Mexico Health Sciences Center Laboratory Animal Care and Use Committees and the National Institutes of Health. Coronal striatal slices were prepared from approximately 21 - 28 day old C57/Bl6 mice as previously described (Schiess et al., 2006) and electrophysiological techniques were identical to those described in the Methods.

HFS Paradigm

To assess long-term synaptic plasticity in the cortico-striatal field, a 10 minute baseline was established at ½ maximum stimulus intensity, then one of 7 high frequency stimulus (HFS) paradigms with stimulus pulses at either half maximum or maximum intensity was applied, and finally 30 minutes of recordings were obtained again at ½ maximum stimulus intensity. The average amplitude of the final 10 PSs during the 30 minute period was compared to the average amplitude of 32 PSs during the 10 minute pre-HFS baseline in order to determine the percentage of change relative to the baseline. The six HFS paradigms consisted of the following: 4 sets of 10, 30, or 100 Hz pulses (each train 100 pulses) at the half maximum or maximum stimulus intensity (except 30 Hz done only at maximum intensity) separated by 1 minute per set for 400 stimuli total; or a continual 5 minute train of 10 Hz pulses at half maximum or maximum stimulus intensity for 3000 stimuli total.

Electrophysiology Filtering Paradigm

The filter properties of the cortico-striatal field were determined by an additional stimulus paradigm, which was applied before and after the assessment of long-term synaptic plasticity. In this random frequency train paradigm, 5 Hz to 60 Hz instantaneous frequency pulse trains were produced by a waveform stimulus file in Clampex (Molecular Devices, Sunnyvale, CA

Frequency response data for PSs were fit with a 3rd order Butterworth low pass filter with a least squares regression using the Levenberg-Marquart method in ProStat (v 6, Poly Software International, Pearl River NY) using equations 1 and 2.

$$V_{mean} = A \times \log_{10}(1 + fr^6) \ldots (1)$$

$$fr = \frac{Hz}{CoF} \ldots (2)$$

where: V_{mean} is the frequency-dependent gain that was fit to the average PS amplitude during the binned PS amplitudes generated by the random frequency protocol, Hz is the stimulus frequency, CoF is the cutoff frequency for a low pass filter, and A is a scaling factor that is directly proportional to the roll off of the filter.

To assess changes in frequency filtering during long-term synaptic plasticity in the cortico-striatal field, (a) a 10 minute baseline was established at ½ maximum stimulus intensity, (b) the first set of random stimulus pulse trains above was delivered, (c) the 10 Hz stimulus (HFS) paradigm above (400 pulses) with stimulus pulses at ½ maximum or maximum intensity was applied, (d) 30 minutes of recordings were obtained again at ½ maximum stimulus intensity and (e) the second set of random stimulus pulse trains above was delivered. The average amplitude of the final 10 population spikes during the 30 minute period was compared to the average amplitude of 32 population spikes during the 10 minute pre-HFS baseline in order to determine the percentage of change relative to the baseline.

Drugs

Picrotoxin (Tocris, Ellisville, MO, USA) was stored frozen in aliquots and diluted to the appropriate concentration in ACSF for electrophysiology on the day of the experiment, or the appropriate concentrations as dictated by the pharmacological assays.

Statistical Analysis

SPSS 16.0 (SPSS, Inc., Chicago, IL) was used for statistical analysis of data. Numerical values for data measurements are expressed as the mean ± standard error unless otherwise specified. Statistical *p* values were represented as follows: * $p < 0.05$;

** $p < 0.01$ and *** $p<0.001$. ANOVA analysis followed by a Tukey's HSD post-hoc test was carried out to compare different frequency paradigms. Cluster analysis was performed as described in the Methods.

Figures

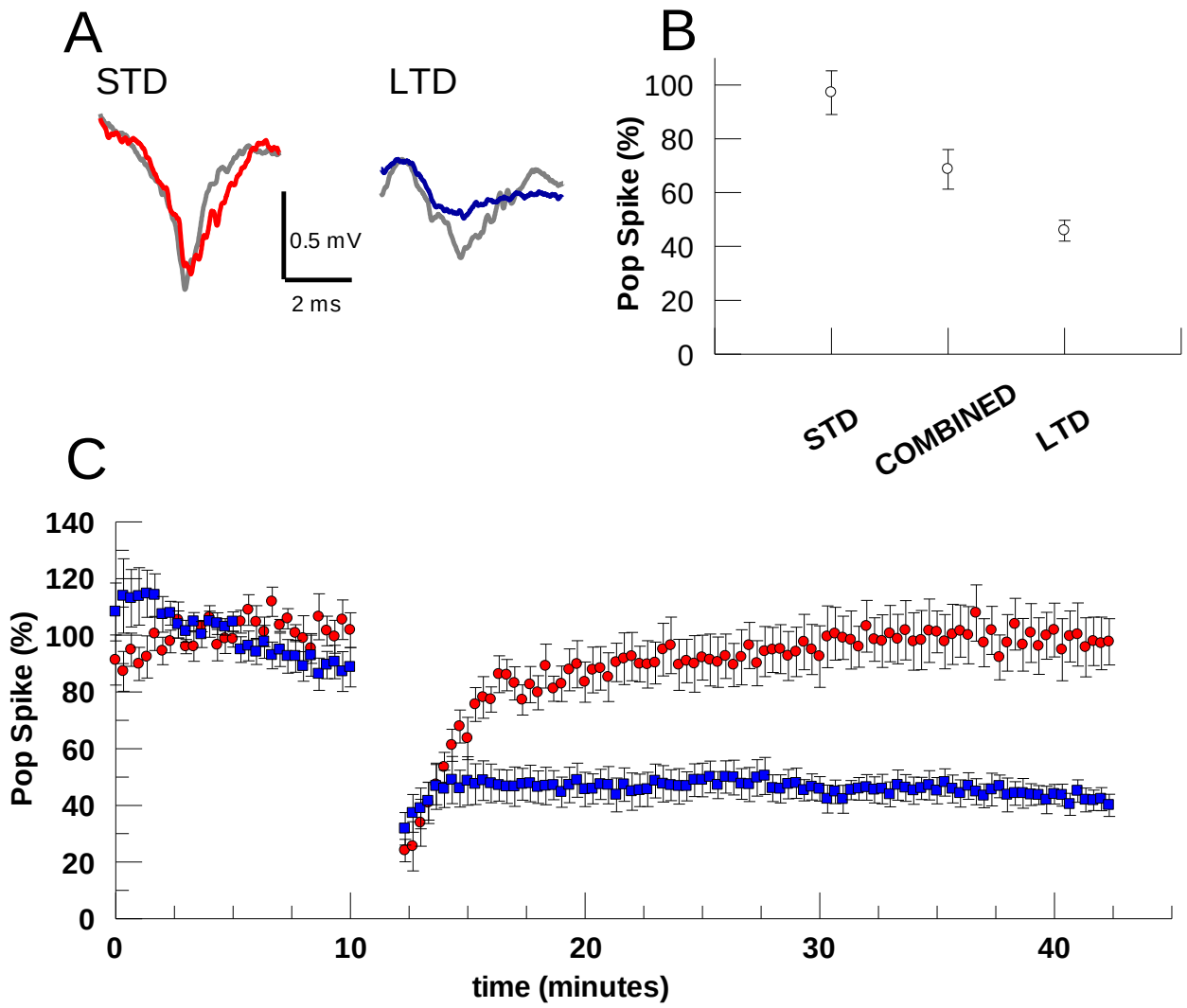

Fig. A2.1: Cluster analysis determination of 10 Hz 400 stimuli maximum input HFS paradigm. A Representative example of population spikes traces before (gray) and after (colored) in 10 Hz 4x 1s maximum input HFS paradigm for STD cluster (> 70% recovery, n = 8, red) and LTD cluster (<60% recovery, n = 10, blue). **B** Mean +/- SEM of individual LTD and STD clusters and combined data for PS amplitudes shown in C. Cluster analysis assigns data points to clusters such that individual SEMs will have minimal overlap with combined SEM. **C** Time course of normalized population spike amplitudes separated into 2 groups determined by cluster analysis of PS amplitudes 30 min after HFS.

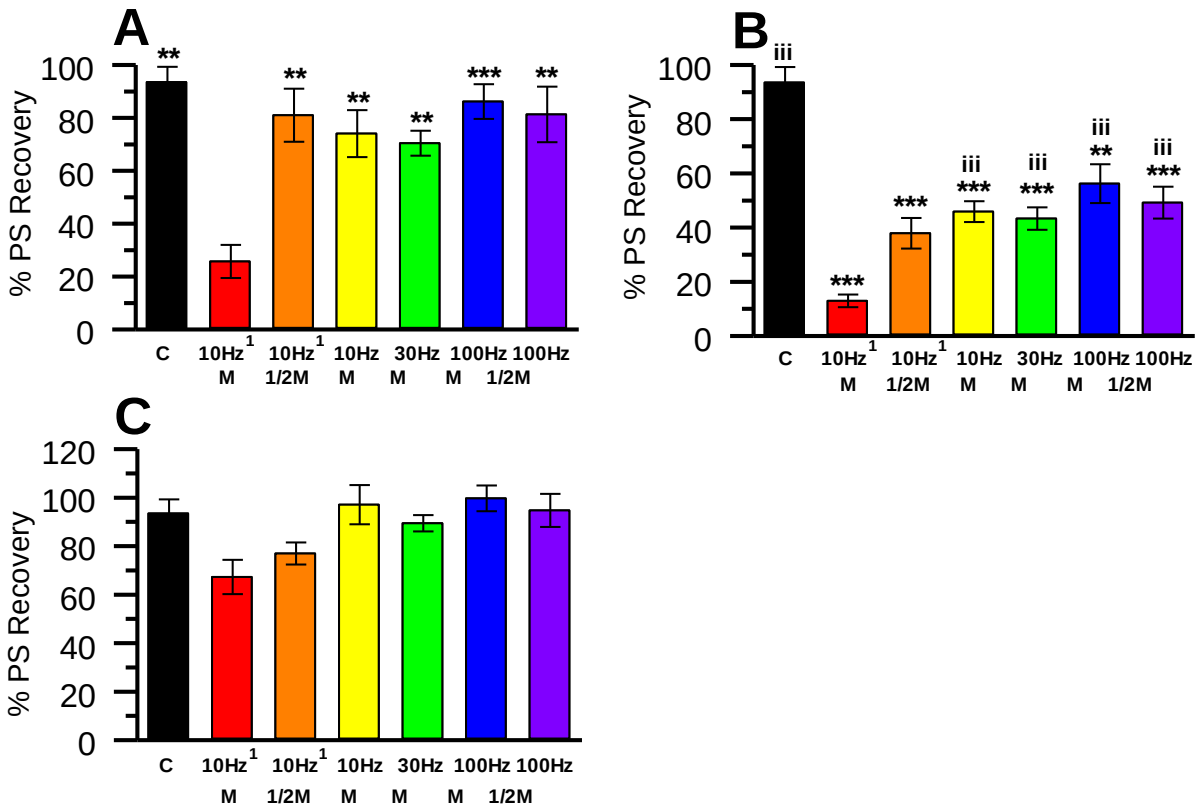

Fig. A2.2: Comparison of STD and LTD clusters in different HFS paradigms. A All experiments no clustering. Percent recovery of population spike amplitudes before cluster analysis following each of 6 HFS protocols. Note 1: 10 Hz 3000 stimuli HFS paradigm at maximum (M) or half-maximum (1/2M) input stimulus. All other HFS paradigms were 4 trains with a total of 400 stimuli. **B** Clusters with least recovery (LTD). Percent recovery of population spike amplitude for clusters with the least recovery following each of 6 HFS protocols. Note iii: These clusters were significantly different from the 10 Hz 3000 stimuli HFS paradigm as well as controls. **C** Clusters with greatest recovery (STD). Percent recovery of population spike amplitude for clusters with the greatest recovery following each of 6 HFS protocols. Statistics: ANOVA multiple comparisons and Scheffe's post hoc tests.

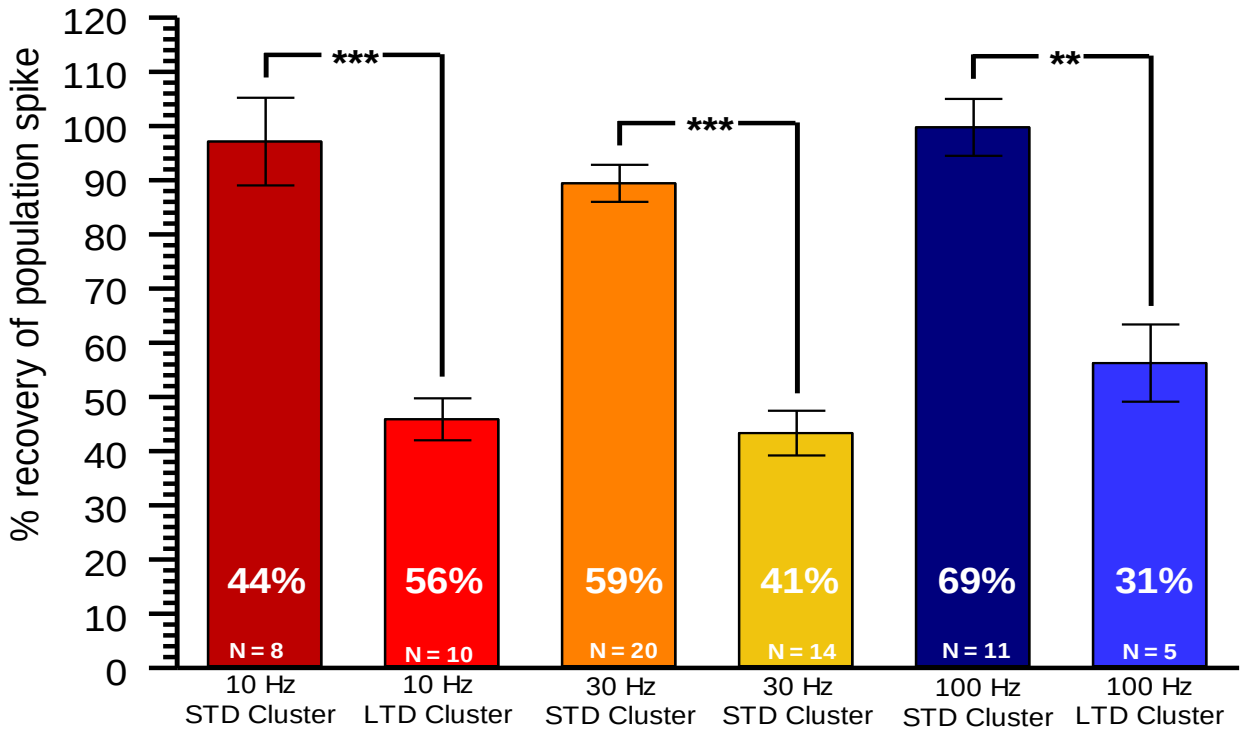

Fig. A2.3: Comparison of STD and LTD clusters. Clusters with 400 stimuli at maximum input stimulus. Percent recovery of population spike amplitude for all clusters with a HFS paradigm with 4 x 100 stim at maximum I_{stim}. Statistics: ANOVA multiple comparisons, 2 × 3, mean squares between groups = 7790.4, F = 29.2047, $p < 0.0001$, with Scheffe's post hoc.

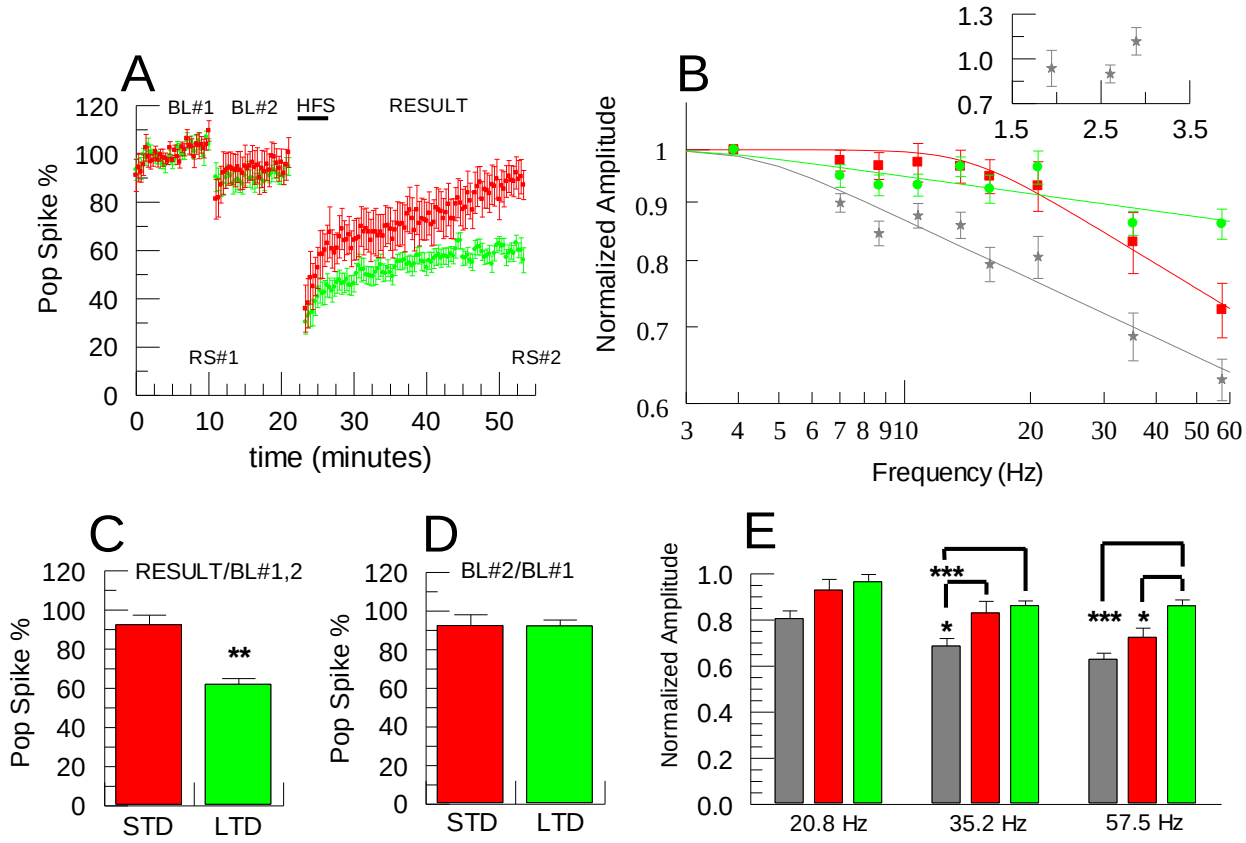

Fig. A2.4: Effect of long-term plasticity on filtering for 10 Hz 400 stimuli maximum input HFS paradigm. A Time course of normalized population spike amplitudes separated into 2 groups (STD and LTD) determined by cluster analysis of amplitudes during test period (30 min after HFS). A 10 minute baseline (BL#1) was followed by a random stimulus paradigm (RS# 1), followed by a second 10 minute baseline (BL#2). Next a 10 Hz, 400 stimuli HFS paradigm was done followed by a 30 minute recovery period (RESULT). Finally, this was followed by an identical random stimulus paradigm (RS#2). Averages of the last 10 readings 30 minutes after the HFS were divided by averages of each of the 10 minute baselines to obtain the % of recovery of the pop spike following HFS. The average of recovery/BL#1 and recovery/BL#2 was used to then perform cluster analysis to obtain STD and LTD populations. **B** Low pass filter properties for 10 Hz, 400 stimuli at maximum intensity. 3rd order Butterworth low pass filter fits to random frequency stimuli either before or after 10 Hz HFS paradigm. Clusters (RS# 1 (grey), COF = 4.3688 Hz, A=0.0185, n=22; RS# 2 STD cluster (red): COF = 14.2026 Hz, A = 0.0370; n = 7; RS# 2 LTD cluster (green): COF = 3.4474, A=0.0084; n=15). Inset shows averages of the lowest 3 frequencies used in random stimulus paradigm (n=6). **C** Bar graph of STD (mean 92.50 +/- 4.87, red) and LTD (62.11 +/- 2.78, green) clusters of results 30 minutes after HFS from time course plots in A. **D** Bar graph of ratio of 10 minute BL#1 to BL#2 for STD and LTD clusters. **E** Comparison of RS# 1 (grey), RS# 2 STD cluster (red), and RS# 2 LTD cluster (green) frequency responses at 20.8 Hz, 35.2 Hz and 57.5 Hz.

References

Adermark, L., Talani, G., Lovinger, D.M., 2009. Endocannabinoid-dependent plasticity at GABAergic and glutamatergic synapses in the striatum is regulated by synaptic activity. Eur J Neurosci. 29**,** 32-41.

American Psychiatric Association, Diagnostic and statistical manual of mental disorders: DSM-IV-TR, 2000.

Ashby, M.C., De La Rue, S.A., Ralph, G.S., Uney, J., Collingridge, G.L., Henley, J.M., 2004. Removal of AMPA receptors (AMPARs) from synapses is preceded by transient endocytosis of extrasynaptic AMPARs. J Neurosci. 24**,** 5172-6.

Baca, M., Allan, A.M., Partridge, L.D., Wilson, M.C., 2013. Gene-environment interactions affect long-term depression (LTD) through changes in dopamine receptor affinity in Snap25 deficient mice. Brain Res. 1532**,** 85-98.

Balleine, B.W., Delgado, M.R., Hikosaka, O., 2007. The role of the dorsal striatum in reward and decision-making. J Neurosci. 27**,** 8161-5.

Beaulieu, J.M., Gainetdinov, R.R., 2011. The physiology, signaling, and pharmacology of dopamine receptors. Pharmacol Rev. 63**,** 182-217.

Biederman, J., Fried, R., Petty, C.R., Wozniak, J., Doyle, A.E., Henin, A., Corkum, L., Claudat, K., Faraone, S.V., 2011. Cognitive development in adults with attention-deficit/hyperactivity disorder: a controlled study in medication-naive adults across the adult life cycle. J Clin Psychiatry. 72**,** 11-6.

Bolam, J.P., Hanley, J.J., Booth, P.A., Bevan, M.D., 2000. Synaptic organisation of the basal ganglia. J Anat. 196 (Pt 4)**,** 527-42.

Braun, J.M., Kahn, R.S., Froehlich, T., Auinger, P., Lanphear, B.P., 2006. Exposures to environmental toxicants and attention deficit hyperactivity disorder in U.S. children. Environ Health Perspect. 114**,** 1904-9.

Bruno, K.J., Freet, C.S., Twining, R.C., Egami, K., Grigson, P.S., Hess, E.J., 2007. Abnormal latent inhibition and impulsivity in coloboma mice, a model of ADHD. Neurobiol Dis. 25**,** 206-16.

Calabresi, P., Maj, R., Pisani, A., Mercuri, N.B., Bernardi, G., 1992. Long-term synaptic depression in the striatum: physiological and pharmacological characterization. J Neurosci. 12**,** 4224-33.

Caspi, A., McClay, J., Moffitt, T.E., Mill, J., Martin, J., Craig, I.W., Taylor, A., Poulton, R., 2002. Role of genotype in the cycle of violence in maltreated children. Science. 297**,** 851-4.

Caspi, A., Sugden, K., Moffitt, T.E., Taylor, A., Craig, I.W., Harrington, H., McClay, J., Mill, J., Martin, J., Braithwaite, A., Poulton, R., 2003. Influence of life stress on depression: moderation by a polymorphism in the 5-HTT gene. Science. 301**,** 386-9.

Castellanos, F.X., Proal, E., 2012. Large-scale brain systems in ADHD: beyond the prefrontal-striatal model. Trends Cogn Sci. 16**,** 17-26.

Castillo, P.E., Younts, T.J., Chavez, A.E., Hashimotodani, Y., 2012. Endocannabinoid signaling and synaptic function. Neuron. 76**,** 70-81.

Centonze, D., Picconi, B., Gubellini, P., Bernardi, G., Calabresi, P., 2001. Dopaminergic control of synaptic plasticity in the dorsal striatum. Eur J Neurosci. 13**,** 1071-7.

Cho, D.I., Zheng, M., Kim, K.M., 2010. Current perspectives on the selective regulation of dopamine D(2) and D(3) receptors. Arch Pharm Res. 33**,** 1521-38.
Choi, S., Lovinger, D.M., 1997a. Decreased frequency but not amplitude of quantal synaptic responses associated with expression of corticostriatal long-term depression. J Neurosci. 17**,** 8613-20.
Choi, S., Lovinger, D.M., 1997b. Decreased probability of neurotransmitter release underlies striatal long-term depression and postnatal development of corticostriatal synapses. Proc Natl Acad Sci U S A. 94**,** 2665-70.
Citri, A., Malenka, R.C., 2008. Synaptic plasticity: multiple forms, functions, and mechanisms. Neuropsychopharmacology. 33**,** 18-41.
Corradini, I., Donzelli, A., Antonucci, F., Welzl, H., Loos, M., Martucci, R., De Astis, S., Pattini, L., Inverardi, F., Wolfer, D., Caleo, M., Bozzi, Y., Verderio, C., Frassoni, C., Braida, D., Clerici, M., Lipp, H.P., Sala, M., Matteoli, M., 2012. Epileptiform Activity and Cognitive Deficits in SNAP-25+/- Mice are Normalized by Antiepileptic Drugs. Cereb Cortex.
David, H.N., Ansseau, M., Abraini, J.H., 2005. Dopamine-glutamate reciprocal modulation of release and motor responses in the rat caudate-putamen and nucleus accumbens of "intact" animals. Brain Res Brain Res Rev. 50**,** 336-60.
Di Filippo, M., Picconi, B., Tantucci, M., Ghiglieri, V., Bagetta, V., Sgobio, C., Tozzi, A., Parnetti, L., Calabresi, P., 2009. Short-term and long-term plasticity at corticostriatal synapses: implications for learning and memory. Behav Brain Res. 199**,** 108-18.
Ding, J., Peterson, J.D., Surmeier, D.J., 2008. Corticostriatal and thalamostriatal synapses have distinctive properties. J Neurosci. 28**,** 6483-92.
Falconer, D.S., 1989. Introduction to quantitative genetics. Vol., Longman Wiley, Burnt Mill, Harlow, Essex, England, New York.
Fan, X., Hess, E.J., 2007. D2-like dopamine receptors mediate the response to amphetamine in a mouse model of ADHD. Neurobiol Dis. 26**,** 201-11.
Fan, X., Xu, M., Hess, E.J., 2010. D2 dopamine receptor subtype-mediated hyperactivity and amphetamine responses in a model of ADHD. Neurobiol Dis. 37**,** 228-36.
Fan, X., Bruno, K.J., Hess, E.J., 2012. Rodent models of ADHD. Curr Top Behav Neurosci. 9**,** 273-300.
Faraone, S.V., Sergeant, J., Gillberg, C., Biederman, J., 2003. The worldwide prevalence of ADHD: is it an American condition? World Psychiatry. 2**,** 104-13.
Faraone, S.V., Perlis, R.H., Doyle, A.E., Smoller, J.W., Goralnick, J.J., Holmgren, M.A., Sklar, P., 2005. Molecular genetics of attention-deficit/hyperactivity disorder. Biol Psychiatry. 57**,** 1313-23.
Faraone, S.V., Mick, E., 2010. Molecular genetics of attention deficit hyperactivity disorder. Psychiatr Clin North Am. 33**,** 159-80.
Gainetdinov, R.R., Premont, R.T., Bohn, L.M., Lefkowitz, R.J., Caron, M.G., 2004. Desensitization of G protein-coupled receptors and neuronal functions. Annu Rev Neurosci. 27**,** 107-44.
Gerfen, C.R., Surmeier, D.J., 2011. Modulation of striatal projection systems by dopamine. Annu Rev Neurosci. 34**,** 441-66.
Gertler, T.S., Chan, C.S., Surmeier, D.J., 2008. Dichotomous anatomical properties of adult striatal medium spiny neurons. J Neurosci. 28**,** 10814-24.

Giuffrida, A., Parsons, L.H., Kerr, T.M., Rodriguez de Fonseca, F., Navarro, M., Piomelli, D., 1999. Dopamine activation of endogenous cannabinoid signaling in dorsal striatum. Nat Neurosci. 2**,** 358-63.
Gold, A.B., Keller, A.B., Perry, D.C., 2009. Prenatal exposure of rats to nicotine causes persistent alterations of nicotinic cholinergic receptors. Brain Res. 1250**,** 88-100.
Goutelle, S., Maurin, M., Rougier, F., Barbaut, X., Bourguignon, L., Ducher, M., Maire, P., 2008. The Hill equation: a review of its capabilities in pharmacological modelling. Fundam Clin Pharmacol. 22**,** 633-48.
Heck, H.D., 1971. Statistical theory of cooperative binding to proteins. The Hill equation and the binding potential. J Am Chem Soc. 93**,** 23-9.
Hein, P., Bunemann, M., 2009. Coupling mode of receptors and G proteins. Naunyn Schmiedebergs Arch Pharmacol. 379**,** 435-43.
Hess, E.J., Jinnah, H.A., Kozak, C.A., Wilson, M.C., 1992. Spontaneous locomotor hyperactivity in a mouse mutant with a deletion including the Snap gene on chromosome 2. J Neurosci. 12**,** 2865-74.
Hess, E.J., Collins, K.A., Copeland, N.G., Jenkins, N.A., Wilson, M.C., 1994. Deletion map of the coloboma (Cm) locus on mouse chromosome 2. Genomics. 21**,** 257-61.
Hess, E.J., Collins, K.A., Wilson, M.C., 1996. Mouse model of hyperkinesis implicates SNAP-25 in behavioral regulation. J Neurosci. 16**,** 3104-11.
Jahn, R., Scheller, R.H., 2006. SNAREs--engines for membrane fusion. Nat Rev Mol Cell Biol. 7**,** 631-43.
Jeans, A.F., Oliver, P.L., Johnson, R., Capogna, M., Vikman, J., Molnar, Z., Babbs, A., Partridge, C.J., Salehi, A., Bengtsson, M., Eliasson, L., Rorsman, P., Davies, K.E., 2007. A dominant mutation in Snap25 causes impaired vesicle trafficking, sensorimotor gating, and ataxia in the blind-drunk mouse. Proc Natl Acad Sci U S A. 104**,** 2431-6.
Jelinek, D.A., Partridge, L.D., 2012. GABA(A) receptor mediated inhibition contributes to corticostriatal frequency filtering. Neurosci Lett. 530**,** 133-7.
Kano, M., Ohno-Shosaku, T., Hashimotodani, Y., Uchigashima, M., Watanabe, M., 2009. Endocannabinoid-mediated control of synaptic transmission. Physiol Rev. 89**,** 309-80.
Kheirbek, M.A., Britt, J.P., Beeler, J.A., Ishikawa, Y., McGehee, D.S., Zhuang, X., 2009. Adenylyl cyclase type 5 contributes to corticostriatal plasticity and striatum-dependent learning. J Neurosci. 29**,** 12115-24.
Kim-Cohen, J., Caspi, A., Taylor, A., Williams, B., Newcombe, R., Craig, I.W., Moffitt, T.E., 2006. MAOA, maltreatment, and gene-environment interaction predicting children's mental health: new evidence and a meta-analysis. Mol Psychiatry. 11**,** 903-13.
Kreitzer, A.C., Malenka, R.C., 2005. Dopamine modulation of state-dependent endocannabinoid release and long-term depression in the striatum. J Neurosci. 25**,** 10537-45.
Kreitzer, A.C., Malenka, R.C., 2007. Endocannabinoid-mediated rescue of striatal LTD and motor deficits in Parkinson's disease models. Nature. 445**,** 643-7.
Kreitzer, A.C., Malenka, R.C., 2008. Striatal plasticity and basal ganglia circuit function. Neuron. 60**,** 543-54.

Lee, S.P., So, C.H., Rashid, A.J., Varghese, G., Cheng, R., Lanca, A.J., O'Dowd, B.F., George, S.R., 2004. Dopamine D1 and D2 receptor Co-activation generates a novel phospholipase C-mediated calcium signal. J Biol Chem. 279**,** 35671-8.

Levant, B., Grigoriadis, D.E., DeSouza, E.B., 1992. Characterization of [3H]quinpirole binding to D2-like dopamine receptors in rat brain. J Pharmacol Exp Ther. 262**,** 929-35.

Lewis, C.M., Levinson, D.F., Wise, L.H., DeLisi, L.E., Straub, R.E., Hovatta, I., Williams, N.M., Schwab, S.G., Pulver, A.E., Faraone, S.V., Brzustowicz, L.M., Kaufmann, C.A., Garver, D.L., Gurling, H.M., Lindholm, E., Coon, H., Moises, H.W., Byerley, W., Shaw, S.H., Mesen, A., Sherrington, R., O'Neill, F.A., Walsh, D., Kendler, K.S., Ekelund, J., Paunio, T., Lonnqvist, J., Peltonen, L., O'Donovan, M.C., Owen, M.J., Wildenauer, D.B., Maier, W., Nestadt, G., Blouin, J.L., Antonarakis, S.E., Mowry, B.J., Silverman, J.M., Crowe, R.R., Cloninger, C.R., Tsuang, M.T., Malaspina, D., Harkavy-Friedman, J.M., Svrakic, D.M., Bassett, A.S., Holcomb, J., Kalsi, G., McQuillin, A., Brynjolfson, J., Sigmundsson, T., Petursson, H., Jazin, E., Zoega, T., Helgason, T., 2003. Genome scan meta-analysis of schizophrenia and bipolar disorder, part II: Schizophrenia. Am J Hum Genet. 73**,** 34-48.

Linnet, K.M., Dalsgaard, S., Obel, C., Wisborg, K., Henriksen, T.B., Rodriguez, A., Kotimaa, A., Moilanen, I., Thomsen, P.H., Olsen, J., Jarvelin, M.R., 2003. Maternal lifestyle factors in pregnancy risk of attention deficit hyperactivity disorder and associated behaviors: review of the current evidence. Am J Psychiatry. 160**,** 1028-40.

Lovinger, D.M., Tyler, E.C., Merritt, A., 1993. Short- and long-term synaptic depression in rat neostriatum. J Neurophysiol. 70**,** 1937-49.

Lovinger, D.M., 2010. Neurotransmitter roles in synaptic modulation, plasticity and learning in the dorsal striatum. Neuropharmacology. 58**,** 951-61.

Luscher, C., Huber, K.M., 2010. Group 1 mGluR-dependent synaptic long-term depression: mechanisms and implications for circuitry and disease. Neuron. 65**,** 445-59.

Marsden, C.D., 1987. What do the basal ganglia tell premotor cortical areas? Ciba Found Symp. 132**,** 282-300.

Martinez, E.J., Kolb, B.L., Bell, A., Savage, D.D., Allan, A.M., 2008. Moderate perinatal arsenic exposure alters neuroendocrine markers associated with depression and increases depressive-like behaviors in adult mouse offspring. Neurotoxicology. 29**,** 647-55.

Mathur, B.N., Lovinger, D.M., 2012. Endocannabinoid-dopamine interactions in striatal synaptic plasticity. Front Pharmacol. 3**,** 66.

Mink, J.W., 1996. The basal ganglia: focused selection and inhibition of competing motor programs. Prog Neurobiol. 50**,** 381-425.

Oliver, P.L., Davies, K.E., 2009. Interaction between environmental and genetic factors modulates schizophrenic endophenotypes in the Snap-25 mouse mutant blind-drunk. Hum Mol Genet. 18**,** 4576-89.

Partridge, J.G., Tang, K.C., Lovinger, D.M., 2000. Regional and postnatal heterogeneity of activity-dependent long-term changes in synaptic efficacy in the dorsal striatum. J Neurophysiol. 84**,** 1422-9.

Partridge, J.G., Apparsundaram, S., Gerhardt, G.A., Ronesi, J., Lovinger, D.M., 2002. Nicotinic acetylcholine receptors interact with dopamine in induction of striatal long-term depression. J Neurosci. 22**,** 2541-9.
Paz, R., Barsness, B., Martenson, T., Tanner, D., Allan, A.M., 2007. Behavioral teratogenicity induced by nonforced maternal nicotine consumption. Neuropsychopharmacology. 32**,** 693-9.
Penny, G.R., Afsharpour, S., Kitai, S.T., 1986. The glutamate decarboxylase-, leucine enkephalin-, methionine enkephalin- and substance P-immunoreactive neurons in the neostriatum of the rat and cat: evidence for partial population overlap. Neuroscience. 17**,** 1011-45.
Pletnikov, M.V., Ayhan, Y., Nikolskaia, O., Xu, Y., Ovanesov, M.V., Huang, H., Mori, S., Moran, T.H., Ross, C.A., 2008. Inducible expression of mutant human DISC1 in mice is associated with brain and behavioral abnormalities reminiscent of schizophrenia. Mol Psychiatry. 13**,** 173-86, 115.
Polanczyk, G., de Lima, M.S., Horta, B.L., Biederman, J., Rohde, L.A., 2007. The worldwide prevalence of ADHD: a systematic review and metaregression analysis. Am J Psychiatry. 164**,** 942-8.
Quik, M., Bordia, T., O'Leary, K., 2007. Nicotinic receptors as CNS targets for Parkinson's disease. Biochem Pharmacol. 74**,** 1224-34.
Rampersaud, E., Mitchell, B.D., Pollin, T.I., Fu, M., Shen, H., O'Connell, J.R., Ducharme, J.L., Hines, S., Sack, P., Naglieri, R., Shuldiner, A.R., Snitker, S., 2008. Physical activity and the association of common FTO gene variants with body mass index and obesity. Arch Intern Med. 168**,** 1791-7.
Rizo, J., Sudhof, T.C., 2012. The membrane fusion enigma: SNAREs, Sec1/Munc18 proteins, and their accomplices--guilty as charged? Annu Rev Cell Dev Biol. 28**,** 279-308.
Ronesi, J., Lovinger, D.M., 2005. Induction of striatal long-term synaptic depression by moderate frequency activation of cortical afferents in rat. J Physiol. 562**,** 245-56.
Ryan, T.A., Reuter, H., Wendland, B., Schweizer, F.E., Tsien, R.W., Smith, S.J., 1993. The kinetics of synaptic vesicle recycling measured at single presynaptic boutons. Neuron. 11**,** 713-24.
Schiess, A.R., Scullin, C.S., Partridge, L.D., 2006. Neurosteroid-induced enhancement of short-term facilitation involves a component downstream from presynaptic calcium in hippocampal slices. J Physiol. 576**,** 833-47.
Schultz, W., Tremblay, L., Hollerman, J.R., 2003. Changes in behavior-related neuronal activity in the striatum during learning. Trends Neurosci. 26**,** 321-8.
Seeman, P., Van Tol, H.H., 1994. Dopamine receptor pharmacology. Trends Pharmacol Sci. 15**,** 264-70.
Seeman, P., Weinshenker, D., Quirion, R., Srivastava, L.K., Bhardwaj, S.K., Grandy, D.K., Premont, R.T., Sotnikova, T.D., Boksa, P., El-Ghundi, M., O'Dowd B, F., George, S.R., Perreault, M.L., Mannisto, P.T., Robinson, S., Palmiter, R.D., Tallerico, T., 2005. Dopamine supersensitivity correlates with D2High states, implying many paths to psychosis. Proc Natl Acad Sci U S A. 102**,** 3513-8.
Seeman, P., Schwarz, J., Chen, J.F., Szechtman, H., Perreault, M., McKnight, G.S., Roder, J.C., Quirion, R., Boksa, P., Srivastava, L.K., Yanai, K., Weinshenker, D.,

Sumiyoshi, T., 2006. Psychosis pathways converge via D2high dopamine receptors. Synapse. 60, 319-46.
Shen, W., Flajolet, M., Greengard, P., Surmeier, D.J., 2008. Dichotomous dopaminergic control of striatal synaptic plasticity. Science. 321, 848-51.
Singla, S., Kreitzer, A.C., Malenka, R.C., 2007. Mechanisms for synapse specificity during striatal long-term depression. J Neurosci. 27, 5260-4.
Sovago, J., Dupuis, D.S., Gulyas, B., Hall, H., 2001. An overview on functional receptor autoradiography using [35S]GTPgammaS. Brain Res Brain Res Rev. 38, 149-64.
Sung, K.W., Choi, S., Lovinger, D.M., 2001. Activation of group I mGluRs is necessary for induction of long-term depression at striatal synapses. J Neurophysiol. 86, 2405-12.
Surmeier, D.J., Song, W.J., Yan, Z., 1996. Coordinated expression of dopamine receptors in neostriatal medium spiny neurons. J Neurosci. 16, 6579-91.
Surmeier, D.J., Ding, J., Day, M., Wang, Z., Shen, W., 2007. D1 and D2 dopamine-receptor modulation of striatal glutamatergic signaling in striatal medium spiny neurons. Trends Neurosci. 30, 228-35.
Swanson, J.M., Kinsbourne, M., Nigg, J., Lanphear, B., Stefanatos, G.A., Volkow, N., Taylor, E., Casey, B.J., Castellanos, F.X., Wadhwa, P.D., 2007. Etiologic subtypes of attention-deficit/hyperactivity disorder: brain imaging, molecular genetic and environmental factors and the dopamine hypothesis. Neuropsychol Rev. 17, 39-59.
Thapar, A., Langley, K., Asherson, P., Gill, M., 2007. Gene-environment interplay in attention-deficit hyperactivity disorder and the importance of a developmental perspective. Br J Psychiatry. 190, 1-3.
Threlfell, S., Lalic, T., Platt, N.J., Jennings, K.A., Deisseroth, K., Cragg, S.J., 2012. Striatal dopamine release is triggered by synchronized activity in cholinergic interneurons. Neuron. 75, 58-64.
Tisch, S., Silberstein, P., Limousin-Dowsey, P., Jahanshahi, M., 2004. The basal ganglia: anatomy, physiology, and pharmacology. Psychiatr Clin North Am. 27, 757-99.
Ueda, N., Tsuboi, K., Uyama, T., 2013. Metabolism of endocannabinoids and related N-acylethanolamines: canonical and alternative pathways. FEBS J. 280, 1874-94.
Uher, R., McGuffin, P., 2008. The moderation by the serotonin transporter gene of environmental adversity in the aetiology of mental illness: review and methodological analysis. Mol Psychiatry. 13, 131-46.
Usiello, A., Baik, J.H., Rouge-Pont, F., Picetti, R., Dierich, A., LeMeur, M., Piazza, P.V., Borrelli, E., 2000. Distinct functions of the two isoforms of dopamine D2 receptors. Nature. 408, 199-203.
Vallone, D., Picetti, R., Borrelli, E., 2000. Structure and function of dopamine receptors. Neurosci Biobehav Rev. 24, 125-32.
van der Sluijs, P., Hoogenraad, C.C., 2011. New insights in endosomal dynamics and AMPA receptor trafficking. Semin Cell Dev Biol. 22, 499-505.
van Wieringen, J.P., Booij, J., Shalgunov, V., Elsinga, P., Michel, M.C., 2013. Agonist high- and low-affinity states of dopamine D(2) receptors: methods of detection and clinical implications. Naunyn Schmiedebergs Arch Pharmacol. 386, 135-54.
Wang, Z., Kai, L., Day, M., Ronesi, J., Yin, H.H., Ding, J., Tkatch, T., Lovinger, D.M., Surmeier, D.J., 2006. Dopaminergic control of corticostriatal long-term synaptic

depression in medium spiny neurons is mediated by cholinergic interneurons. Neuron. 50**,** 443-52.
Washbourne, P., Thompson, P.M., Carta, M., Costa, E.T., Mathews, J.R., Lopez-Bendito, G., Molnar, Z., Becher, M.W., Valenzuela, C.F., Partridge, L.D., Wilson, M.C., 2002. Genetic ablation of the t-SNARE SNAP-25 distinguishes mechanisms of neuroexocytosis. Nat Neurosci. 5**,** 19-26.
Wermter, A.K., Laucht, M., Schimmelmann, B.G., Banaschweski, T., Sonuga-Barke, E.J., Rietschel, M., Becker, K., 2010. From nature versus nurture, via nature and nurture, to gene x environment interaction in mental disorders. Eur Child Adolesc Psychiatry. 19**,** 199-210.
Wilson, M.C., 2000. Coloboma mouse mutant as an animal model of hyperkinesis and attention deficit hyperactivity disorder. Neurosci Biobehav Rev. 24**,** 51-7.
Yao, W.D., Spealman, R.D., Zhang, J., 2008. Dopaminergic signaling in dendritic spines. Biochem Pharmacol. 75**,** 2055-69.
Yin, H.H., Mulcare, S.P., Hilario, M.R., Clouse, E., Holloway, T., Davis, M.I., Hansson, A.C., Lovinger, D.M., Costa, R.M., 2009. Dynamic reorganization of striatal circuits during the acquisition and consolidation of a skill. Nat Neurosci. 12**,** 333-41.
Zhang, T., Zhang, L., Liang, Y., Siapas, A.G., Zhou, F.M., Dani, J.A., 2009. Dopamine signaling differences in the nucleus accumbens and dorsal striatum exploited by nicotine. J Neurosci. 29**,** 4035-43.
Zucker, R.S., Regehr, W.G., 2002. Short-term synaptic plasticity. Annu Rev Physiol. 64**,** 355-405.